TECHNICAL UNIVERSITY OF LIBEREC
Faculty of Mechanical Engineering

EXPERIMENTAL AND THEORETICAL STUDY OF THE HEATED COANDA JET

by

Tomáš Vít

Doctoral Degree Programme:
Applied Mechanics / Fluid Mechanics and Thermodynamics

Supervisor:
Prof. Ing. František Maršík, DrSc.

Liberec 2004

Abstract

The transition from laminar to turbulent flow occurs for certain magnitude of the Reynolds number in the case of plane wall jet as well as curved wall jet. This transition in the case of curved wall jet is well observed owing to the tendency of laminar flow to separate from the wall. On the other hand turbulent flow has a strong tendency to remain attached to the surface. Both flow separation and flow transition into turbulence are phenomena that have not been so far satisfactory described by any of complex theories. Therefore they represent very complex problem and it is necessary to take into consideration knowledge from the theory of turbulence and the theory of stability of boundary layer to succeed in solving.

There are the results of experimental and analytical study of the effect of temperature and temperature gradient on the character and stability of boundary layer in the case of air flow along the curved wall presented in this thesis. The thesis was focused on obtaining experimental results primarily. For this reason large number of experiments by "Smoke wire" method was carried out. These experiments showed that already a small change of the temperature of the wall can lead to significant change of the character of the flow. These tendencies were also proved by the measuring of the Hot wire anemometry method where the development of the velocity and the temperature profiles and the magnitudes of intensity of turbulence in the cases of the heated and unheated wall were observed.

The results obtained on the basis of experiments were compared with the analytical solution carried out by the similarity solution method and numerical simulation by finite volume method. The forms of the velocity profiles and the profiles of higher velocity derivations were calculated on the basis of similarity solution. These values were used to analyze the stability of boundary layer according to the Rayleigh and the Thermodynamic criterion of stability. By the analysis of the thermodynamic criterion the stabilizing effect of heating up the circumfluenced wall for low velocity of flow was shown. Obtained results proved conclusions published before and they also deepened the knowledge of problems of the heated Coanda jet. The analysis of the results also showed the directions for further research in above mentioned field of study.

Prohlášení

Byl jsem seznámen s tím, že na mou diplomovou *(bakalářskou, doktorskou)* práci se plně vztahuje zákon č. 121/2000 o právu autorském, zejména § 60 (školní dílo) a § 35 (o nevýdělečném užití díla k vnitřní potřebě školy).

Beru na vědomí, že TUL má právo na uzavření licenční smlouvy o užití mé práce a prohlašuji, že **s o u h l a s í m** s případným užitím mé práce (prodej, zapůjčení apod.).

Jsem si vědom toho, že užít své diplomové *(bakalářské, doktorské)* práce či poskytnout licenci k jejímu využití mohu jen se souhlasem TUL, která má právo ode mne požadovat přiměřený příspěvek na úhradu nákladů, vynaložených univerzitou na vytvoření díla (až do jejich skutečné výše).

Datum

8. 10. 2004

Podpis

Tomáš Lít

Anotace

V případě stěnového proudu podél rovinné stěny i v případě stěnového proudu podél zakřivené stěny dochází při určité velikosti Reynoldsova čísla k přechodu proudění z laminární do turbulentní formy. Pro stěnový proud podél zakřivené stěny je tento přechod velmi dobře pozorovatelný díky tendenci laminárního proudu odtrhnout se od obtékaného povrchu. Turbulentní proud má naopak silnou tendenci zůstat k obtékanému povrchu přilnutý. Kromě geometrického uspořádání a materiálových vlastností proudícího média je charakter proudění možné ovlivnit i jinými faktory, jako je drsnost povrchu nebo zde sledovaná teplota obtékaného povrchu.

Zde publikovaná práce aplikuje poznatky z teorie stability a z teorie turbulence na úlohu proudění podél zakřivené válcové stěny, která spojuje jak problematiku odtržení mezní vrstvy, tak i problematiku přechodu do turbulence. V této práci jsou uvedeny výsledky experimentů, společně s výsledky výpočtů, které sledují vliv teploty obtékané stěny a teplotního gradientu v mezní vrstvě na stabilitu mezní vrstvy a tím pádem na charakter stěnového proudu podél zakřivené stěny.

Práce byla v první řadě zaměřena na získání experimentálních výsledků. Za tímto účelem bylo provedeno velké množství experimentů metodou kouřového drátku. Výsledky experimentů ukázaly, že již malá změna teploty stěny může vést k výrazné změně charakteru proudění. Pozorované tendence byly rovněž potvrzeny měřením metodou drátkové anemometrie, kdy byl sledován vývoj rychlostních a teplotních profilů a velikosti intensity turbulence pro případy obtékání zahřívané a nezahřívané stěny.

Výsledky získané na základě experimentů byly následně porovnány s analytickým řešením provedeným metodou podobných profilů a numerickou simulací metodou konečných objemů, tak jak je aplikována v softwaru Fluent. Na základě výsledků získaných metodou podobných profilů byly vypočteny tvary rychlostních profilů a hodnoty vyšších derivací rychlosti. Tyto hodnoty posloužily k vyhodnocení stability mezní vrstvy z pohledu Rayleigho a termodynamického kriteria stability. Analýzou termodynamického kritéria stability byl ukázán stabilizující vliv ohřevu obtékané stěny na mezní vrstvu při malých rychlostech proudění.

Získané výsledky potvrdily dříve publikované závěry a zároveň prohloubily znalost problematiky proudění termoviskozní tekutiny podél zahřívané stěny. Rozbor výsledků rovněž naznačil směry dalšího výzkumu v uvedené oblasti.

Acknowledgement

I would like to express here my thanks to those who helped me with preparation, writing and handling with this thesis. In the first place, I would like to thank to Prof. Ing. František Maršík, DrSc. who devoted his time to my problems for his advice and suggestions during the implementation of the project and for his remarks to the results of the thesis. My thanks also belong to Ing. Zdeněk Trávníček, CSc. for his help and advice not only during the preparation of the experiments.

It is also necessary to thank to Jaroslav Kneř and Petr Jerje for the completing of the experimental setup and for their help with setting up and carrying out the experiments. I would like to thank to all members of the Department of Power Engineering Equipment and to the management of the Technical University of Liberec for the support during my studies and handling my diploma thesis as well as to C.C.M. Rindt and to the Technical University of Eindhoven for the opportunity to spend time at the University in Eindhoven.

Last but not least my thanks belong to Jitka, Jana and Hana for their help with the translation and for the following emendation.

My thanks also belong to all my colleagues and friends at the Technical University of Liberec, to the Institute of the Thermomechanics of the Academy of Sciences and to Lenam company, who never rejected to help me.

The costs of this thesis were paid from the financial resources of the Department of Power Engineering Equipment and from the research project of the Ministry of Education, Youth and Sports of Czech republic number MSM 24210 0001. Both of them also deserve my thanks.

CONTENTS

LIST OF SYMBOLS

A		calibration constant - eq. (3.5)
a	$[K^{-1}]$	constant in a model of viscosity - eq. (4.35)
A^*		calibration function - eq. (3.11)
A^+		constant - eq. (2.87)
a_h	[1]	overheat ratio - eq. (3.10)
B	[1]	calibration constant - eq. (3.5)
b	[1]	constant in a model of viscosity - eq. (4.35)
b	[m]	slot width
B^*		calibration function - eq. (3.11)
B_w		additive constant in the law of the wall - eq. (2.81)
C		calibration constant - eq. (3.15)
c		parameter of velocity profile - eq. (4.21)
c	$[ms^{-1}]$	phase velocity
C_c		constant in the Clauser turbulence model - eq. (2.90)
C_1		constant - eq. (2.95)
C_2		function of a distance from the wall - eq. (2.99)
c_p	$[Jkg^{-1}K^{-1}]$	specific heat of fluid at constant pressure
c_s	$[ms^{-1}]$	velocity of sound
d	[m]	diameter
d	$[s^{-1}]$	tensor of strain rate
$d_{(1)}$	$[s^{-1}]$	the first invariant of the tensor of strain rate
D		calibration constant - eq. (3.16)
da	$[m^2]$	element of area
E	[V]	anemometer output voltage
E_{acq}	[V]	voltage measured at temperature of the fluid - eq. (4.4)
E_{wire}	[V]	wire voltage - eq. (4.4)
e	[1]	Euler strain tensor
f	$[Jkg^{-1}]$	specific free energy
F		invariant - eq. (4.34)
f		stream function - eq. (4.21)
f(x)		function of x
g	$[Nm^{-3}]$	external volume force
g(x)		function of x
h	$[Wm^{-2}K^{-1}]$	heat transfer coefficient
h_c	$[Jkg^{-1}K^{-1}]$	specific total enthalpy - eq. (2.48)
I	[A]	current
$J(\Phi)$		total flow of quantity Φ - eq. (2.2)
K		flow stability parameter - eq. (2.96)
k	$[m^{-1}]$	wave number

L	[m]	relaxation length - eq. (2.100)
l_m	[m]	mixing length - eq. (2.79)
m	[kg]	mass
m, n		boundary layer parameters - eq. (4.21)
n		vector in normal direction
n_c		calibration exponent
p	[Pa]	pressure
p		vector of density of flux
$P(\Phi)$		total production of quantity Φ - eq. (2.3)
Pr	[1]	Prandtl number, $Pr = \nu/\lambda$
Q	[W]	heat flux
q	[Wm^{-2}]	specific heat flux
$\tilde{q}$	[Wm^{-2}]	external heat flux
r	[m]	radial coordinate
R	[m]	radius of curvature
R_0	[Ω]	resistance of wire at 0°C
R_1, R_2, R_3	[Ω]	resistors in Wheatstone bridge
R_{20}	[Ω]	resistance of wire at 20°C
R_a	[Ω]	resistance of wire at ambient temperature T_a
Re	[1]	Reynolds number $Re = U_b\sqrt{Rb}/\sqrt{2}\nu_\infty$
Re_b	[1]	Reynolds number $Re_b = U_b b/\nu_\infty$
Re_c	[1]	critical Reynolds number
$\tilde{Re}$	[Ω]	Reynolds number $\tilde{Re} = \nu_e\delta^*/\nu$
R_L	[Ω]	resistance of probe lead and cables
R_{wire}	[Ω]	resistance of heated wire at temperature T_{wire}
S	[JK^{-1}]	entropy
s	[$Jkg^{-1}K^{-1}$]	specific entropy
$S_{u,CC}$	[$Vm^{-1}s$]	CC mode velocity sensitivity - eq. (3.8)
$S_{u,CT}$	[$Vm^{-1}s$]	CT mode velocity sensitivity - eq. (3.6)
$S_{\theta,CC}$	[VK^{-1}]	CC mode temperature sensitivity - eq. (3.9)
$S_{\theta,CT}$	[VK^{-1}]	CT mode temperature sensitivity - eq. (3.7)
T	[K]	temperature
t	[s]	time
T_a	[K]	ambient temperature
T_{cal}	[K]	temperate during calibration - eq. (4.5)
T^*	[1]	temperature ratio $T^* = T_w/T_\infty$
TI	[1]	turbulence intensity - eq. (4.8)
T_w	[K]	temperature of wall
T_{wire}	[K]	temperature of heated wire
U	[ms^{-1}]	measured/ calculated velocity
u	[Jkg^{-1}]	specific internal energy

u'	[ms^{-1}]	fluctuating part of measured velocity
U_R	[ms^{-1}]	measured/calculated velocity in radial direction
U_{Ref}	[ms^{-1}]	reference velocity
U_φ	[ms^{-1}]	measured/calculated velocity in tangential direction
$\dot{V}$	[m^3s^{-1}]	flow rate
V	[m^3]	volume
v^*	[ms^{-1}]	friction velocity - see footnote 1 on page 39
v^+	[1]	dimensionless, sublayer-scaled, velocity - see footnote 1 on page 39
v_e	[ms^{-1}]	velocity of external flow
v_i	[ms^{-1}]	component of velocity vector ($i = x, y, z, R, \varphi$)
x, y, z		Cartesian coordinates, curvilinear orthogonal coordinates
y	[m]	distance from the wall
y^+	[1]	dimensionless, sublayer-scaled, distance - see footnote 1 on page 39
z	[m]	lengthwise direction
α	[1]	dimensionless parameter of curvature $\tilde{R} = \alpha\tilde{x}^n$
α_0	[K^{-1}]	temperature coefficient of resistivity at 0°C
α_{20}	[1]	temperature coefficient of resistivity at 20°C
δ	[m]	thickness of the boundary layer
δ^*	[m]	displacement thickness of the boundary layer
δ_{BL}	[m]	velocity boundary layer thickness
δp	[Pa]	deviation of pressure
δs	[$Jkg^{-1}K^{-1}$]	deviation of entropy
δ_{TBL}	[m]	temperature boundary layer thickness
δv	[ms^{-1}]	disturbance of velocity
∂V	[m^2]	boundary of volume
δ_v^*	[m]	velocity thickness of boundary layer
ϕ		potential function of body forces
η	[1]	dimensionless coordinate - eq. (4.21)
φ	[°]	angle
Φ, ϕ		general physical quantity - eq. (2.1)
χ_{wire}	[Ωm]	resistivity
κ		constant - eq. (2.87)
κ_w		Kármán constant - eq. (2.81)
λ	[$Wm^{-1}K^{-1}$]	thermal conductivity
λ_v	[m]	wavelength of disturbance
μ	[$kgm^{-1}s^{-1}$]	molecular viscosity
μ_{it}	[$kgm^{-1}s^{-1}$]	isothermal molecular viscosity - eq. (4.48)
μ_t	[$kgm^{-1}s^{-1}$]	turbulent viscosity - eq. (2.78)
μ_{tc}	[$kgm^{-1}s^{-1}$]	turbulent viscosity of curved flow - eq. (2.98)
μ_{temp}	[$kgm^{-1}s^{-1}$]	temperature dependent molecular viscosity - eq. (4.48)

μ_{teq}	[$kgm^{-1}s^{-1}$]	equilibrium turbulent viscosity - eq. (2.100)
μ_v	[$kgm^{-1}s^{-1}$]	volume viscosity
ν	[m^2s^{-1}]	kinematic molecular viscosity
ν_t	[m^2s^{-1}]	kinematic turbulent viscosity
$\pi,\tilde{\pi}$	[$Jm^{-3}s^{-1}$]	density of energy dissipation - eq. (2.25), - eq. (2.51) resp.
Θ	[1]	dimensionless temperature difference $\Theta = (T - T_w)/(T_\infty - T_w)$
ρ	[kgm^{-3}]	density of fluid
σ		standard deviation
$\sigma(\Phi)$		density of quantity Φ production - eq. (2.3)
τ	[Pa]	shear stress
τ_{diss}	[Pa]	dissipative part of stress tensor - eq. (4.42)
τ_{el}	[Pa]	elastic part of stress tensor
τ_{it}	[Pa]	isothermal part of shear stress - eq. (4.49)
τ_t	[Pa]	turbulent shear stress - eq. (2.78)
τ_{temp}	[Pa]	temperature-dependent part of shear stress - eq. (4.49)
τ_{tot}	[Pa]	total shear stress $\tau_{tot} = \tau + \tau_t$
τ_w	[Pa]	wall shear stress $\tau_w = \mu(\partial\overline{v}_x/\partial y)_w$
ϑ_x, ϑ_y, ϑ_{xy}	[m^3s^{-3}]	production rate of turbulence energy - eq. (2.92), (2.93), (2.94)
ω		exponent in the model of viscosity - eq. (2.58)
ξ	[1]	normalised radial coordinate $\xi = y/y_{0.5}$
ψ	[1]	stream function - eq. (4.20)

Subscripts and superscripts

A	attached flow
I	inflection point on velocity profile
i,j,k,l,m	components
max	maximum
S	separated flow
w	wall
0.5	position above surface where is velocity the half of velocity maximum
~	dimensionless quantities
∞	free stream condition
-	time mean value

Abbreviations

CC	constant current
CT	constant temperature
HWA	hot wire anemometry
NS	Navier-Stokes equation

Chapter 1

INTRODUCTION

The Coanda jet is one case of a flow along a curved wall. To investigate it more in detail, we can start from a fluid flow along the plain wall, Fig.1.1, where the surrounding fluid is steady. This type of flow was named "Wall Jet" by Glauert. Glauert[12] presents similarity solution for laminar as well as for turbulent wall jet.

Wall jet can be understood as a combination developed by interaction of two shear layers. The inner region is in its character very similar to the boundary layer. In comparison to it, the outer region is similar to the jet.

Glauert solution of laminar wall jet belongs to the typical examples of similarity solution of velocity profiles. Glauert presumed constant turbulent viscosity in outer region (if Görter hypothesis, that the velocity profile of a turbulent jet is the same as the velocity profile of a laminar jet, is valid) and he used Prandtl model of turbulence for the similarity solution of the turbulent wall jet. He used Blasius model of turbulent viscosity for the inner region that must follow the influence of the wall and where constant turbulent viscosity cannot be presumed. Final profiles can be seen in Fig.1.2.

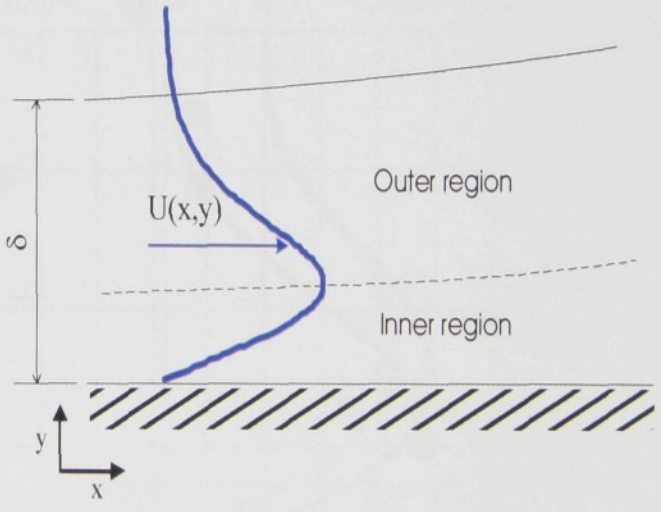

Fig.1.1 Schema of a wall jet. Splitting of the wall jet layers. The layer from the wall to the velocity maximum is marked as inner region. The layer from the velocity maximum up to the edge of the boundary layer is called the outer region

A known result of several experiments dealing with a wall jet is that the point where the sign of shear stress changes does not correspond to the point of zero velocity gradient but this point shifts closer to the

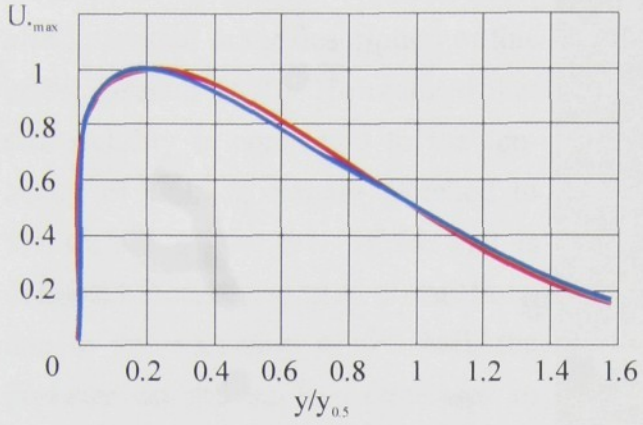

Fig.1.2 Turbulent velocity profile calculated on the basis of Glauert solution (After Glauert[12]-red line). Measured turbulent velocity profile is presented to make comparison (After Guitton[14]-blue line)

wall. The point of zero shear stress shifts much closer to the wall in the curved wall jet (see Fig.1.3)

Among the significant studies dealing with the problems of a wall jet, the study by Irvin[17], which contains some very detailed measurements in a self preserving flow, is worth mentioning. Kruka[23] have measured longitudinal fluctuations and shear stress and Kacker[20] have measured all the non-zero stress components.

1.1 Coanda[1] effect

Wall jet and mainly curved wall jet are the examples of very interesting flows, which are in its essence about one degree more complex than a boundary layer. Wall jet is easy to carry out in laboratory and it has a lot of applications in engineering practice in those branches that deal with film cooling and advanced airfoil design. These are the reasons why the wall jet has received a considerable attention from experimenters and modelers.

There is a phenomenon known from everyday life where the fluid flow has a strong tendency to remain attached to the wall close to it and then follow this wall. A typical example can be stable, equilibrium position which has a ball "floating" on the top of a vertical symmetric flow of

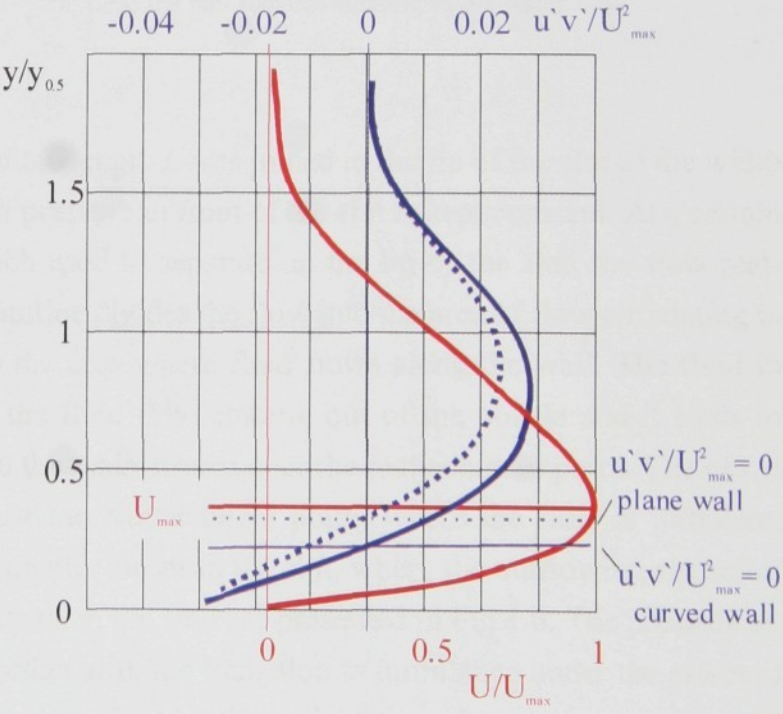

Fig.1.3 The comparison of velocity profile and shear stress profile. The shift of minimum shear stress from the position of the velocity maximum towards the wall is evident (After Dakos[7])

1. Henry Coanda (1886-1972), Romanian technician and physics. In addition to aeronautics, he was also interested in metallurgy and petrochemistry. He presented the first plane with a jet propelled engine at the II. International Aeronautic Exhibition in Paris in 1910.

water or air - Fig.1.4. O. Reynolds was also interested in the description of this effect (around 1870). He realized that this stability is connected to the tendency of fluid to remain attached to the surface of the ball. If the ball is deflected from the centre of the flow, due to the curvature of the ball, the pressure on the surface decreases in the positions that are closer to the centre and a force, which originates in this process, returns the ball back into the equilibrium position.

Fig.1.4 Example of Coanda effect. Fluid remains attached to the surface of the ball. Negative pressure occurs in this case in the upper part of the surface of the ball that is sufficient enough to keep the ball remains floating in the water flow.

The phenomenon in which the fluid flow remains attached to the wall is usually associated with the name of Henry Coanda who used this effect in some of his inventions (for example to improve the scavenging of internal combustion engines, to increase the maximum lift coefficient of a wing). His experiment is presented in Fig.1.5.

In this experiment the wall of the length L was joined to the lip of the slot of the width b. This wall is beveled at the angle α. Air pressure in front of the slot is kept constant. At a certain magnitude of L/b ratio of the flow, which used to separate on the lip of the slot, the flow reattaches to the wall again. Reattached streamline divides the flow into the area of flow circulating in a so called "separated bubble" and into the area where fluid flows along the wall. The fluid in the "separated bubble" is entrained by the fluid flow coming out of the nozzle and it leads to the return of the part of the fluid back to the main stream near the reattachment point. The effect of the entrainment is much stronger near the reattachment point, where the flow is turbulent, whereas the effect of the entrainment is smaller closer to the slot, where the outflowing stream of fluid is laminar. Measured values of pressure on the wall are presented in Fig.1.6. The pressure on the wall is constant closer to the lip. Together with the transition to turbulence under the effect of more intensive entrainment of the surrounding fluid by the main stream the pressure on the wall starts to decrease until it reaches lower values than the pressure of the air surrounding it. The pres-

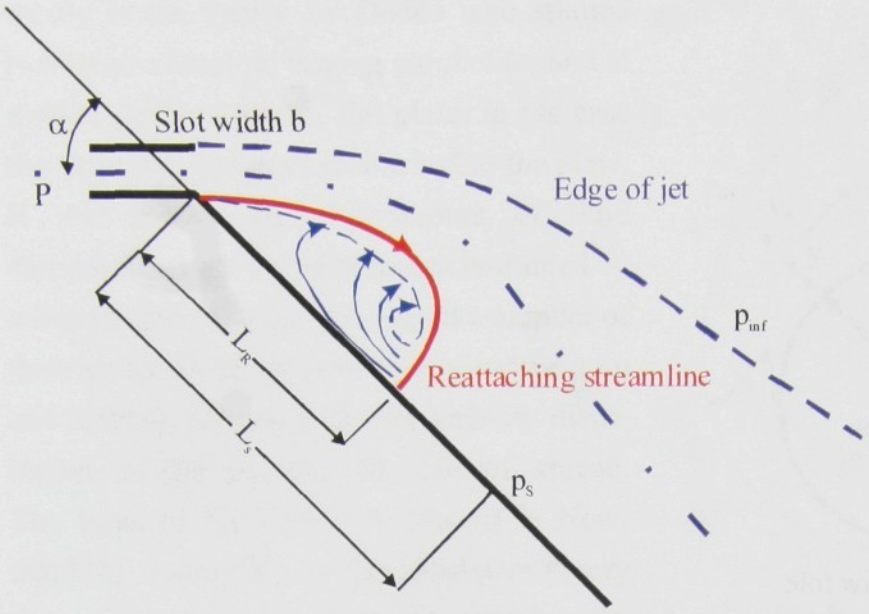

Fig.1.5 Coanda's experimental setup (After Newman[28]).

sure increases again while it flows along the wall until it corresponds to the values of the pressure of the surroundings.

The explanation of the phenomenon can be found in Squire[38]. Let's imagine a free fluid flow which entrains surrounding fluid along its sides. If this flow gets close to the wall in a restricted area between the flow and the wall, the velocity increases together with the decrease of the pressure on the wall. The pressure on the wall reaches lower values than the pressure of the surroundings does and so the fluid flow gets attached to the wall. This phenomenon can be best observed in a two-dimensional or nearly two-dimensional flow. In the case of a three-dimensional flow, air from lateral direction can be sucked, the pressure on the wall will remain on the same level as the pressure of the surroundings and the effect of the fluid attachment to the wall does not occur. That is why it is necessary to design the experimental setup as the two-dimensional one and for this purpose we have to equip the setup with end plates or we have to ensure the two-dimensional flow by another possible way.

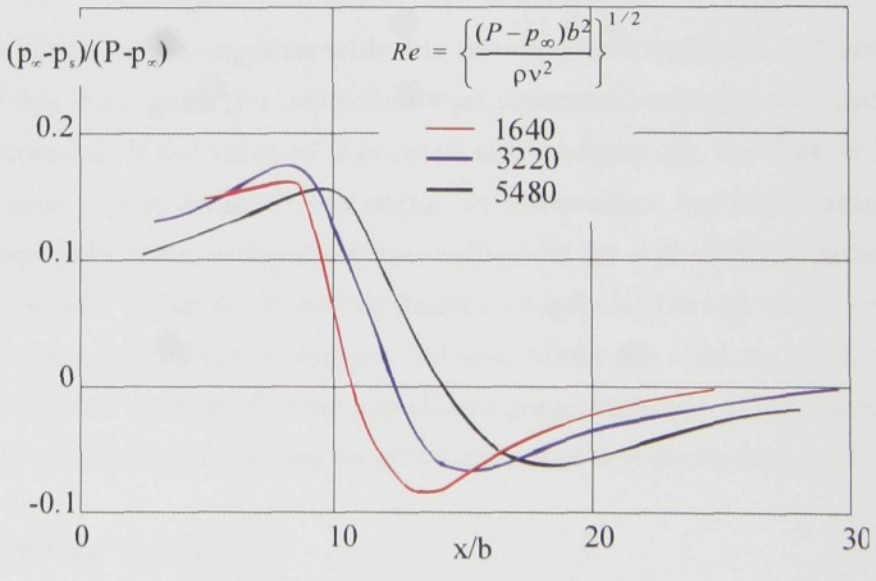

Fig.1.6 Variation of surface pressure distribution along the wall for different Reynolds number at $\alpha=45^{o}$(After Newman[28])

Many investigations have been made for the case of deflection of the plane jets by adjacent boundaries. An entrainment

theory is the theory by Dodds who studied two-dimensional jet issuing parallel to, and at a short distance above, flat plate. In his case the flow also becomes reattached to the plate. It was found, that the amount of fluid entrained had been similar to that entrained by a free jet. Bourque has developed a number of theories by using the principle of momentum and making allowance for the velocity distribution in the jet and its rate of spread. The basis of his theory are shown in Newman[28]. According to the Bourques theory the maximum value of α, for which reattached flow is possible, is 90° and then the separation bubble is infinitely long. The maximum value, which has so far been obtained experimentally, is 75° with $L_R/b=2000$.

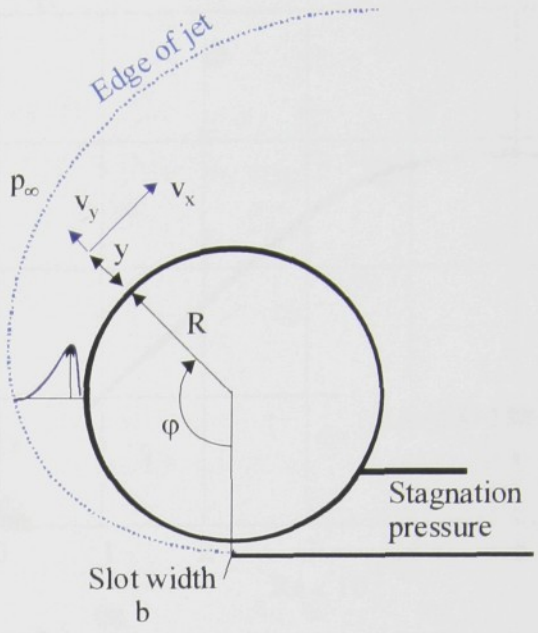

Fig.1.7 Flow of a two-dimensional jet round a circular cylinder

Glahn studied the influence of compressibility on the deflection of plane jets by adjacent boundaries and he found out that for the pressure ratios P/p_∞, which are lower than those required for chocking reattachment, distance increases as the pressure ratio increases. But these experiments were carried out under the conditions that are far from the conditions in our experiments.

The hysteresis effect which occurs together with this flow is also mentioned in Newman[28], moreover it was found that the regime (jet reattached × jet separated) actually obtained, depends on the way the flow is initiated. If the value of α is small at the beginning, the flow will be reattached and remains reattached within the dual-flow region as α increases. For high values of α the flow will always be completely separated and for low values the jet will always remain reattached. This phenomenon was also observed in circumfluence round the curved wall (see Trávníček[45]). Hysteresis occurs not only when α changes but also when the velocity of flow changes and it can be presumed that the change of other significant parameters (as the temperature ratio in case of a heated wall) will lead to hysteresis between separated and reattached flows.

1.2 Wall jet over convex surface

Nowadays, the circumfluence of curved convex wall (as shown in Fig.1.7) is considered to be a typical example of Coanda effect. One lip of α slot of the width b is joined to the cylinder wall of the radius R. If the values of the Reynolds number are high and R/b ratios are high,

the angle of separation reaches the values over 180°. Some publications present the angles of separation over 230°. It is possible to assume that under such conditions the distance of the separation point depends mainly on the geometric arrangement of the experiment.

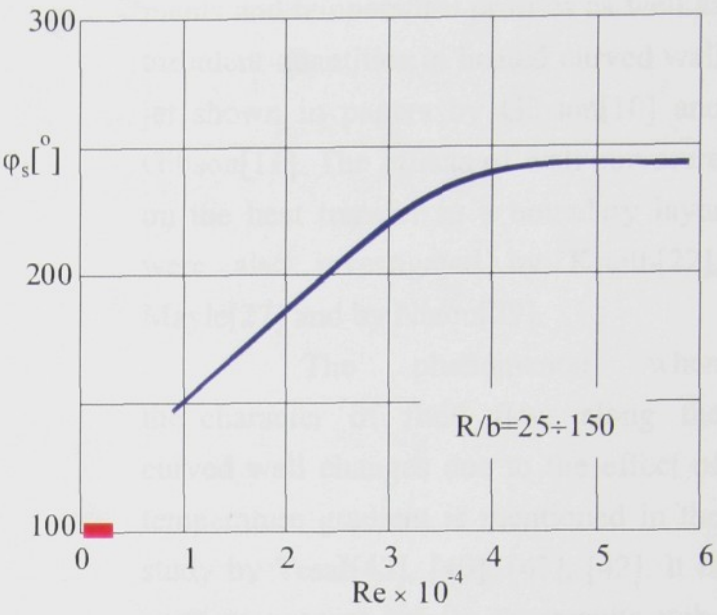

Fig.1.8 The position of separation for high *R/b*. (6 in. dia. cylinder). Reynolds number is defined as in (4.3) (After Newman[28]). Area of our interest is marked by red line.

If we presume the flow of ideal fluid (non-viscid, non-turbulent), it is possible to imagine that the flow will not entrain the surrounding fluid, the width of flow will be constant and the distribution of velocity in the flow will be the same for the various angles φ. Static pressure on the wall will also be constant. The flow separation will never occur in the flow of such fluid. Although the behavior of real fluid is far from ideal state, it is possible that the flow of real fluid will remain attached to the wall even when the values of φ will be very high (see Fig.1.8).

The entrainment of fluid from the surroundings occurs in the flow of real fluid, the width of the boundary layer rises and the velocity of the flow decreases. It leads to the increase of pressure and finally to the separation of flow from the wall.

The first significant study dealing with a curved wall jet is an article by Newman published in Newman[28]. There are the first extensive measurements of the wall jets in the self-preserving flow on logarithmic spiral in Guitton[14]. The results of experiments in constant curvature flow are mentioned in Dakos[7]. At the higher Reynolds number the turbulence intensities and shear stress in the destabilized outer region increase with the distance downstream to levels significantly higher than those recorded on self-preserving plane flow are the main results of these measurements. Consequently, the spreading rate also increases with the distance along the plate. At the same time, the stabilizing effect of the wall curvature in the inner region causes the position of zero shear to move away from the velocity maximum and approaching the wall. Coanda effect is also mentioned in studies dealing with the application of the wall jet in technical practice.

The study of Trávníček[45] is worth mentioning. The problems of impact drying of plain materials with the use of supporting effect developed by Coanda effect are described there.

Much smaller attention in scientific publications was given to the problems of a curved wall jet over heated/cooled surface. There are the results of detailed velocity measure-

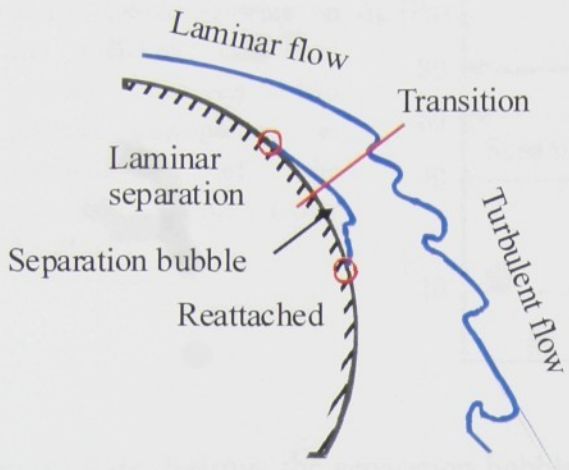

Fig.1.9 Principle of separation bubble, as a description of heated laminar wall jet behavior (After Tesař[44])

ments and temperature profiles as well as turbulent quantities in heated curved wall jet shown in papers by Gibson[10] and Gibson[11]. The effects of wall curvature on the heat transfer in a boundary layer were also investigated by Kreith[22], Mayle[27] and by Nizou[29].

The phenomenon when the character of fluid flow along the curved wall changes due to the effect of temperature gradient is mentioned in the study by Tesař[43], [40], [41], [42]. It is good to present briefly the results published by Tesař because his study is closely connected to the problem being solved in the present thesis

Mainly the results of the experiments are worth mentioning. They show the dependence of the point of transition from separated to attached state on the Reynolds number and *R/b* ratio. The particular state depends on the value of Re_b and on the temperature of the wall. The effect of the temperature on the shift of the point of separation to higher values of Re_b is shown in Fig.1.10. This shift mentioned by Tesař[44] is explained by postponing the transition to turbulence due to the decrease of the local Reynolds number, which is caused by the increase of viscosity with temperature.

Tesař states the hypothesis that evident destabilization due to the wall temperature is connected to the presence of a so called "separation bubble". The "separation bubble" is called the area where the separation of a laminar flow and consecutive fast transition to turbulence occur. The separation from the wall leads to the increase of fluctuations which were inhibited by the presence of the wall. The rate of the increase of the turbulent boundary layer thickness is big enough for the flow to get reattached to the wall. The turbulent flow is then able to keep following the wall. The introduced tempera-

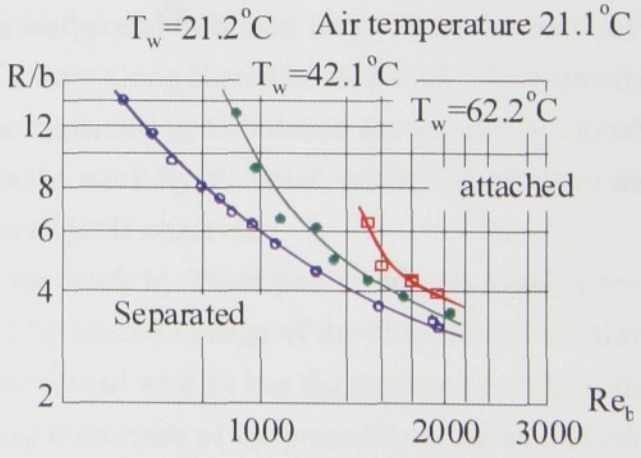

Fig.1.10 The separation of air flow as a function of temperature of the wall and R/b ratio (After Tesař[44])

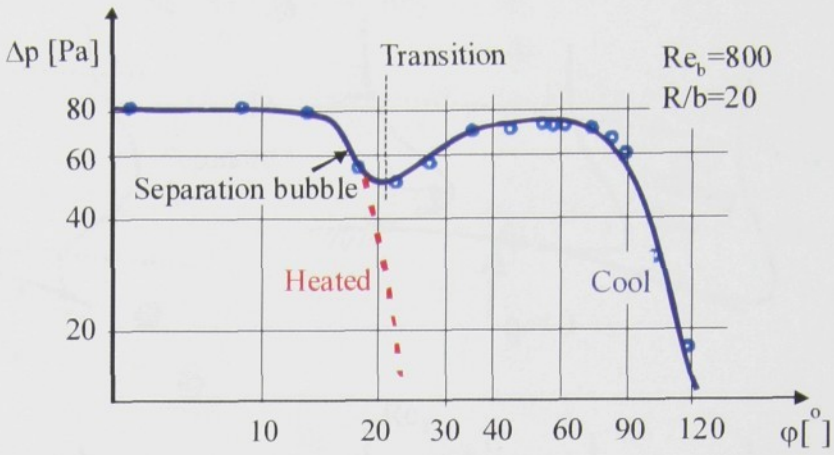

Fig.1.11 Distribution of subatmospheric pressure on the wall-with the local extreme between two plateaux interpreted as manifestation of the separation bubble (After Tesař[44])

ture gradient destroys the separation bubble probably by delaying the transition. The turbulent layer then forms too far downstream so that it fails to reach towards the wall and to reattach. The separating bubble principle is shown in Fig.1.9. The distribution of pressure on a heated and an unheated wall (Fig.1.11) published by Tesař supports his hypothesis of the separation bubble.

1.3 Research objectives

This thesis deals with the problems of stability of a laminar boundary layer, the loss of stability of the boundary layer and the transition to turbulence in the flow of fluid along the curved wall in the cases where the boundary layer is influenced by the temperature gradient. The thesis describes the problems of a curved wall jet around a heated surface and the effect of the temperature and the temperature gradient in the circumfluous air on the stability of the fluid flow coming out off the narrow nozzle.

As it is clear from the abstract in the previous paragraphs, most of the papers dealing with the problems of Coanda jet are interested in a isothermal turbulent flow. There are only several pieces of work that deal with the problems of a flow along heated/cooled wall. The problems of the laminar Coanda jet and the problems of the transition to turbulence are usually marginalized in the literature. The only known exception is the work by V. Tesař, where the effect of the temperature gradient on the character of a curved wall jet is observed.

At the same time it is also clear, and the work by Tesař published previously prove that the transition to the turbulence is accompanied by a rapid change of the character of the flow in the case of the Coanda jet (Fig.1.12). The laminar curved wall jet has the tendency to follow the circumfluenced wall only for a small angle φ_S. A rapid increase of the pressure on the wall occurs under the influence of the curvature of the wall and an adverse pressure gradient in the direction of the flow leads to the separation of the flow. On the other hand, the turbulent flow has a strong tendency to remain attached to the circumfluenced wall. There are values of the separation angle around $\varphi_S=270^o$ presented in literature. The magnitude of the angle of separation depends on

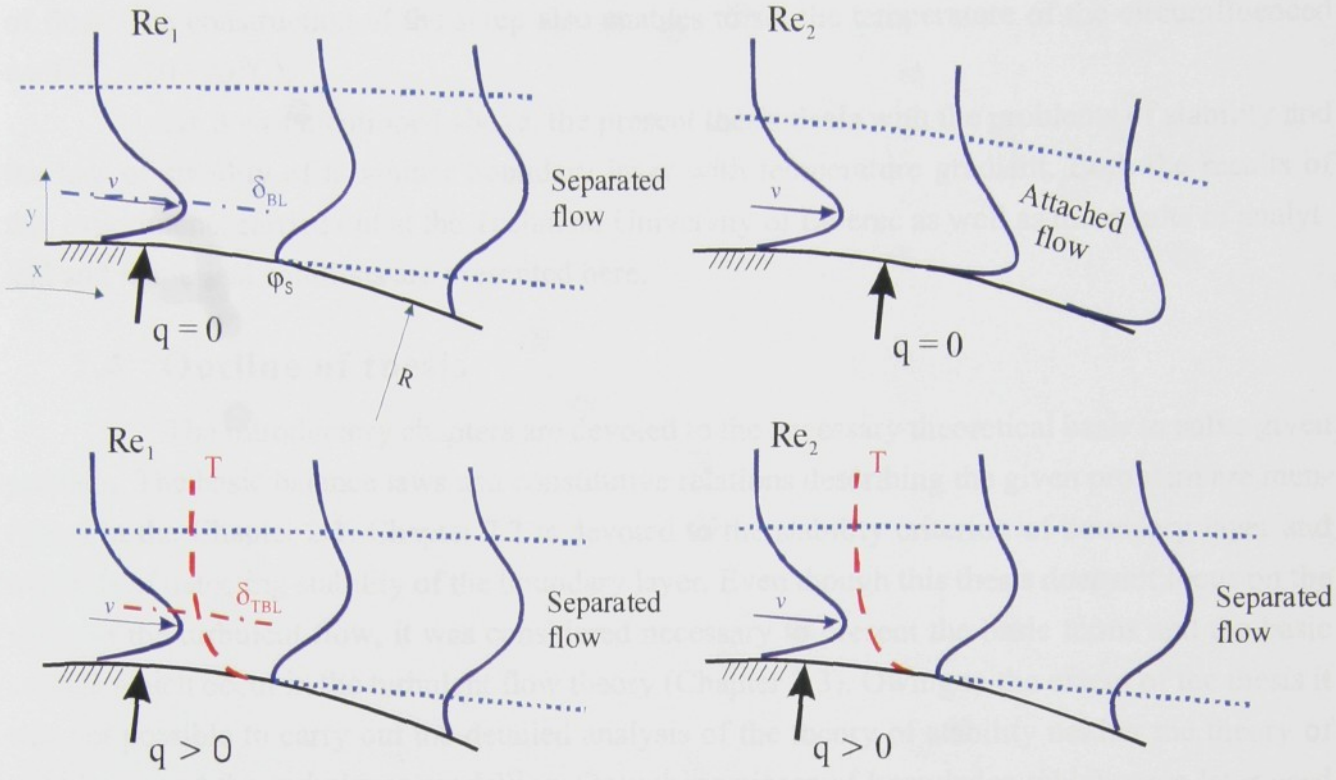

Fig.1.12 Development of flow in case of isothermal and heated Coanda jet. In the picture $Re_1 < Re_2$ is valid.

the geometric arrangement of the experiment (ratio of the radius of the wall R and the width of the nozzle R/b) and on the magnitude of the Reynolds number.

If we increase the velocity of the flow in the nozzle for same geometric arrangement from the values which correspond to the laminar flow up to the values which correspond to the fully developed turbulent flow, we do not observe a continuous increase of the angle of separation. The flow has a laminar character for low values of Re and the increase of the angle of separation with increasing Re is very small. A sudden change of the angle of separation occurs for a certain value of the Reynolds number (Re_c). This change is in connection with the transition of the flow to the turbulent regime. A further increase of the flow velocity leads to a gradual increase of the angle of separation. Only for high values of Re the angle of separation is not dependant on the magnitude of Re. That is why the Coanda jet seems to be an ideal arrangement for the investigation of the stability of a boundary layer and for observing the influence of particular parameters (velocity of flow, temperature, temperature gradient etc.) on the transition to the turbulence.

The aim of the present thesis was to obtain precise experimental results and to complete these experiments with an analysis carried out on the basis of numerical simulations (Finite Volume Method) and on the similarity solution of velocity profiles. For this reason it was necessary to assemble an experimental setup of the Coanda jet type that enables to set various regimes

of flow. The construction of the setup also enables to set the temperature of the circumfluenced wall (T_w=20÷90°C).

As it was mentioned above, the present thesis deals with the problems of stability and the loss of stability of a laminar boundary layer with temperature gradient. Both the results of the experiments carried out at the Technical University of Liberec as well as the results of analytical and numerical solutions are presented here.

1.4 Outline of thesis

The introductory chapters are devoted to the necessary theoretical basis to solve given problem. The basic balance laws and constitutive relations describing the given problem are mentioned in the Chapter 2.1. Chapter 2.2 is devoted to the stability criterion of boundary layer and methods of detecting stability of the boundary layer. Even though this thesis does not focus on the study of the turbulent flow, it was considered necessary to present the basic terms and the basic models which occur in the turbulent flow theory (Chapter 2.3). Owing to the extent of the thesis it was not possible to carry out the detailed analysis of the theory of stability neither the theory of turbulence and the turbulence modelling. Only those pieces of knowledge which were later used to analyze the observed phenomenon were chosen out of these two wide areas. Detailed explanation of terms which exceed the extent of this thesis is represented by the references to literature.

The following chapters already deal directly with the solution of the given problem. The basis of the applied experimental and numerical methods are presented in the Chapter 3.1. The difficulties which can be met when studying the flow with the temperature gradient are presented here. This chapter is followed by the Chapter 3.2 where the experimental setup is described.

The Chapter 4.1 is devoted to the results of the experiments carried out by the "Smoke Wire" and the CTA methods. The Chapters 4.2÷4.5 which follow describe the results obtained by the method of similar profiles and the numerical simulation by the Final Volume method. It is necessary to highlight the derivation of the similarity solution of a laminar boundary layer along a heated convex wall as well as the stability criterion, presented in this case in curve-linear orthogonal coordinates.

The Chapter 5 summarizes the results presented in the previous chapters and it shows a possible explanation of the studied phenomenon.

Chapter 2

CURRENT STATE OF KNOWLEDGE

2.1 Fundamental equations

Regarding the problem solution, most of the balance equations and the relations based on these equations used in the following chapters are formulated by the spatial[1] (Euler) description. A detailed derivation of the balance principles can be found for example in Maršík[26], in the English references for example in Bird[1].

The balance of mass, total energy and momentum are the most often used terms in mechanics and in fluid mechanics. Regarding the later use of the stability criterion of processes which is directly derived from the balance of entropy, the relation of the balance of entropy will be mentioned in this chapter too.

2.1.1 General balance principles

Regardless the choice of the system of coordinates, we can set a general schema for the balance of a general physical quantity Φ according to the principle:

$$\frac{d\Phi(t)}{dt} = J(\Phi) + P(\Phi) \tag{2.1}$$

This equation reflects the experience that time change of the quantity Φ is in particular volume caused by the inflow/outflow of the quantity Φ through the boundary of the volume and by production (annihilation) the quantity Φ inside the volume.

---

1. The spatial (Euler) description is closely connected to a fixed system of coordinates. The observed volume V bound by surface ∂V does not move in space. Fluid does not flow through the observed volume. The use of the substantial (Lagrange) description in mechanics of solid body is more pragmatic in many cases. This description deals with the observed volume which contains the same elements in every moment.

The total flow of the quantity Φ through the boundary V can be formulated by the surface integral (in spatial coordinates)

$$J(\Phi) = \int_{\partial V} j^k(\Phi) da_k \tag{2.2}$$

Total production of the quantity Φ can be formulated as:

$$P(\Phi) = \int_V \sigma(\Phi) dV \tag{2.3}$$

If we substitute the relations (2.2) and (2.3) to basic relation (2.1), and if we use substantial derivation and Gauss theorem[1], we get the equation for the balance quantity Φ for the whole volume:

$$\int_V \left[\frac{\partial \phi}{\partial t} + \frac{\partial (\phi v^k)}{\partial x^k} - \frac{\partial j^k(\Phi)}{\partial x^k} - \sigma(\Phi) \right] dV = 0 \tag{2.4}$$

As this equation is valid for any fixed and closed observed volume, it must be valid for an infinitely small volume too. As a result of this,

$$\frac{\partial \phi}{\partial t} + \frac{\partial (\phi v^k)}{\partial x^k} - \frac{\partial j^k}{\partial x^k} - \sigma(\Phi) = 0 \tag{2.5}$$

The equations of the balance of mass, momentum, kinetic and total energy, inner energy, enthalpy and entropy will be derived in accordance with the schema mentioned above in the following paragraphs.

2.1.2 Balance of mass

If we substitute the general quantity Φ with the mass m, which is:

$$m(t) = \int_V \rho(x, t) dV \tag{2.6}$$

---

1. Gauss theorem: $\int_V \frac{\partial \mathbf{p}_i}{\partial x_i} dv = \int_{\delta V} p_j n_j d(\delta V)$ where $\mathbf{p}=(p_1; p_2; p_3)$ is a vector of flux density of quantity through surface ∂V. It states that the flux of vector a through close surface equals to the volume integral from divergence of vector $\mathbf{p}$.

and then if we substitute m in relation (2.5), we get the form of the mass balance in the spatial coordinates

$$\frac{\partial \rho}{\partial t} + \frac{\partial(\rho v^k)}{\partial x^k} = 0, \tag{2.7}$$

if we assume that $J(m) = 0$ and $P(m) = 0$. It is possible to formulate this equation in the form

$$\frac{\partial v^k}{\partial x^k} = 0, \tag{2.8}$$

if $d\rho = 0$ (incompressible fluid).

2.1.3 Balance of momentum

The balance of momentum expresses the balance of forces which affect the volume. Forces which affect the volume can be divided into forces affecting the surface element of the volume. Those forces can be, for example, the forces caused by the static pressure viscose friction or the skin-effect. Other forces affecting the volume element have the character of gravity forces or forces generated by the transformation of system of coordinates (see centrifugal and Coriolos forces in the equation (4.9)).

The total momentum of body is defined by the integral:

$$\int_V \rho(x, t) v^k(x, t) dV. \tag{2.9}$$

The total force effect on the surface of the body can be expressed in the spatial coordinates by the surface integral:

$$\int_{\partial V} \tau^{ki}(x, t) n_k da, \tag{2.10}$$

where τ^{ki} are the components of the stress tensor[1].

The momentum produced by the external volume forces can be formulated as:

$$\int_V \rho g^i dV. \tag{2.11}$$

1. It is common to divide the stress tensor into a part characterizing scalar pressure and a part characterizing dissipative stress in fluid mechanics. See (2.32).

If we substitute (2.9), (2.10) and (2.11) into the equation for the balance of general quantity (2.1), we get the momentum balance in the spatial coordinates in the form:

$$\frac{\partial(\rho v^i)}{\partial t} + \frac{\partial(\rho v^i v^k)}{\partial x^k} - \frac{\partial \tau^{ki}}{\partial x^k} - \rho g^i = 0. \tag{2.12}$$

2.1.4 Balance of mechanical energy

The balance equation for mechanical energy will be derived from the inner product of the momentum balance (2.12) and the velocity vector v_i with the use of the balance of mass (2.7). The form of the quantity for the balance of mechanical energy in the spatial coordinates can be formulated as:

$$\frac{\partial}{\partial t}\left(\rho \frac{v^i v_i}{2}\right) + \frac{\partial}{\partial x^k}\left(\rho v^k \frac{v^i v_i}{2}\right) - \frac{\partial \tau^{ki}}{\partial x^k} v_i - \rho g^i v_i = 0 \tag{2.13}$$

Let us also mention the equation for mechanical energy for the whole body

$$\int_V \rho \frac{\overset{\cdot}{\overline{v^i v_i}}}{2} dV - \int_{\partial V} \tau^{ki} v_i da_k - \int_V \left(\rho g^i - \tau^{ki} \frac{\partial v_i}{\partial x^k}\right) dv = 0 \tag{2.14}$$

2.1.5 Balance of total energy

Total energy of a body can be obtained as a sum of mechanical energy (2.13) and internal energy of the body

$$\int_V \rho \left[\frac{v^i v_i}{2} + u\right] dV \tag{2.15}$$

The total energy flux through the boundary of a system ∂V can be formulated as:

$$\int_{\partial V} (\tau^{ki} v_i - q^k) da_k, \tag{2.16}$$

where q^k is the heat flux in the spatial coordinates.

The total production of energy in a body

$$\int_V (\rho f^i v_i + \tilde{q}) dV \tag{2.17}$$

is a sum of the energy source $\rho g^{i} v_i$ caused by the external volume forces (balance of mechanical energy) and the external heat flux $\tilde{q}$ which can be, for example, radiation.

Balance of the total energy in the spatial coordinates can be formulated as

$$\overline{\int_V \rho\left(\frac{v^i v_i}{2} + u\right) dv} - \int_{\partial V} (\tau^{ki} v_i - q^k) da_k - \int_V \rho(g^{i} v_i + \tilde{q}) dV = 0 \tag{2.18}$$

$$\frac{\partial}{\partial t}\left[\rho\left(\frac{v^i v_i}{2} + u\right)\right] + \frac{\partial}{\partial x^k}\left[\rho v^k\left(\frac{v^i v_i}{2} + u\right) - \tau^{ki} v_i + q^k\right] - \rho g^{i} v_i - \tilde{q} = 0 \tag{2.19}$$

Balance of internal energy: By subtracting the relations (2.14) and (2.19) we get the relation for the balance of internal energy. This relation is the First Law of Thermodynamics:

$$\frac{\partial(\rho u)}{\partial t} + \frac{\partial(\rho v^k u)}{\partial x^k} + \frac{\partial q^k}{\partial x^k} - \tau^{ki}\frac{\partial v_i}{\partial x^k} - \tilde{q} = 0 \tag{2.20}$$

2.1.6 Balance of entropy

The entropy was formulated by the Clausius inequality in the form:

$$\frac{dQ}{T} \leq dS. \tag{2.21}$$

The total entropy of the system can be defined as:

$$S = \int_V \rho(x,t) s(x,t) dV \tag{2.22}$$

where s is the specific entropy. The Clausius inequality for the whole system can be written in the form:

$$\overline{\int_V \rho s dV} \geq -\int_{\partial V} \frac{q^k}{T} da_k + \int_V \frac{\tilde{q}}{T} dV \tag{2.23}$$

The total production of entropy can be defined as follows:

$$\sigma(S) = \rho\dot{s} + \frac{\partial}{\partial x^k}\left(\frac{q^k}{T}\right) - \frac{\tilde{q}}{T} \geq 0 \tag{2.24}$$

If we use the balance of internal energy (2.20) we can transform the equation (2.24) into the so called fundamental thermodynamic inequality:

$$\pi = T\sigma(S) = \rho(T\dot{s} - \dot{u}) - \frac{\partial}{\partial x^k}\left(\frac{q^k}{T}\right) + \tau^{ki}\frac{\partial v_i}{\partial x^k} \geq 0 \tag{2.25}$$

This inequality will be used to derive the constitutive relations and mainly the thermodynamic criterion of stability.

2.1.7 Constitutive relations for thermo-viscid fluid

The basic equations to solve velocity, pressure and temperature fields in a thermo-viscid fluid flow are the momentum balance equation (2.12), mass balance equation (2.17) (so called continuity equation), energy balance equation (2.19) and entropy balance equation (2.25). There are 22 unknown quantities (x^i, T, ρ, u, s, q^i, v^i, τ^{ij}) in these 9 equations and one inequality. It is clear that it is necessary to define 22-9=13 unknown functions and to satisfy generally valid requirements known as axioms of the constitutive theory[1].

The aim is to find 11 constrains. We can generally set up constitutive relations of the thermo-viscid fluid for free energy[2] (instead of internal energy), entropy, heat flow and stress tensor (owing to the symmetry, the stress tensor includes only six unknown quantities).

$$f = f\left(\rho, d_{ij}, T, \frac{\partial T}{\partial x^i}\right) \tag{2.26}$$

$$s = s\left(\rho, d_{ij}, T, \frac{\partial T}{\partial x^i}\right) \tag{2.27}$$

$$q^i = q^i\left(\rho, d_{ij}, T, \frac{\partial T}{\partial x^i}\right) \tag{2.28}$$

$$\tau^{ij} = \tau^{ij}\left(\rho, d_{ij}, T, \frac{\partial T}{\partial x^i}\right) \tag{2.29}$$

By substituting the constitutive relations (2.26)-(2.29) into the equation (2.25) we get the expression for the condition of time irreversibility[3] in the form:

---

1. The Basic axioms of constitutive theory are: 1. axiom of causality, 2. axiom of determinism, 3. axiom of equipresence, 4. axiom of objectivity, 5. axiom of material invariance, 6. axiom of surroundings, 7. axiom of memory, 8. axiom of time irreversibility, 9. axiom of maximum probability. The results of each axiom and its use when deriving constitutive relations are mentioned, for example, in Maršík[26]
2. Free energy $f(x, t) = u - Ts$

$$\pi = -\rho\left(\frac{\partial f}{\partial T} + s\right)\dot{T} + \left(\tau^{ki}{}_{el} + \tau^{ki}{}_{dis} + \rho^2\frac{\partial f}{\partial \rho}\delta^{ki}\right)d_{ki} \tag{2.30}$$

$$-\frac{q^k}{T}\frac{\partial T}{\partial x^k} - \rho\frac{\partial f}{\partial\left(\frac{\partial T}{\partial x^k}\right)}\left(\frac{\dot{\partial T}}{\partial x^k}\right) - \rho\frac{\partial f}{\partial d_{ki}}\dot{d}_{ki} \geq 0$$

where d_{ki} is the tensor of the strain rate. The stress tensor was divided into the elastic part τ_{el} and the dissipative part τ_{dis}.

An isotropic model of fluid which is called the Newton fluid describes exactly enough fluids considered by us. The heat flux and the stress tensor are described by linear equations in this model:

$$q^i = -\lambda(\rho, T)\delta^{ij}\frac{\partial T}{\partial x^j} \tag{2.31}$$

$$\tau^{ij} = -p(\rho, T)\delta^{ij} + \tau^{ij}{}_{dis} \tag{2.32}$$

where $\tau^{ij}{}_{dis}$ is the dissipative part of the stress tensor and for the Newton fluid it can be formulated as:

$$\tau^{ij}{}_{dis} = \mu_v(\rho, T)d_{(1)}\delta^{ij} + 2\mu(\rho, T)d^{kl} \tag{2.33}$$

where $d_{(1)}$ is the first invariant of the tensor of the strain rate, μ_v is the volume viscosity and η is the shear viscosity. With respect to the continuity equation for the incompressible fluid ($d_{(1)} = \frac{\partial v^i}{\partial x_i} = 0$) and the dissipative part of the stress tensor, (2.33) can be written in the form:

$$\tau^{ij}{}_{diss} = 2\mu(\rho, T)d^{kl} \tag{2.34}$$

---

3. The tensor of velocity gradient $\partial v_i/\partial x_j$ was in the derivation replaced by the sum of the symmetric tensor d_{ij} (tensor of strain rate) and the anti-symmetric tensor w_{ij} (spin tensor). The inner product of the tensor w and the stress tensor equals zero. For the small strain: $\dot{e}_{ij} \approx d_{ij}$ is valid.

2.2 Stability of a boundary layer

The basis of most theses dealing with stability and loss of stability of a laminar boundary layer is the idea that laminar fluid flow is exposed to the effect of small disturbances. They can be either disturbances resulting from the initial state of flow, or disturbances resulting from the effect of circumfluous surface (roughness and friction on the wall) or from the effect of shear layers (non-uniformity of external velocity field).

The aim of the theoretical investigation of the boundary layer with regard to its stability is to observe the time development of small disturbances, which are superimposed to the main fluid flow. If these disturbances damp in the course of time, it is possible to consider the flow as stable. On the contrary, intensifying disturbances lead to a destabilization of flow and to the transition of flow into another steady form. As an example we can mention the development of Kármán vortex street or transition to turbulence. This simplified formulation presents the basic idea of the theory of a stability of boundary layer that can lead as its consequence, to the determination of the critical Reynolds number from the known velocity profile.

2.2.1 History

The first important thesis dealing with studying hydrodynamic stability can be found in the work of Helmholtz (1868) (the development of so called Kelvin-Helmholtz vortices is shown in Fig.2.2). Previous authors were aware of the fact that the phenomenon of the loss of stability exists, but their theses did not mostly go beyond the scope of a description of the problem. It is worth mentioning here the sketches of eddies by Leonardo da Vinci (15th century- Fig.2.1) and the experiments by Hagen (1855).

Fig.2.1 In an early study of turbulence Leonardo da Vinci wrote "Observe the motion of the surface of the water, which resembles that of hair, which has two motions, of which one is caused by the weight of the hair, the other by the direction of the curls; thus the water has eddying motions, one part of which is due to the principal current, the other to random and reverse motion." (After Lumley, J.L., 1997. Phys. Fluids A, 4, 203)

O. Reynolds (Fig.2.3 and Fig.2.4) laid the foundations for studying the loss of stability and transition to turbulence. He proceeded from an assumption that laminar flow presents solution of differential equations in hydrodynamics. After crossing a certain limit which is determined by the magnitude of the critical Reynolds number the flow is getting unstable and it changes into turbulent flow.

Lord Rayleigh was occupied by the problems of transition at the same time as O. Reynolds was. His first theory, inspired by flame stability of the gas burner, dealt with the flow stability from the nozzle. Besides that, the most

known piece of knowledge from his work is the information about the existence of the point of inflexion of velocity profile which affects the stability and some knowledge of flow stability between rotating cylinders. In the course of development it was getting clearer that to explain the presence of the critical Reynolds number and its theoretical calculation is not a trivial problem. On the contrary, the real knowledge led to a necessity to include both the second-order derivation of the velocity profile and the effect of viscosity into the analysis.

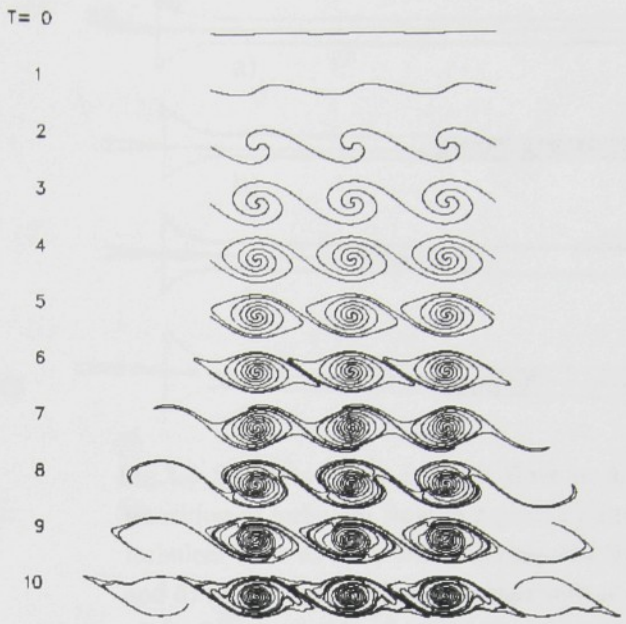

Fig.2.2 A flat vortex sheet of constant strength separates two streams of fluid moving in opposite directions. When the sheet is given a small perturbation, it rolls up into a periodic array of spiral vortices (from www.math.lsa.umich.edu/~krasny/k-h.html)

The equation derived independently by Orr and Sommerfeld in 1907 and 1908 was considered as the basic equation for solving the problem of the loss of stability for a long time. At the time of its derivation this equation get aroused optimism and it was considered as the way of answering finally the questions to the problems of turbulence. But it soon turned out that the equation is successfully solvable only in special cases and so the Orr-Sommerfeld equation remained unsolved for a long time. Only in 1929 Tollmien published the first calculations of the critical *Re* obtained through the analysis of the Orr-Sommerfeld equation.

Only in the 30's of the last century the team around L.Prandtl succeeded in solving the problem of theoretical determination of the critical *Re*. Prandtl's results were confirmed later by way of experiment, even though there were some qualitative differences in the value of the critical Reynolds number.

Together with the linearized Orr-Sommerfeld theory, the non-linear theory (Synge, 1936), also began to develop. It should have eliminated evident faults of the linearized theory. Only the beginnings of numerical solution methods of differential equations and the development of computer technology enabled rational solution of the problems of stability. Even though some solutions have appeared on the basis of direct solution of the Navier-Stokes equation in the last 20 years, the classical Orr-Sommerfeld equation remains one of the basic points in the contemporary interpretation of the theory of turbulence.

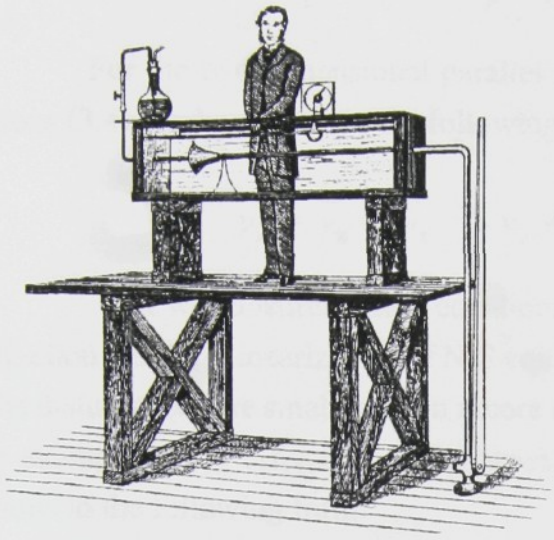

Fig.2.3 The configuration of Reynolds experiment on flow along a pipe (1883)

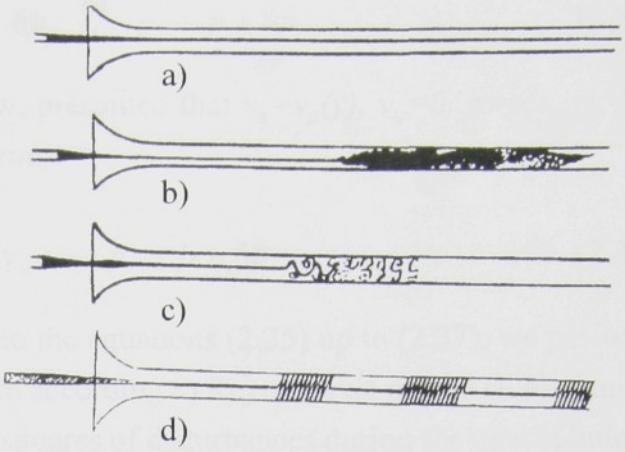

Fig.2.4 Sketches of a) laminar flow in a pipe; b) transition to turbulent flow in a pipe; c) transition to turbulent flow as seen when illuminated by a spark and d) flashes which show the intermittent character of the flow caused by the disturbances - experiments by Reynolds (Both after Cheng[5])

2.2.2 Basis of the "Small disturbance method"

This part of the thesis describes briefly the way of treating the flow stability by the method of small disturbances. Even though the other part of the thesis deals with the fluid flow along the curved wall, the basic description will be performed on an example of two-dimensional flow in carthesian coordinates and the required equations will be transformed into cylindrical coordinates in the following chapters.

The basic equations, that means the equation of continuity and the balance of momentum, for the two-dimensional laminar flow can be written in the following forms:

$$\frac{\partial v_x}{\partial x} + \frac{\partial v_y}{\partial y} = 0 \tag{2.35}$$

$$\frac{\partial v_x}{\partial t} + v_x \frac{\partial v_x}{\partial x} + v_y \frac{\partial v_x}{\partial y} = -\frac{1}{\rho}\frac{\partial p}{\partial x} + \nu\left(\frac{\partial^2 v_x}{\partial x^2} + \frac{\partial^2 v_x}{\partial y^2}\right) \tag{2.36}$$

$$\frac{\partial v_y}{\partial t} + v_x \frac{\partial v_y}{\partial x} + v_y \frac{\partial v_y}{\partial y} = -\frac{1}{\rho}\frac{\partial p}{\partial y} + \nu\left(\frac{\partial^2 v_y}{\partial x^2} + \frac{\partial^2 v_y}{\partial y^2}\right) \tag{2.37}$$

Pressure and velocity components (v_x, v_y and p) can be divided into components representing the average values of laminar flow ($\bar{v}_x$, $\bar{v}_y$ and $\bar{p}$) and into fluctuating components (δv_x, δv_y and δp). So we can write:

$$v_x = \bar{v}_x + \delta v_x \qquad v_y = \bar{v}_y + \delta v_y \qquad p = \bar{p} + \delta p \tag{2.38}$$

For the two-dimensional parallel flow, presumed that $v_x=v_x(y)$, $v_y=0$, $p=p(x, y)$, the equations (3.4) can be written in the following form:

$$v_x = \bar{v}_x + \delta v_x \qquad v_y = \delta v_y \qquad p = \bar{p} + \delta p \tag{2.39}$$

If we substitute these equations into the equations (2.35) up to (2.37), we perform linearization (see e.g. linearization of N-S equation according to Reynolds on page 37). Presumed that the disturbances are small, we can ignore the squares of disturbances during the next solution, as for example $(\delta v_x)^2$, $\delta v_x \delta v_y$. After necessary arrangements we get a system of differential equations in the following form:

$$\frac{\partial \delta v_x}{\partial x} + \frac{\partial \delta v_y}{\partial y} = 0 \tag{2.40}$$

$$\frac{\partial \delta v_x}{\partial t} + v_x \frac{\partial \delta v_x}{\partial x} + \delta v_y \frac{\partial v_x}{\partial y} = -\frac{1}{\rho}\frac{\partial \delta p}{\partial x} + \nu\left(\frac{\partial^2 \delta v_x}{\partial x^2} + \frac{\partial^2 \delta v_x}{\partial y^2}\right) \tag{2.41}$$

$$\frac{\partial \delta v_y}{\partial t} + v_x \frac{\partial \delta v_y}{\partial x} = -\frac{1}{\rho}\frac{\partial \delta p}{\partial y} + \nu\left(\frac{\partial^2 \delta v_y}{\partial x^2} + \frac{\partial^2 \delta v_y}{\partial y^2}\right) \tag{2.42}$$

If we apply an operator *rot* into equations (2.41) and (2.42) we can eliminate the terms with pressure gradient. Using the equation of continuity we introduce the relation for flow function of disturbance that is possible to formulate in the form of travelling wave with the amplitude $\delta\hat{v}_y$:

$$\delta v_y = \delta \hat{v}_y e^{ik(x-ct)}, \tag{2.43}$$

where k is wave number and c is phase velocity (complex number $c = c_r + i.Im(c)$). We get a differential equation for the disturbance amplitude in the form:

$$(v_x - c)\left(\frac{d^2 \delta \hat{v}_y}{dy^2} - k^2 \delta \hat{v}_y\right) - \frac{\partial^2 v_x}{\partial y^2}\delta \hat{v}_y + \frac{i\nu}{k}\left(\frac{d^4 \delta \hat{v}_y}{dy^4} - 2k^2 \frac{d^2 \delta \hat{v}_y}{dy^2} + k^4 \delta \hat{v}_y\right) = 0. \tag{2.44}$$

Applying non-dimensional quantities

$$\tilde{\eta} = \frac{y}{\delta^*}, \tilde{v} = \frac{v_x}{v_e}, \tilde{Re} = \frac{v_e \delta^*}{\nu}, \tilde{k} = k\delta^*, \gamma = \frac{c}{v_c}, \tilde{\delta v} = \frac{\delta v_y}{v_e \delta^*}, \tag{2.45}$$

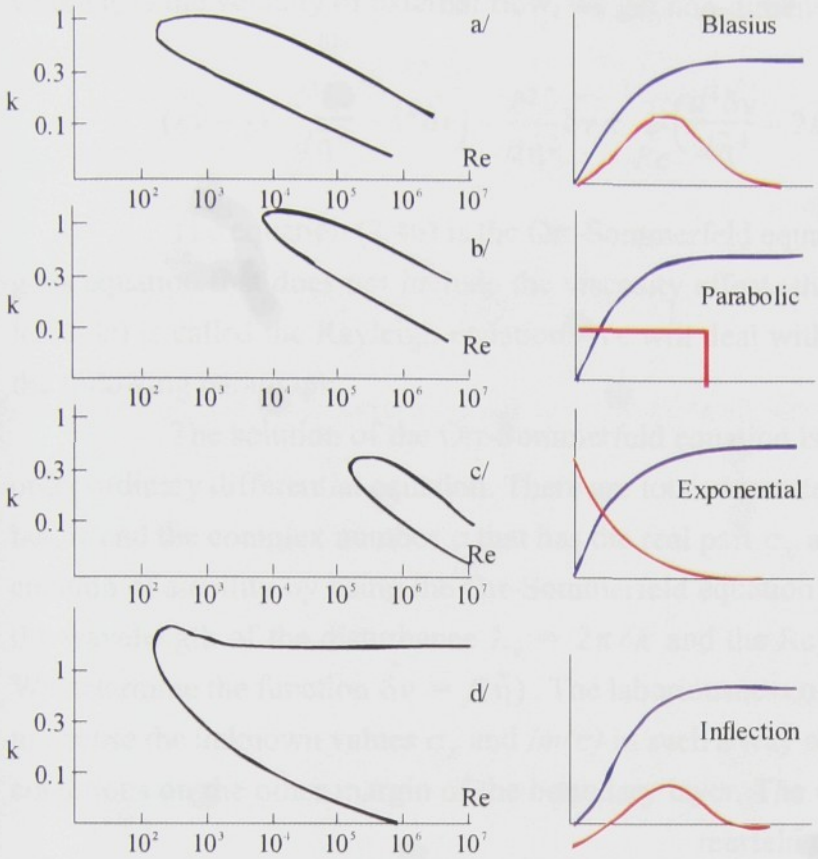

Fig.2.5 Stability (neutral curves) of various profiles. Red lines show the second derivation of the velocity profile. a/ corresponds to Blasius, b/ parabolic c/ exponential d/ profile with inflec-tion. The exponential velocity profile is encountered in the flow over a porous plate, when there is a continuous suction of the fluid through the plate. Because the curvature of the mean profile is concentrated near the wall, we can see that the oscillations occur at high Reynolds numbers and therefore the suction has a stabilizing effect. (After Betchov[3])

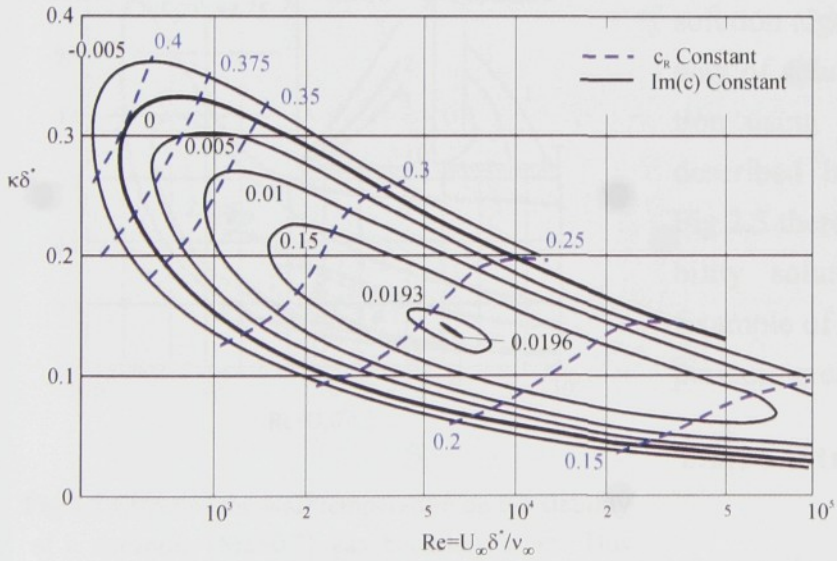

Fig.2.6 Eigenvalues for the Blasius boundary layer (After Betchov[3]). δ^* is displacement thickness

where v_e is the velocity of external flow, we get non-dimensional form of equation (2.44)

$$(\tilde{k}\tilde{v}-\gamma)\left(\frac{d^2\tilde{\delta v}}{d\tilde{\eta}^2}-\tilde{k}^2\tilde{\delta v}\right)-\frac{\partial^2\tilde{v}}{\partial\tilde{\eta}^2}\tilde{\delta v}+\frac{i}{\tilde{Re}}\left(\frac{d^4\tilde{\delta v}}{d\tilde{\eta}^4}-2\tilde{k}^2\frac{d^2\tilde{\delta v}}{d\tilde{\eta}^2}+\tilde{k}^4\tilde{\delta v}\right)=0 \qquad (2.46)$$

The equation (2.46) is the Orr-Sommerfeld equation we have searched for. The analogous equation that does not include the viscosity effect (that means without the last term on the left side) is called the Rayleigh equation. We will deal with the analysis of Rayleigh equation in the following paragraph.

The solution of the Orr-Sommerfeld equation is the question of solution of the fourth order ordinary differential equation. There are four parameters in the equation, the Reynolds number, α and the complex number c that has the real part c_r and the imaginary part $Im(c)$. The calculation of stability by using the Orr-Sommerfeld equation proceeds as follows - first we choose the wavelength of the disturbance $\lambda_v = 2\pi/k$ and the Reynolds number of the basic flow $\tilde{Re}$. We determine the function $\tilde{\delta v} = f(\tilde{\eta})$. The laboriousness of the solution is based on the necessity to choose the unknown values c_r and $Im(c)$ in such a way so that the solution meets the boundary conditions on the other margin of the boundary layer. The examples of solution of the Orr-Sommerfeld equation for different velocity profiles are presented in Betchov[3], where even some solution algorithms are described. The modern way of solution of the Orr-Sommerfeld equation using the Chebishev transformation is described in Zebib[59]. In the Fig.2.6 and Fig.2.5 there are shown some examples of stability solution of some velocity profiles. Example of stability curves for flow with temperature gradient are presented in Fig.2.7.

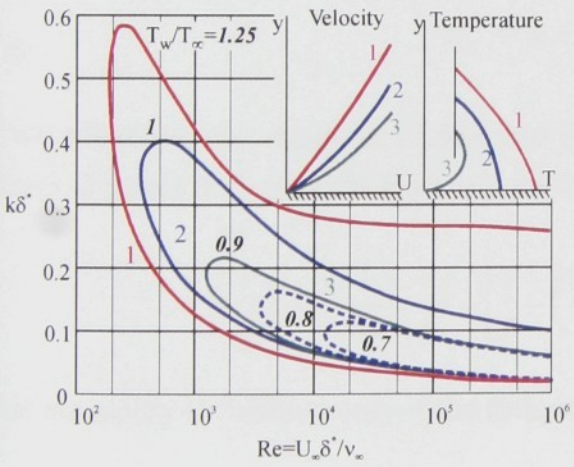

Fig.2.7 Effect of the wall temperature on the stability of a subsonic (Ma=0.7) gas boundary layer. This shows that the gas-flow boundary layer can be destabilized by heating the wall. This example is only in evident discrepancy with the main idea of this thesis which tries to show stabilizing effect of heating the wall. The explanation is directly derived from the equation (2.64). (After White[51])

2.2.3 Stability criterion

As mentioned above, it is possible to describe the state of the system by means of temperature and velocity fields (density is a function of temperature and pressure). It is possible to consider the dependence of all important variables on the spatial coordinates

and on time as steady if a small change of initial conditions in time t_0 initiates a small change of observed variables in time $t>t_0$.

The derivation of the below mentioned thermodynamic stability condition is based on Ljapunov theory of stability, its mathematical formulation is given in Maršík[26]. Here will be given only an idea how to derive the thermodynamic stability criterion of thermoviscous fluid with convection and the reasonable connection of this criterion with before published stability criteria (Rayleigh, Fjörtoft) published before will be shown.

To derive the stability criterion of flowing thermoviscous fluid we use the fundamental thermodynamic inequality (2.25) completed with the balance of kinetic energy and with the relation for stress tensor for thermoviscous fluid (2.32). So we get the equation in the following form:

$$\pi = \rho\left[T\dot{s} + \frac{1}{\rho}\frac{\partial p}{\partial t} - \overline{\left(\frac{|v_i|^2}{2} + u + \frac{p}{\rho} + \phi\right)}^{\cdot} \right] - \frac{q^k}{T}\frac{\partial T}{\partial x^k} + \frac{\partial \tau_{dis}^{ki}}{\partial x^k} v_i + \tau_{dis}^{ki}\frac{\partial v_i}{\partial x^k} \geq 0 \tag{2.47}$$

where ϕ is the potential function of body forces. The total specific energy can be defined as follows:

$$h_c = u + \frac{p}{\rho} + \frac{|v_i|^2}{2} + \phi \tag{2.48}$$

If we substitute the equation (2.48) into the equation (2.47), presumed that the total specific energy depends only on enthalpy s and on the pressure p, we get the following inequality:

$$\pi = \rho\left[T - \left(\frac{\partial h_c}{\partial s}\right)_p \right]\dot{s} - \left[\frac{1}{\rho} - \left(\frac{\partial h_c}{\partial s}\right)_s \right]\frac{\partial p}{\partial t} - \frac{q^k}{T}\frac{\partial T}{\partial x^k} + \frac{\partial(\tau_{dis}^{ki} v_i)}{\partial x^k} \geq 0 \tag{2.49}$$

This inequality is fulfilled only if the following equations are valid:

$$T = \left(\frac{\partial h_c}{\partial s}\right)_p, \quad \frac{1}{\rho} = \left(\frac{\partial h_c}{\partial s}\right)_s, \tag{2.50}$$

$$\tilde{\pi} = \frac{q^k}{T}\frac{\partial T}{\partial x^k} + \frac{\partial(\tau_{dis}^{ki} v_i)}{\partial x^k} \geq 0 \tag{2.51}$$

The total specific energy can be written then as follows:

$$\dot{h}_c = T\dot{s} + \frac{1}{\rho}\frac{\partial p}{\partial t} \tag{2.52}$$

If the deviations δh_c, δp , δs from the reference state of system $h_{0c} = T_0\dot{s} + \frac{1}{\rho_0}\frac{\partial p}{\partial t}$ fulfill the following inequality

$$T_0\dot{s} + \frac{1}{\rho_0}\frac{\partial p}{\partial t} - \dot{h}_c = T_0(\dot{s}_0 + \dot{\overline{\delta s}}) + \frac{1}{\rho_0}\left(\frac{\partial p_0}{\partial t} + \frac{\partial \delta p}{\partial t}\right) - \left\{h_{0c} + \left(\frac{\partial h_{0c}}{\partial s}\right)_0 \dot{\overline{\delta s}} + \left(\frac{\partial h_c}{\partial p}\right)_0 \frac{\partial \delta p}{\partial t}\right. \tag{2.53}$$

$$\left. + \left[\frac{1}{2}\left(\frac{\partial^2 h_c}{\partial s^2}\right)_0 \dot{\overline{(\delta s)^2}} + 2\left(\frac{\partial^2 h_c}{\partial s \partial p}\right)_0 \dot{\overline{\delta s \delta p}} + \left(\frac{\partial^2 h_c}{\partial p^2}\right)_0 \frac{\partial (\delta p)^2}{\partial t}\right]\right\} \geq 0$$

then we can write the thermodynamic stability condition of processes in fluids with convection in the following form:

$$\frac{\rho_0}{2}\left[\frac{T}{c_p}\dot{\overline{(\delta s)^2}} + 2\left(\frac{\partial T}{\partial p}\right)_s \dot{\overline{\delta s \delta p}} + \left(\frac{\partial\left(\frac{1}{\rho}\right)}{\partial p}\right)_s \frac{\partial (\delta p)^2}{\partial t}\right] = -\tilde{\pi} \leq 0 \tag{2.54}$$

The term in the brace formulates the second differential of total specific energy.

Introducing the velocity of sound $c_s = (\partial p / \partial \rho)_s^{1/2}$, using the definition of entropy for the calculation of entropy fluctuation $\delta s = \frac{c_p}{T}\delta T + \frac{1}{T}\left[\left(\frac{\partial h}{\partial p}\right)_T - \frac{1}{\rho}\right]\delta p$ and applying the partial derivative $\left(\frac{\partial T}{\partial p}\right)_s = -\frac{1}{c_p}\left(\frac{\partial h}{\partial p} - \frac{1}{\rho}\right)$ we get the thermodynamic criterion of stability for the processes in the fluid with convection:

$$\frac{\rho}{2}\dot{\overline{d^2 h_c}} = \frac{\rho}{2}\left[\frac{c_p}{T}\dot{\overline{(\delta T)^2}} - \frac{1}{\rho^2 c_p^2}\frac{\partial (\delta p)^2}{\partial t}\right] = -\tilde{\pi} \leq 0 \tag{2.55}$$

If we substitute the constitutive relations (2.31) and (2.32) into the equation (2.51) and presumed that there is the two-dimensional flow near the wall for which we can suppose the following simplifications:

$$v_x << v_y, \quad \left|\frac{\partial v_x}{\partial x}\right| << \left|\frac{\partial v_y}{\partial x}\right|, \quad \left|\frac{\partial v_y}{\partial y}\right| << \left|\frac{\partial v_x}{\partial y}\right|, \quad \left|\frac{\partial T}{\partial x}\right| << \left|\frac{\partial T}{\partial y}\right|. \tag{2.56}$$

The thermodynamic stability criterion (2.55) gets after the substitution and after all the arrangements a simpler form:

$$-\frac{\rho_0}{2}\dot{\overline{d^2h_c}} = \frac{\lambda}{T}\left(\frac{\partial T}{\partial y}\right)^2 + \mu\left(\frac{\partial v_x}{\partial y}\right)^2 + \mu v_x\left[\frac{d\ln\mu}{dT}\frac{\partial T}{\partial y}\frac{\partial v_x}{\partial y} + \frac{\partial^2 v_x}{\partial (y)^2}\right] = \tilde{\pi} \geq 0 \qquad (2.57)$$

The following paragraph deals with the analysis of in this way formulated thermodynamic stability criterion.

The first and the second term in the equation (2.57), taking into consideration the positive values of transport coefficients λ and μ - are bigger or they equal zero. The last term plays the crucial role in stability of boundary layer. The existence of steady laminar layer is obvious from the equation, because for $v_x \to 0$ the last term is always smaller than the first two terms. The term $\partial^2 v_x / \partial (y)^2$ can take either positive or negative values and even higher order values than the magnitudes of other terms. Even for isothermal flow this term is responsible for the instability of boundary layer.

In non-isothermal flow, magnitudes of other terms must be taken into consideration. If the gas flow along the wall are being cooled off ($\partial T / \partial y > 0$), and presumed that $d\mu / dT > 0$, the first term in the brackets is positive and the thermal gradient leads in this case to the stabilization of the flow. The case of a heated wall should by analogy lead to destabilization of the boundary layer. But the problem is more complicated and a detailed analysis is necessary.

Destabilization effect of heating the wall is probably valid only for high flow velocities. Analyzing the particular case we can find, at least approximately, the relation between the flow velocity and intensity of the thermal gradient (the wall heating).

Let us suppose the viscosity temperature dependence on the temperature in the following form:

$$\mu = \mu_0\left(\frac{T}{T_0}\right)^{\omega} \quad ; \quad \omega = 0.7774 \text{ (for air according to Hilsenrath[15])} \qquad (2.58)$$

Arranging the stability condition (2.55):

$$\frac{\lambda}{T}\left(\frac{\partial T}{\partial y}\right)^2\left[1 + \frac{\omega\mu v_x}{\lambda}\frac{\partial y}{\partial T}\frac{\partial v_x}{\partial y}\right] + d^2h_c\big|_{isoterm} \geq 0 \qquad (2.59)$$

we derived the influence of the thermal gradient from the isothermal shear layer. The second term

$$d^2h_c\big|_{isoterm} = \mu\left(\frac{\partial v_x}{\partial y}\right)^2 + \mu v_x\frac{\partial^2 v_x}{\partial (y)^2} \geq 0 \qquad (2.60)$$

is exactly the thermodynamic stability condition only for an isothermal shear layer. If we substitute the derivatives by differences,

$$\frac{\partial v_x}{\partial y} = \frac{\Delta v_x}{\delta_{BL}}; \quad \frac{\partial T}{\partial y} = \frac{\Delta T}{\delta_{TBL}}; \quad \Delta v_x = v_{x0} - 0; \quad \Delta T = T_0 - T_w \tag{2.61}$$

and if we presume that

$$\frac{\delta_{TBL}}{\delta_{BL}} \cong 1.026 Pr^{-1/3} \cong Pr^{-1/3}, \text{ see Schlichting[34]} \tag{2.62}$$

we can arrange the first term in the relation (2.59) as follows

$$1 + \frac{\omega \mu v_x}{\lambda} \frac{\delta_{TBL}}{\delta_{BL}} \frac{\partial v_x}{\Delta T} \cong 1 + \frac{\omega Pr^{2/3} (v_{x0})^2}{c_p \Delta T} > 0 \tag{2.63}$$

δ_{BL} and δ_{TBL} are convectional thicknesses of velocity and thermal boundary layers respectively. At the heated wall there is $\Delta T < 0$ and the shear layer is stabilized if the following inequality is fulfilled

$$-\frac{c_p \Delta T}{(v_{x0})^2/2} = \frac{c_p (T_w - T_0)}{(v_{x0})^2/2} > 2\omega Pr^{2/3} = 2 \cdot 0.78 \cdot 0.80 = 1.25 \tag{2.64}$$

For the air it is valid: $c_p \cong 1000\ \mathrm{Jkg^{-1}K^{-1}}$ and low velocity $v_{x0} \approx 10^0 \div 10^1$. This condition is already fulfilled at very small temperature differences. The results published in this thesis show the correctness of this simplified relation. We come across the stabilizing effect of heating the wall in a curved wall jet published here as well. Another typical example of a stabilizing effect of the positive temperature gradient in the case of gas-flow is a laminar vortex shedding behind a heated cylinder (see Wang[49]). We must take into consideration that the experiments mentioned above are carried out for a low velocity. On the other hand, destabilization of a boundary layer occurs for high velocities (or for extremely low temperature gradients) (Fig.2.7).

The stability criterion for isothermal flow like the Rayleigh and Fjörtoft criteria can be derived from the thermodynamic stability condition (2.60). The Rayleigh criterion is based on the Orr-Sommerfeld equation (2.44) for inviscid flow in the form of so called Rayleigh equation:

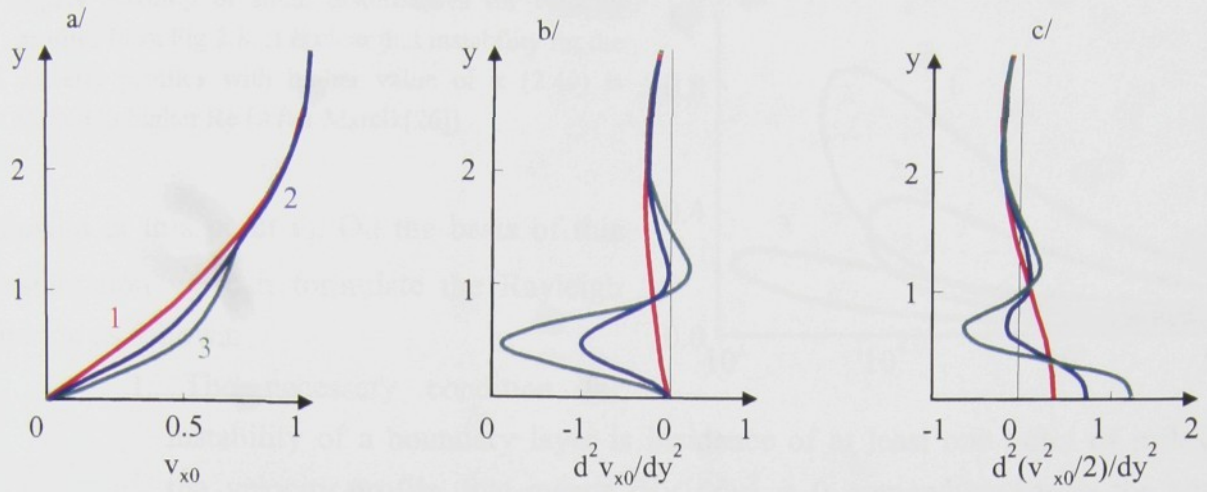

Fig.2.8 a/ Velocity profiles. 1-Pohlhausen velocity profile $v_{x0}=2(y/\delta)-2(y/\delta)^3+(y/\delta)^4$; 2, 3 - Velocity profiles 1 with disturbances; b/ Curves of Rayleigh criterion of stability; c/ curves of thermodynamic criterion of stability of processes. (After Maršík[26])

c/

$$(v_x - c)\left(\frac{d^2\delta\hat{v}_y}{dy^2} - k^2\delta\hat{v}_y\right) - \frac{\partial^2 v_x}{\partial y^2}\delta\hat{v}_y = 0 \qquad (2.65)$$

This equation can be arranged by multiplying the complex conjugated functions $\delta\hat{v}^*_y$ to the function of the amplitude disturbance $\delta\hat{v}_y$. If we take into consideration the boundary conditions for disturbance amplitude function:

$$\delta\hat{v}_y\Big|_{y=0} = \delta\hat{v}_y\Big|_{y=\infty} = 0 \qquad (2.66)$$

and if we perform the integration of equation (2.65), we get:

$$-\int_{y0}^{y1}\left(\left|\delta\hat{v}_y\right|^2 + k^2\left|\delta\hat{v}_y\right|^2\right)dy = \int_{y0}^{y1}(v_x - c_r)\frac{\partial^2 v_x}{\partial y^2}\frac{\left|\delta\hat{v}_y\right|^2}{\left|v_x - c\right|^2}dy < 0, \quad \text{for real part} \qquad (2.67)$$

$$iIm(c)\int_{y0}^{y1}\frac{\partial^2 v_x}{\partial y^2}\frac{\left|\delta\hat{v}_y\right|^2}{\left|v_x - c\right|^2}dy = 0, \quad \text{for imaginary part} \qquad (2.68)$$

This inequality is valid both for amplified and for damped disturbances only if $Im(c) \neq 0$. To fulfill the equation (2.67) for imaginary part the condition: $\frac{\partial^2 v_x}{\partial y^2} = 0$ must be fulfilled at some point y_I of velocity profile. That means that the velocity profile has the point of

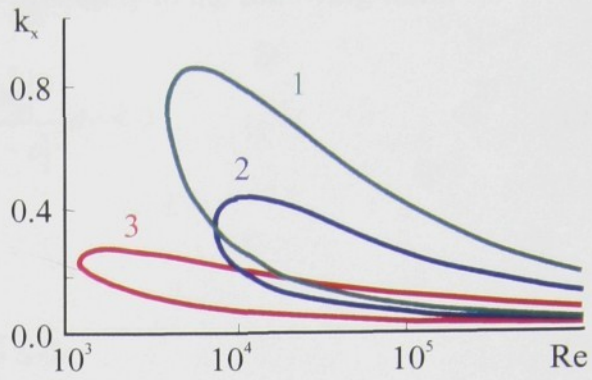

Fig.2.9 Stability of small disturbances for velocity profiles from Fig.2.8. It is clear that instability for the velocity profiles with higher value of π (2.49) is shifted to higher Re (After Maršík[26])

inflexion at this point y_I. On the basis of this consideration we can formulate the Rayleigh criterion as follows:

1. The necessary condition for instability of a boundary layer is incidence of at least one point of inflexion of the velocity profile, that means $\partial^2 v_x / \partial y^2 = 0$ somewhere inside the boundary layer.
2. The sufficient condition for stability of the boundary layer is the absence of the point of inflexion, that means $\partial^2 v_x / \partial y^2 \neq 0$ somewhere inside the boundary layer.

The extension of the Rayleigh criterion is the Fjörtoft theorem. The velocity at the point of inflexion is $v_1(y_I) = v_{1I}$ and imaginary part of the equation (2.67) can be written as:

$$(c_r - v_{xI}) \int_{y0}^{y1} \frac{\partial^2 v_x}{\partial y^2} \frac{|\delta \hat{v}_y|^2}{|v_x - c|^2} dy = 0 \qquad (2.69)$$

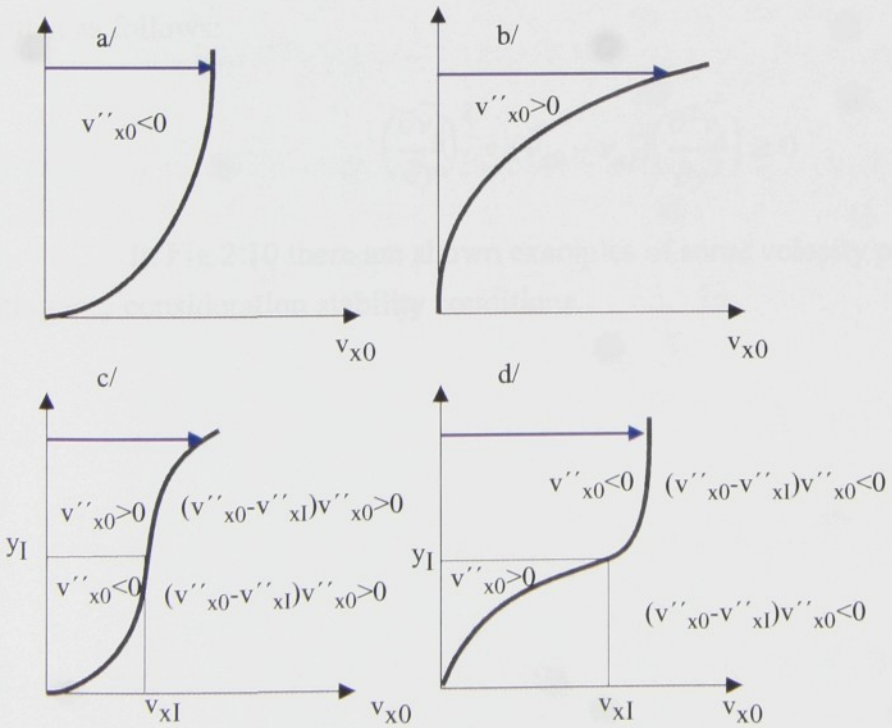

Fig.2.10 Classification of the velocity profiles. Typical examples of stable and unstable velocity profiles. a/ ,b/ velocity profiles stable according to the Rayleigh criterion c/ velocity profile with inflection; unstable by the Rayleigh criterion, stable according to Fjörtoft and thermodynamic criteria d/ velocity profile which can be unstable both according to the Rayleigh criterion and the Fjörtoft and thermodynamic criteria (After Maršík[25])

Adding the real part (2.67) we get the condition of instability in the following form:

$$\int_{y0}^{y1} (v_x - v_{xI}) \frac{\partial^2 v_x}{\partial y^2} \frac{\left|\delta \hat{v}_y\right|^2}{\left|v_x - c\right|^2} dy \leq 0 \tag{2.70}$$

This condition can be fulfilled only if it is valid:

$$(v_x - v_{xI}) \frac{\partial^2 v_x}{\partial y^2} \leq 0 \tag{2.71}$$

somewhere in the flow field:

The condition (2.71) is necessary for instability of the velocity flow field with the point of inflexion.

Remarkable is the comparison of (2.71) with the thermodynamic stability condition (2.60) for isothermal flow. Introducing the inequality

$$\left(\frac{\partial v_x}{\partial y}\right)^2 + v_x \left(\frac{\partial^2 v_x}{\partial y^2}\right) = \frac{\partial^2}{\partial y^2}\left(\frac{v_x^2}{2}\right) \tag{2.72}$$

it is obvious that the Rayleigh criterion directly results from the thermodynamic stability condition.

Analogously we get the Fjöerteft criterion when we substitute the transformed velocity by relation $\overline{v_x} = v_{x0} + v_{xI}$ into the equation (2.72). Then the condition for flow stability can be written as follows:

$$\left(\frac{\partial \overline{v_x}}{\partial y}\right)^2 + (\overline{v_{x0}} - v_{xI}) \left(\frac{\partial^2 \overline{v_x}}{\partial y^2}\right) \geq 0 \tag{2.73}$$

In Fig.2.10 there are shown examples of some velocity profiles and their classification taking into consideration stability conditions.

2.3 Basic concepts of turbulence theory

2.3.1 Reynolds equation

Flow of Newtonian fluid is described by Navier-Stokes Equation which we get when we substitute the constitutive relation (2.33) to the momentum balance equation (2.12). Navier-Stokes equation for flow of incompressible fluid can be written in the form:

$$\frac{\partial(\rho v^i)}{\partial t} + \frac{\partial(\rho v^i v^k)}{\partial x^k} + \frac{\partial p}{\partial x^k} + -\frac{\partial}{\partial x^k}\left(\mu\left(\frac{\delta v^i}{\delta x_k} + \frac{\delta v^k}{\delta x_i}\right)\right) - \rho g^i = 0 \tag{2.74}$$

The Navier-Stokes equation is valid for the motion of each particular element of fluid. If viscous stress in fluid dominates it leads to fast damping of small and fast flow fluctuations and the flow field can be defined on the basis of time averaged velocity of fluid. This type of flow is called the laminar flow. If the velocity of flow increases, the effect of inertial forces starts to grow and small disturbances, which were formerly damped by viscosity, start to increase. It leads to transition to turbulence. The Navier-Stokes equation can be generally used to analyze both laminar and turbulent flow (time scale for the smallest eddies is much longer then the period between the collisions of molecules). That is why it is possible to use equations (2.74) describing flow of a continuum for turbulent flow as well. Because of the much time consuming calculations it is possible to use the N-S equation only to solve the simple problems of turbulent flow. We come across three-dimensional, stochastic and unsteady flow with spectrum of scales ranging from the largest to the smallest velocity fluctuations. Solving turbulence flow, in most cases it is necessary to use methods which enable us to obtain at least the fluctuation distribution of time averaged values of observed variables.

One of the most developed methods is so called statistic approach that deals with the time averaged Navier-Stokes equation. The basic presumption is to calculate time averaged values of statistically steady flow described by Navier-Stokes equation. Each observed variable (v_i, p) can be divided into a mean value $\bar{v}_i$ and a fluctuating part δv_i. Then, for example, velocity can be written as:

$$v_i = \bar{v}_i + \delta v_i \tag{2.75}$$

if (2.75) are substituted to Navier-Stokes equation and to continuity equation and if time averaging[1] is applied we get a so called Reynolds equation for incompressible fluid in the form:

$$\frac{\partial(\rho\bar{v}^i)}{\partial t} + \frac{\partial(\rho\bar{v}^i\bar{v}^k)}{\partial x^k} + \frac{\partial\bar{p}}{\partial x^k} - \frac{\partial}{\partial x^k}\left(\mu\left(\frac{\partial\bar{v}^i}{\partial x_k} + \frac{\partial\bar{v}^k}{\partial x_i}\right)\right) + \frac{\partial}{\partial x^k}(\overline{\rho\delta v^i\delta v^k}) - \rho g^i = 0 \tag{2.76}$$

and a continuity equation for incompressible fluid in the form:

$$\frac{\partial \delta v^i}{\partial x^i} = 0 \tag{2.77}$$

In comparison with the Navier-Stokes equation for laminar flow the additional quantity $\overline{\rho \delta v^i \delta v^k}$, appears here. This quantity is known as the Reynolds-Stress tensor and has similar meaning in equation as the quantity representing the shear stress tensor in laminar model of flow. According to Boussinesq it is possible to express this quantity with the help of μ_t variable which is called turbulent viscosity. Turbulent viscosity is for two-dimensional boundary layer defined by the relation

$$-\overline{\rho \delta v_x \delta v_y} = \tau_t = \mu_t \frac{\partial \overline{v_x}}{\partial y} \tag{2.78}$$

Other important form of turbulent viscosity was published by Prandtl (1925)

$$\tau_t = -\overline{\rho \delta v_x \delta v_y} = \rho l_m^2 \left| \frac{\partial \overline{v_x}}{\partial y} \right| \frac{\partial \overline{v_x}}{\partial y} \tag{2.79}$$

where l_m is a so called mixing-length[1]. The mixing-length is similar to the mean free path of molecules in this equation and is similar to the mean distance where the interaction among eddy structures takes place. Prandtl presumed that the mixing-length in a turbulent boundary layer is proportional to the distance from the wall $l_m = k \cdot y$.

Unknown general formula for the turbulent viscosity (or turbulent shear stress or other corresponding variable in the fluid flow) are the obstacles in solving the Reynolds equations. That is why it is necessary to close the system of equations with the use of certain, mostly semi-empirical formulas for turbulent viscosity or for other corresponding quantities. Various models of turbulence are used for this closure.

---

1. Time averaging is defined by: $\overline{f(x)} = \lim_{t \to \infty} \frac{1}{t} \int_0^t f(x, t)\, dt$. When we consider functions $f = f_0 + \delta f$ and $g = g_0 + \delta g$ then $\overline{\delta f} \equiv 0$, $\bar{f} = f_0$ is valid, and: $\overline{fg} = f_0 g_0 + \overline{\delta f \delta g}$.
1. The Prandtl formulation is equivalent to Boussinesq formulation when we write the equation for turbulent viscosity as: $\mu_t = \rho l_m^2 \left| \frac{\partial \overline{v_x}}{\partial y} \right|$.

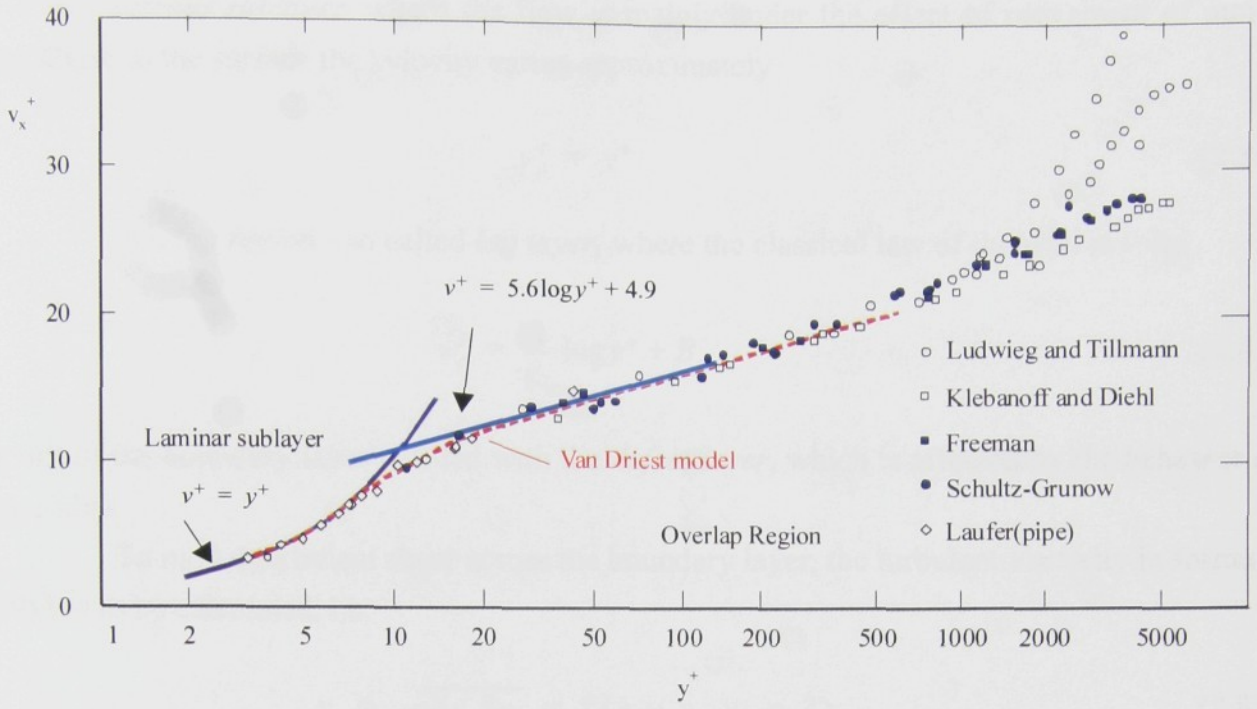

Fig.2.11 Universal law of the wall plot for turbulent boundary layers. Red dotted line corresponds to Van Driest model of turbulent viscosity (After Tennekes[39])

2.3.2 Structure of turbulent flow

The great number of models is published in literature, however, we will concentrate on a brief description of models suitable for solving the problems of a curved wall jet only. We will use the Glauert presumptions to describe a turbulent wall jet. Problems of the wall jet can be divided into two parts, an inner region of flow near the wall where models for a boundary layer can be used and an outer region of flow which is similar to the shear layer known from jets (see Fig.1.1).

a) Inner region - Models for a boundary layer

The results of experiments show that we can find several different layers (Fig.2.11)[1] on the profile of mean velocity of turbulent flow. The turbulent boundary layer can be generally divided into an inner and an outer layer. The inner layer includes regions where the effect of viscosity prevails and these are:

---

1. It is obvious to express velocity in boundary layer in so called wall coordinates: v_y^+, y^+ : $v_y^+ = \frac{\bar{v}_y}{v^*}$, $y^+ = \frac{y v^*}{\nu}$ where friction velocity $v^* = \sqrt{\frac{\tau_w}{\rho}}$.

viscous sublayer, where the flow is mainly under the effect of movement of molecules. Close to the surface the velocity varies approximately

$$v_y^+ = y^+ \tag{2.80}$$

overlap region - so called *log layer,* where the classical law of the wall is valid

$$v_y^+ = \frac{1}{\kappa_w}\log y^+ + B_w \tag{2.81}$$

The rest of the boundary layer is filled with the *defect layer*, which is affected by the behavior of large eddies.

To model turbulent shear across the boundary layer, the turbulent viscosity in formula (2.79) has to be calculated, i.e.

$$\tau_t = -\overline{\rho \delta v_x \delta v_y} = f(x, y, v_x, v_y, p, T) \tag{2.82}$$

Such models of turbulence have to best fit the experimentally obtained data and moreover they also have to be based on clear physical nature so they can be generalized for variety of cases.

When we substitute the relations (2.80) and (2.81) to equation (2.76) we get the equation in the form (Coles (1955)):

$$\frac{\tau + \tau_t}{\tau_w} = 1 + \frac{y}{\tau_w}\frac{dP}{dx} + \frac{\nu}{(v^*)^2}\frac{dv_*}{dx}\int_0^{y^+} g(y^+)^2 dy^+ \tag{2.83}$$

Last two terms can be neglected in comparison with the unity and equation (2.83) can be written in the form

$$\tau + \tau_t = \tau_w = \mu\frac{\partial \overline{v}_x}{\partial y} + \mu_t\frac{\partial \overline{v}_x}{\partial y}. \tag{2.84}$$

Considering $\tau << \tau_T$ is valid in the region of the law of the wall, then substituting τ_w from $v^* = \sqrt{\tau_w/\rho}$ we get the formula for the turbulent viscosity in the log layer

$$\mu_t = \kappa \rho v^* y \tag{2.85}$$

The modification of this model for the inner part of the inner region ($y^+ < 60$) was accomplished by Van Driest model (1965). He completed the factor $[1 - \exp(-y/A)]$ should be

applied to the fluid oscillation to obtain the damping effect of the wall. Finally we can write a model for the whole region according to Van Driest in the form (Tennekes[39]):

$$\tau + \tau_t = \tau_w = \mu\frac{\partial\overline{v}_x}{\partial y} + \rho\kappa^2 y^2\left[1 - \exp\left(\frac{-y}{A}\right)\right]^2\left|\frac{\partial\overline{v}_x}{\partial y}\right|\frac{\partial\overline{v}_x}{\partial y} \tag{2.86}$$

or in its non-dimensional form

$$\frac{\tau + \tau_t}{\tau_w} = \frac{\partial v^+}{\partial y^+} + \rho\kappa^2 (y^+)^2\left[1 - \exp\left(\frac{-y^+}{A^+}\right)\right]^2\left(\frac{\partial v^+}{\partial y^+}\right)^2 = 1 \tag{2.87}$$

The best agreement with experimental data is where $A^+ = 26$ a $\kappa = 0.40$
The equation for turbulent viscosity can be then written as

$$\mu_t = \rho\kappa^2 y^2\left[1 - \exp\left(\frac{-yv_*}{26\nu}\right)\right]^2\frac{\partial\overline{v}_x}{\partial y} \tag{2.88}$$

Let us present model a of mixing-length for the outer part of boundary layer. This model of the mixing length is based on the presumption that the mixing length must be proportional to the same length scale and that it is possible to express it in the form (by Ecsudier -1966):

$$l_m = 0.09\delta \tag{2.89}$$

where δ is the thickness of the boundary layer.

b) Outer region - Models for shear layers

Due to the similarity of the structure of jets and wakes and the structure of flow in the outer part of the boundary layer, the models used for the outer part of the boundary layer are similar to models used for shear layers.

The Clauser model is presented as an example in the form:

$$\nu_t = C_c v_e \delta^* \tag{2.90}$$

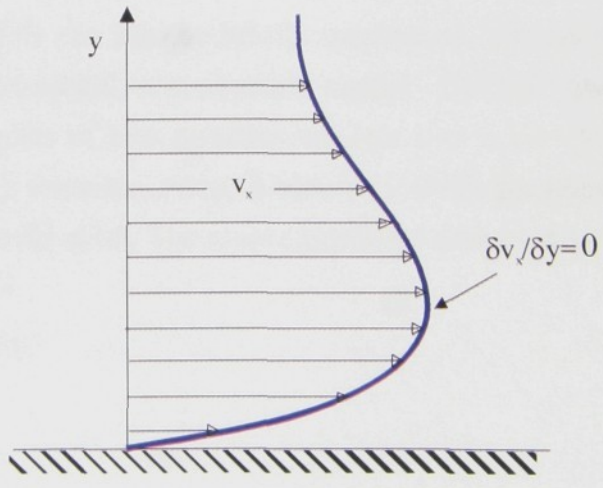

Fig.2.12 Illustration of a turbulent boundary layer velocity profile with a velocity maximum.

where $C_c \approx 0.018$. Other models can be found for example in Wilcox[53], Tennekes[39] or Příhoda[32].

A velocity profile with the velocity maximum shown in Fig.2.12 causes the basic disadvantage of these formulations in the equations (2.78) a (2.79). The wall jet profile must have $\frac{\partial v_x}{\partial y} = 0$. Zero τ_t value must be in this position according to the both formulations for the Reynolds stress tensor. It was verified by many experiments that the turbulent transport of momentum and other variables appear also in positions with zero velocity gradient.

The second disadvantage of algebraic models is the insufficiency of advection of turbulence. It fails to solve the flow behind a grid for example. Certain corrections of basic model are necessary to describe the flow with curved streamlines (See "Correction of models of turbulence for curved flow" on page 43.).

2.3.3 Models of turbulence for complex flows

Other algebraic models are also worth mentioning, such as modification introduced by Corrsin and Kistler (1954) and Klebanoff, which also includes the effect of intermittence, into the models. Model Cebeci-Smith divides the boundary layer into two layers with different turbulent viscosity in inner and outer layers.

The Baldwin-Lomax model is based on the same idea as the Cebeci-Smith two-layer model and is used in those cases where boundary layer properties, such as (δ, δ_v^*, v_e), are difficult to determine. This situation often arises in numerical simulation of separated flows, especially of flows with shock waves. Detailed description of Cebeci-Smith and Baldwin-Lomax models can be found in Wilcox[53].

Apart from algebraic models, other models can also be briefly mentioned. The most used models are so called Johnson-King 1/2 equation model, one equation model - Baldwin and Barth (1990), Spalart-Allmaras (1992), a large number of two equation models k-ω a k-ε (for example: Saffman (1970); Wilcox and Albert (1972); Speziale, Abid, Anderson (1990); Standard k-ε). All these models are based on Boussinesq approximation. The most significant drawbacks of these models are their limitations in calculations of:

* flow with sudden change of the mean strain
* flow along the curved wall
* flow with secondary motion
* flow in rotational channels
* three - dimensional flow
* flow with separation of a boundary layer

Even thought the drawbacks mentioned above appear in most observed cases, the models based on the Boussinesq approximation are used most often. It is mainly because of their simplicity, transparency and also their popularity among the producers of commercial CFD codes.

Models with non-linear formulation of a constitutive relation for turbulent shear stress [Lumley(1970); Saffman (1976)], so called "Second-Order Closure" models [Launder-Reece-Rodi(1975); Wilcox-Rubesin(1980)], try to eliminate the drawbacks mentioned above.

Nowadays we can reach more and more solutions obtained by a "Direct Numerical Simulation" method [article Rogallo-Moin(1984)], which directly solves the Navier-Stokes equation. the "Large Eddy Simulation" method is also used quite often. The motion of large structures is solved directly and the motion of the small ones is modelled. A compact theory using the theory of chaos to model turbulence has not been set up yet.

2.3.4 Correction of models of turbulence for curved flow

It is evident from the experimental results that the streamwise surface curvature strongly affects properties of turbulent flow. Appropriate description of curved flow is necessary for the correct use of models mentioned above, which were derived for the case of curved wall jet. Only the correction for curved wall jet will be mentioned owing to the problems this thesis deals with.

The main difference between a curved wall jet and its plain flow equivalent is the presence of instability in the curved wall jet which is caused by a centrifugal force. This instability introduces rapid mixing of the curved wall jet with its surroundings and causes significant increase in turbulence intensity and the Reynolds shear stress in the boundary layer. Shear stress in boundary layer in curvelinear orthogonal coordinates can be written as combination of viscous and Reynolds stresses:

$$\tau + \tau_t = \mu\left(\frac{\partial \overline{v_x}}{\partial y} - \frac{\overline{v_x}}{R+y}\right) - \overline{\rho \delta v_x \delta v_y} \tag{2.91}$$

The effect of the streamline curvature on the viscous stress is evident in the first term of the equation (2.91). It is necessary to mention the equation describing the production of turbulence energy to explain the effect of the streamline curvature on the Reynolds stress. According to Wilson[55] we can write the equations for the production of turbulence energy for the curved wall in the form

$$\vartheta_x = \frac{-\overline{\delta v_x^2}}{\left(1+\frac{y}{R}\right)}\frac{\partial \overline{v}_x}{\partial x} - \overline{\delta v_x \delta v_y}\frac{\partial \overline{v}_x}{\partial y} - \frac{\overline{\delta v_x^2}\overline{v}_y + \overline{\delta v_x \delta v_y}\overline{v}_x}{R+y} \tag{2.92}$$

$$\vartheta_y = \frac{-\overline{\delta v_x \delta v_y}}{\left(1+\frac{y}{R}\right)}\frac{\partial \overline{v}_y}{\partial x} - \overline{\delta v_y^2}\frac{\partial \overline{v}_y}{\partial y} + \frac{2\overline{\delta v_x \delta v_y}\overline{v}_x}{R+y} \tag{2.93}$$

and the equation for the production of $\overline{\delta v_x \delta v_y}$ in the form

$$\vartheta_{xy} = \frac{\overline{\delta v_x^2}}{\left(1+\frac{y}{R}\right)}\frac{\partial \overline{v}_y}{\partial x} - \overline{\delta v_y^2}\frac{\partial \overline{v}_x}{\partial y} + \frac{2\overline{\delta v_x^2}\overline{v}_x}{R+y} - \frac{\overline{\delta v_y^2}\overline{v}_x}{R+y} \tag{2.94}$$

One of the first attempt to include the streamline curvature effects into the calculation for eddy viscosity was made by Prandtl in 1929. His analyses were revised much later by Sawyer (see Wilson[55] for details) and it resulted in

$$-\rho\overline{\delta v_x \delta v_y} = \mu_t \frac{\partial \overline{v}_x}{\partial y}(1 - C_1 K) \tag{2.95}$$

where:

$$K = \frac{\overline{v}_x}{(R+y)\frac{\partial \overline{v}_x}{\partial y}} \tag{2.96}$$

is a flow stability parameter, C_1 is constant. The positive constant C_1 was determined by Sawyer for curved wall jet on a logarithmic spiral surface as $C_1 \approx 3$ and it varies from $5 < C_1 < 9$ for curved free jet. According to Wilson[55] is $C_1 = 5$ valid for cylindrical wall.

It is possible to determine the parameter ε by the function

$$f(\xi) = \frac{\mu_t}{\rho y_{0.5} \overline{v}_{max}}, \tag{2.97}$$

which is independent of the curvature and may be evaluated from geometrically similar plain flow.

A more realistic approach to the Reynolds Stress is to assume that the magnitude of the product of velocity fluctuations $\overline{\delta v_x \delta v_y}$, is proportional to its local rate of production ϑ_{xy}. When we put ϑ_{xy} in the equation (2.94) proportional to $\overline{\delta v_x \delta v_y}$, we get the equation for a thin shear layer,

$$-\delta\overline{v_x \delta v_y} = \mu_{tc}\frac{\partial \overline{v_x}}{\partial y}\left[1 - 2K\left(\frac{\overline{\delta v_x}^2}{\overline{\delta v_y}^2} - \frac{1}{2}\right)\right], \tag{2.98}$$

where:

$$\frac{\mu_{tc}}{y_{0.5}\overline{v_{max}}} = C_2\frac{\overline{\delta v_y}^2}{\overline{v_{max}}} \tag{2.99}$$

C_2 is the function of the distance y from the wall.

2.3.5 Flow Separation

Flows with adverse pressure gradient cause the boundary layer to separate. The separation occurs, for example, in the case of flow along the curved wall. The topical problem in the theory of turbulence is to find a model of turbulence which could predict the position of separation and its effect on skin friction and heat transfer on circumfluous surface. Unfortunately, algebraic models are quite unreliable for separated flows. The results obtained with the use of algebraic models are questionable. There are several reasons.

The streamlines are no longer nearly parallel to the surface as they are in case of an attached boundary layer when a boundary layer separates. We must solve the full Reynolds-averaged Navier-Stokes equation which includes all the components of the Reynolds stress tensor.

The separated flows cannot be considered "equilibrium" and for that reason the Boussinesq approximation cannot provide an accurate description of separated flows as it is based on the presumption of local equilibrium.

Shang-Hankey (1975) used Cebeci-Smith model and introduced the notion of a relaxation length L to include upstream turbulence history effect:

$$\mu_t = \mu_{teq} - (\mu_{teq} - \mu_{t1})e^{-(x-x_1)/L} \tag{2.100}$$

[see Wilcox[53] for details]. There μ_{teq} is equilibrium eddy viscosity obtained from the Cebeci-Smith model and μ_{t1} is the value of eddy viscosity at a reference point $x = x_1$ upstream of the sep-

aration region. The relaxation length is approximately $5\delta_1$, where δ_1 is the boundary layer thickness at x_1.

The aim of this thesis is not the exact prediction of the position of separation and that is why the Van Driest model (2.88) for inner region and the Clauser model (2.90) for outer region with a streamline curvature effect correction (2.95) will be used to model the turbulent flow. It will be necessary to take into consideration the limits and inaccuracies caused by the use of a simple algebraic model when evaluating the observed results.

Chapter 3

PROBLEM SOLUTION

3.1 Smoke wire visualization

The main means of analyzing the stability of a boundary layer was the "Smoke wire" method, developed by Respet and Moore in the early 1950s Yang[57] - Fig.3.1. The basis of this simple, but powerful, method is a resistively heated thin wire (with the diameter of cca. 0.15mm), on which the oil layer is applied. While heating the wire by means of electricity, oil is evaporated and aerosol of condensed oil vapors produced in this way is sufficient for the visualization of the air flow. Cornell[6] studied the structure of substances used for smoke generation and it results from his conclusions that the "smoke" does not contain products of burning, but condensed particles with the diameter of cca. 1μm. This method is suitable for rough identification of direction of the flow and for identification of large structures in the flow. The results of the visualization of von Kármán vortex street, published by in Travníček[46] (see. Fig.3.2) are worth mentioning. This method is suitable for velocities not exceeding cca. 4m/s. This velocity is limited by ability to saturate a large amount of air on one hand and and by magnitude of critical Reynolds number of the wire on

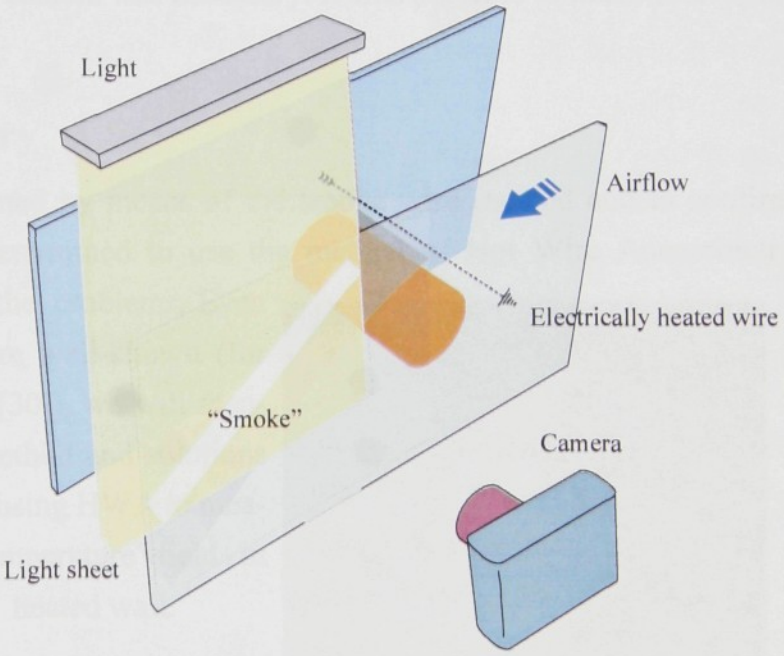

Fig.3.1 Schema of "Smoke Wire" visualization

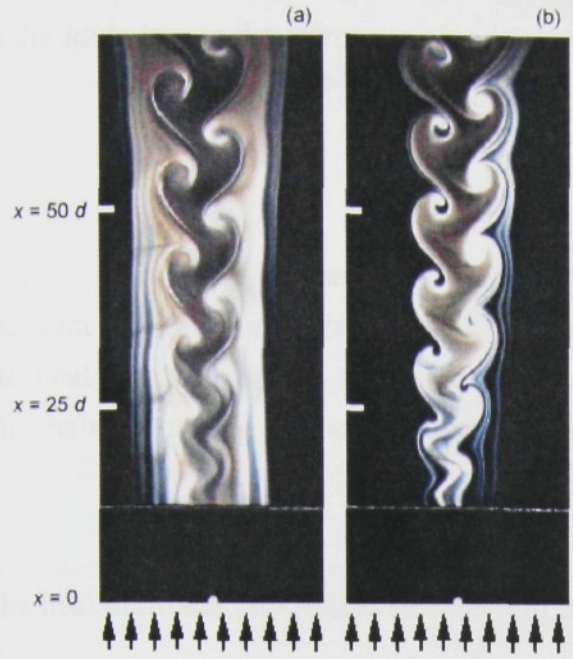

Fig.3.2 Visualization of Kármán vortex street by "Smoke Wire" method at T_∞=144.5°C; Re=61: a/ Isothermal case T*=1; b/ cooled cylinder T*=0.70 (After Travníček[46])

the other hand, so that the Kármán vortex street behind the wire does not develop.

Different kinds of oil were used in the course of experiments. It turned out that the most suitable is ricin oil. Power supply of 12V voltage and of 1.2A current was used for heating the manganin wire of 0.03mm thickness and of cca.110mm length. With regard to a short time of smoke development that ranged from 2-3 s synchronization between the wire and the camera was necessary. It was possible to make cca. 4 pictures in the course of one experiment.

3.2 Hot wire anemometry

In the experiments performed by means of the smoke wire method and to confirm conclusions of calculations, it was determined to use the method of Hot Wire Anemometry (HWA) for more detailed analysis of the problems. Even though the basis of HWA method are well-known (for more information see Bruun[4], Perry[30]), we will mention here the basic principle of this method and solutions of some problems that appeared when using HWA to measure parameters of velocity and temperature field in non-isothermal fluid flow and near the heated wall.

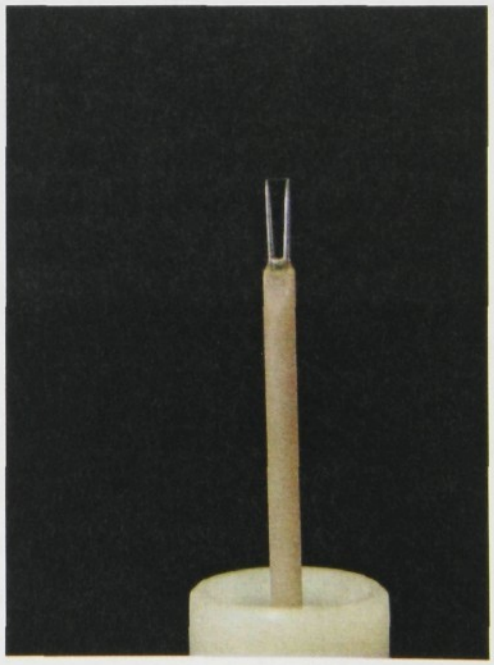

Fig.3.3 Dantec 55P11 probe

3.2.1 HWA principles

HWA method is based on convective heat transfer from the heated body into the surrounding circulating environment. The basic element of the measuring circuit is the probe that is, in the most simple case, in the form of a tungsten wire Fig.3.3 fixed to the prongs of the carrier. The wire is heated by electric current. It is pos-

sible to formulate the heat generated by electric current in the wire element of dx length according to the Joule law in the form:

$$d\dot{Q}_J = \frac{I^2 \chi_{wire}}{S_{wire}} dx \tag{3.1}$$

In the stationary case the heat generated in the wire element (Fig.3.4) must equal the sum of heats transferred into the surrounding, i.e. the convective transferred heat $d\dot{Q}_{conv}$, the heat transferred into the carrier $d\dot{Q}_{cond}$, the heat radiated into the surroundings $d\dot{Q}_{rad}$. The balance of heat can be formulated by the following equation:

$$d\dot{Q}_J = d\dot{Q}_{conv} + d\dot{Q}_{cond} + d\dot{Q}_{rad} \tag{3.2}$$

The heat dissipated by means of radiation is in most cases negligibly low and the heat dissipated from the wire into the carrier can be considered as independent of parameters of the flowing medium. Radiation effect is not negligible when measuring near the wall. We will deal with a proximity effect of the wall in the following paragraph. The heat convective transferred into the flowing medium can be formulated according to the Newton's law for heat transfer:

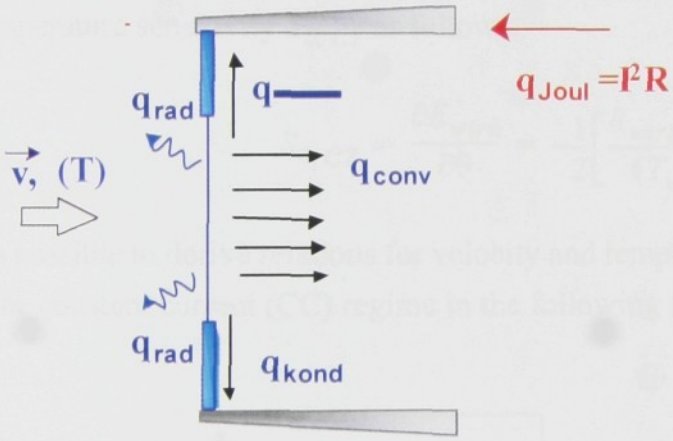

Fig.3.4 Mechanism of heat transfer from the wire element.

$$\dot{Q}_{conv} = \pi d_{wire} l_{wire} h (T_{wire} - T_\infty) \tag{3.3}$$

The transferred heat is then proportional to the fluid velocity (through the heat-transfer coefficient h) and to the temperature difference of the wire T_{wire} and the fluid T_∞. Hence it results that we can use wire anemometry for both velocity and temperature measuring. Simultaneously however, the consequence of the above mentioned dependence is inaccuracy of the velocity measurement in non-isothermal fluid flow. We will deal with the methods for elimination of this inaccuracy in the following chapter.

If we suppose infinitely long wire where we can ignore heat transfer into the holder, the thermal balance is given by:

$$I^2 R_{wire} = \pi d_{wire} l_{wire} h (T_{wire} - T_\infty) \tag{3.4}$$

If we substitute the relation for temperature dependence of resistance $R_{wire} = R_0[1 + \alpha_0(T_{wire} - T_0)]$ and the relation for voltage calculation $E_{wire} = IR_{wire}$, we can rewrite the equation (3.4)) in the form

$$E_{wire}^2 = (A + BU^n)(T_{wire} - T_\infty), \tag{3.5}$$

where A, B and n are the functions of wire diameter and material properties of the wire and of the surrounding fluid whose magnitude we get through calibration.

As mentioned above, HWA probes are sensitive to both velocity of the surrounding fluid and its temperature. Velocity sensitivity of the probe connected in constant temperature (CT) regime $S_{u,CT}$ can be calculated as follows:

$$S_{u,\,CT} = \frac{\partial E_{wire}}{\partial U} = \frac{nBU^{n-1}}{2}\left[\frac{R_{wire}(T_{wire} - T_\infty)}{A + BU^n}\right]^{1/2} \tag{3.6}$$

Temperature sensitivity $S_{\theta,\,CT}$ as follows:

$$S_{\theta,\,CT} = \frac{\partial E_{wire}}{\partial \theta} = -\frac{1}{2}\left[\frac{R_{wire}(A + BU^n)}{(T_{wire} - T_\infty)}\right]^{1/2} \tag{3.7}$$

It is possible to derive relations for velocity and temperature sensitivities for anemometer working in the constant current (CC) regime in the following form:

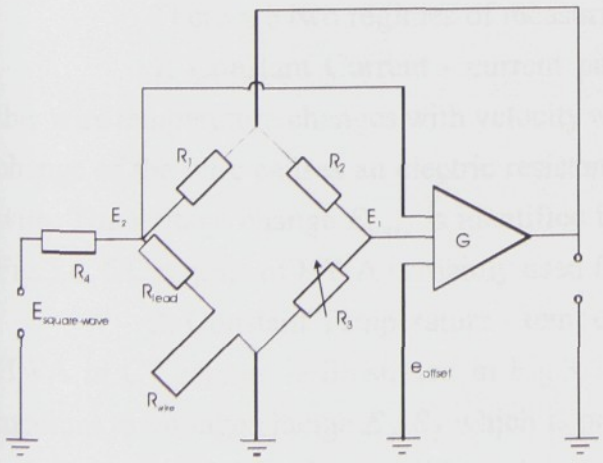

Fig.3.5 Wheatstone bridge for anemometer operating in CT mode

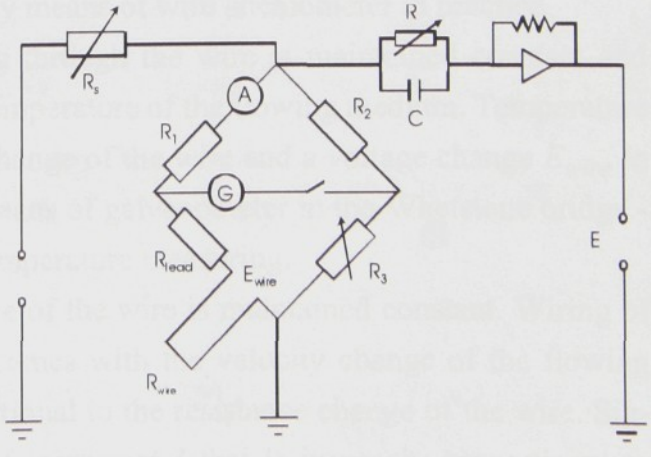

Fig.3.6 Bridge for anemometer operating in CC mode

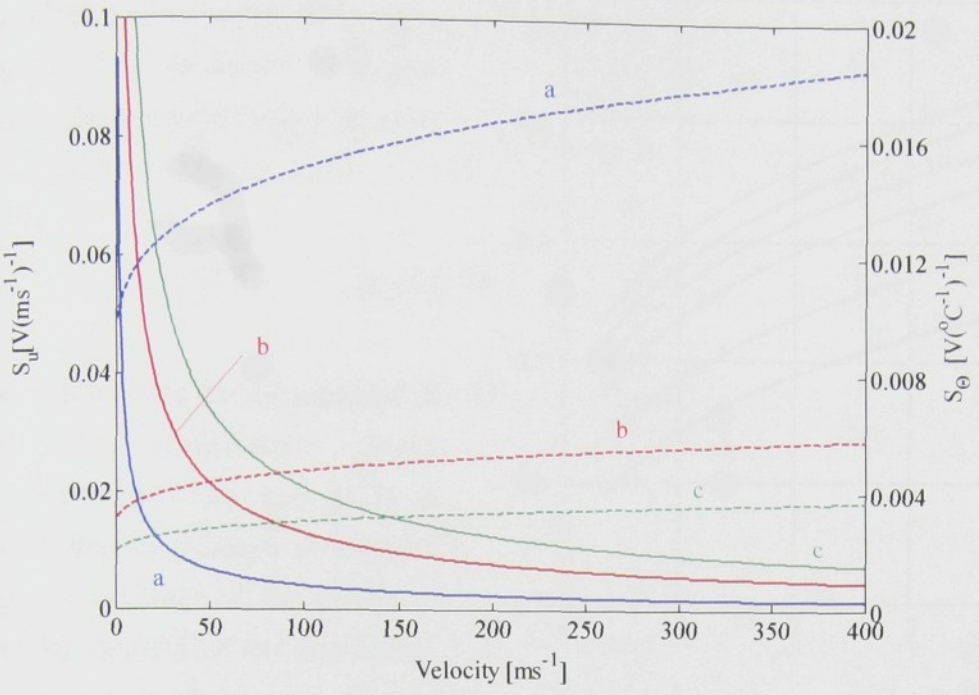

Fig.3.7 The variation in the velocity (line) and temperature (dotted) sensitivity (for CTA bridge) with velocity for temperature differences T_{wire}-T_a of: a/10K, b/100K, c/250K (After Bruun[4])

$$S_{u,\,CC} = \frac{nBI^3\bar{R}_{wire}^2 U^{n-1}}{\bar{R}_\infty (A + B\bar{U}^n)^2} \tag{3.8}$$

$$S_{\theta,\,CC} = \frac{\alpha_0 I \bar{R}_{wire} R_0}{\bar{R}_\infty} \tag{3.9}$$

where the barred values are time averaged values.

There are two regimes of measuring by means of wire anemometer in practice.

1. Constant Current - current passing through the wire is maintained constant and the wire temperature changes with velocity and temperature of the flowing medium. Temperature change of the wire causes an electric resistance change of the wire and a voltage change E_{wire} in wire. The voltage change E_{wire} is identified by means of galvanometer in the Whetstone bridge - Fig.3.6. CC regime of HWA is mainly used for temperature measuring.

2. Constant Temperature - temperature of the wire is maintained constant. Wiring of HWA in CT regime is illustrated in Fig.3.5. It comes with the velocity change of the flowing medium to voltage change E_2-E_1 which is proportional to the resistance change of the wire. Signal E_2-E_1 is led into the amplifier whose output is current I that is inversely proportional to the wire resistance. Conducting this current back into the bridge it comes to a repeated adjustment of initial resistance value of the wire. CT regime is used for velocity measuring.

An important parameter of the probes working in CTA regime is a so called Overheat ratio. The overheat ratio is formulated by the following ratio:

$$a_h = \frac{R_{wire}}{R_a} \qquad (3.10)$$

and it is a guide for adjustment of the wire temperature. From the relations (3.6) and (3.7) it results that the velocity or temperature sensitivity of the probe is directly dependent on the selection of the overheat ratio. Therefore it is recommended for the velocity measuring to select the overheat ratio as high as possible (Maximum values are limited by material properties of the wire, especially then by a tendency to faster corrosion at higher temperatures. In experiments performed in water, the overheat ratio is limited by boiling temperature of water and by the influence of buoyancy measuring).

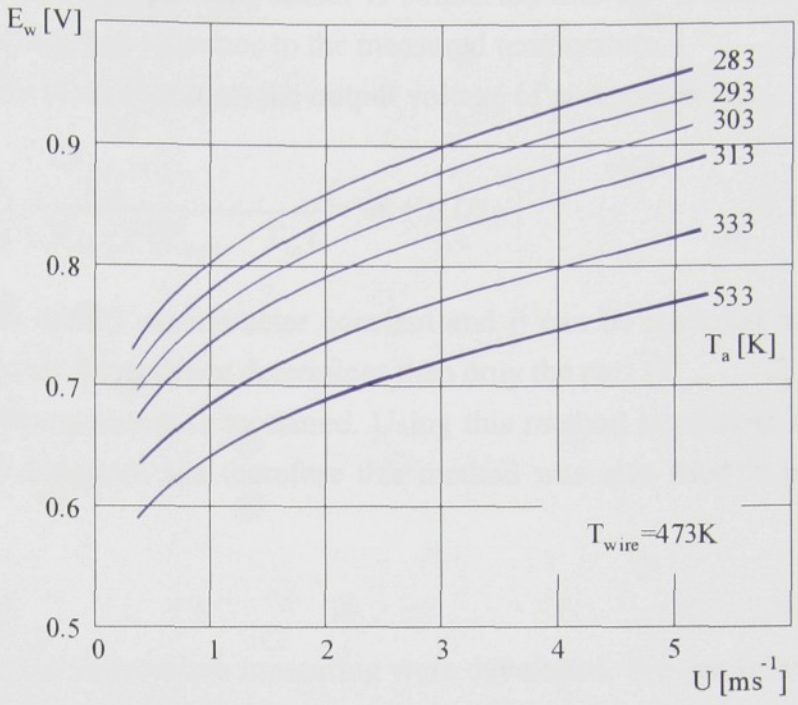

Fig.3.8 The dependence of the hot-wire voltage E_{wire}, on the air velocity U for different ambient fluid temperatures (After Bruun[4] page 209)

3.2.2 Temperature effect

The temperature change in the course of experiment affects recorded velocity values. It results, from the relation (3.5), that the output voltage of anemometer is dependent not only on the velocity, but also on the temperature difference between the wire and the surrounding environment (see Fig.3.8).

To correct the temperature effect on the measured velocity it is possible to use one of the following methods:

1. Velocity and temperature calibration of CT hot-wire probe: Using this method we perform velocity calibration for different temperatures of fluid. From this calibration we can then formulate dependence in the following form:

$$E^2 = A^*(T_\infty) + B^*(T_\infty)U^n \qquad (3.11)$$

2. Automatic compensation - Temperature sensor is connected into the Wheatstone bridge, which compensates the temperature in reference to the measured temperature.

3. Analytic compensation - If we formulate the output voltage of anemometer as:

$$E^* = E^2 \frac{R_w}{(R_1 + R_L + R_{wire})^2 (T_{wire} - T_\infty)} = A + BU^n \tag{3.12}$$

the part $R_{wire}/(R_1 + R_L + R_{wire})^2$ is for CT anemometer constant and it can be included into the calibration coefficients. Temperature dependence determines then only the part $(T_{wire} - T_\infty)$, that we can determine if the current temperature is measured. Using this method is suitable for the evaluation of the results on the computer and therefore this method was also used in our experiments.

3.2.3 Temperature measuring

Also several methods for the temperature measuring were developed. We can briefly mention the Dual CT hot-wire method, where 2 probes (the best if they are identical) work in different overheat ratios. It is possible to determine the temperature through an analysis of an output signal from the both of the probes. In the "multiple overheat ratio" method, measuring is performed by means of one probe that works gradually in more (at least in 3) overheat ratios.

The most simple method for temperature measuring, at least for the subsequent result evaluation, is to use the wire working in CC anemometry regime. Very important for such measuring is the ratio of temperature and velocity sensitivities of the probe. From the relations (3.8) and (3.9) we can formulate a ratio that has the non-dimensional form:

$$\frac{S_{u,CC}}{S_{\theta,CC}} = -\frac{\chi_{wire} Re^{0.45}}{\pi^2 \alpha_0 \bar{U} (0.24 + 0.56 Re^{0.45})^2 d_{wire}^2} \frac{I^2}{} \tag{3.13}$$

It is obvious for the given wire diameter that for the ratio $S_{u,CC}/S_{\theta,CC}$ as high as possible it is necessary to minimize I. We used the wire of 5μm diameter in our experiments. With regard to the used anemometer it was possible to select $I = 0.05mA$ and the error in temperature measuring due to velocity effect should not exceed 1%.

3.2.4 Measuring near the wall

The aim of our experiments is not a detailed determination of velocity and temperature profiles near the wall, but an analysis of stability of a boundary layer as a whole. But it is still suitable to mention here some consequences of using HWA near the wall.

During the measurement of the velocity profile near the wall, approximately in a viscid sublayer $1 < y^+ < 5$, it is necessary to take the following factors into consideration:

1. Flow velocity near the wall is lower than $1 ms^{-1}$. This velocity requires using special calibration techniques (see. Bruun[4]).

2. Presence of the probe in a viscid sublayer leads to the interference of the fluid flow and the holder. Therefore special microprobes were developed for measuring near the wall. If we use classical probes, it is recommended to incline the probe at the angle of cca. 5^o.

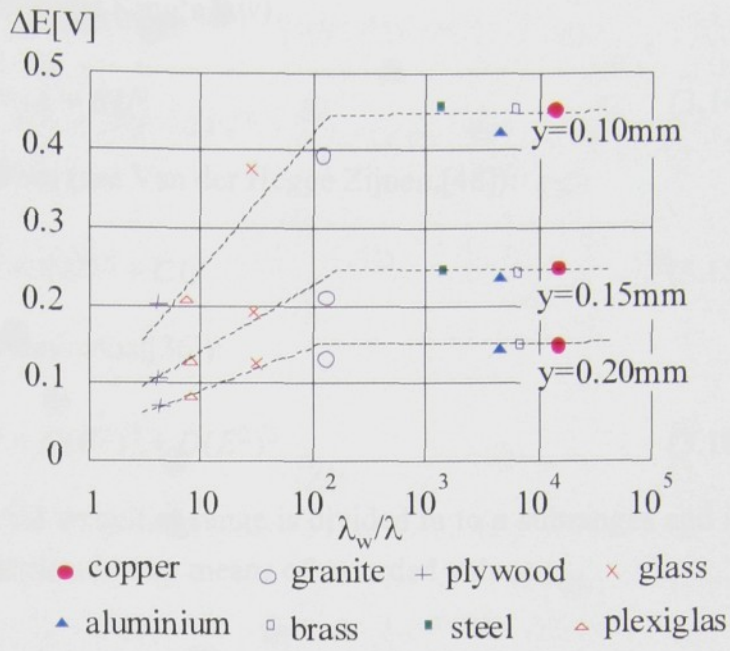

Fig.3.9 The near wall effect on an anemometer signal in still air as a function of the relative thermal conductivity (λ_w,λ – the thermal conductivity of the wall material and of the air respectively) (After Bruun[4])

3. Measuring close to the wall demands increased requirements of accuracy of distance measuring from the wall. Several methods were developed for that purpose (see: Wills[54]).

4. Wall proximity causes also increasing of heat transfer from the probe in the air due to the changes in velocity and temperature field in the environment of the wire (with regard to much higher heat conductivity of water, this effect was not observed in experiments performed in water). The example of affecting the results by the presence of the wall is illustrated in Fig.3.9. Experiments of other authors (see: Polyakov[31], Ligrani[24]) show that deviation from the curve $U^+ = y^+$ for the wall of non-conducting material appears at lower values y^+. With regard to the character of our experiments, selection of copper (that is one of the worst materials for measuring near the wall with regard to its high conductivity) as material of the heated cylinder was necessary.

3.2.5 Probe calibration

Precise calibration of the used probe is An unavoidable part of each measurement. During calibration the constants presented in calibration curve $E = f(U)$ for velocity measurement and $E = f(T)$ for temperature measurement are determined. The most used relations for HWA calibration are:

1. Power law in the form (often called King's law)

$$E^2 = A + BU^n \tag{3.14}$$

2. Extended power law in the form (see Van der Hegge Zijnen,[48]):

$$E^2 = A + BU^{0.5} + CU \tag{3.15}$$

3. Polynomial curve fit (see Swaminathal[36]):

$$U = A + BE^2 + C(E^2)^2 + D(E^2)^3 \tag{3.16}$$

4. Cubic spline fit - the measured velocities range is divided in to n subranges and in each of these subareas there are fitted cubic function by means of recorded values.

To perform experiments precisely it is important to carry out calibration before each measuring and, if necessary, at the end of each measuring, sometimes also several times in the course of measuring. We can consider the results of experiments as satisfactory if the values from both initial and final calibrations do not differ.

We used DANTEC Flow unit for the calibration. Examples of calibration curves for the velocity and the temperature are illustrated in Fig.4.10 on page 72.

3.2.6 Measuring process

We constructed a special traverse mechanism to reach high quality results. This traverse mechanism is fixed to a rotating cylinder. That ensures constant distance from the wall for various angles φ. The micrometer screw is used to adjust the distance of the probe from the wall. DANTEC 55P11 probe was used for the velocity measuring and the same DANTEC 55P11 probe was used for the temperature measuring. DANTEC 56C17 CTA anemometer bridge and DANTEC 90P20 CCA anemometer bridge were used for the velocity and temperature measurements respectively. To evaluate the results we used the software DANTEC Streamline.

3.3 Similarity solution

H. Blasius proposed in his thesis to solve the problems of fluid flow by means of the method of self-similar profiles. The principle of this method is based on transformation of coordinates that transfers the system of partial differential equations describing the velocity of flowing fluid to the system of ordinary differential equations.

We can use this methods only in such cases where we can introduce such longitudinal coordinates, the length and velocity scales of which change in a streamwise direction and all

velocity profiles transform into one shape. The typical similarity solutions are the Blasius solution of a boundary layer without pressure gradient, the Schlichting solution of jet flow, the Glaubert solution of wall jet, the Göertler solution of a mixing layer etc. To the same family belongs the Falkner-Skan solution, which describes flows with adverse pressure gradients.

For the solution of a non-isothermal curved wall jet we used the similarity solution of isothermal curved wall jet as it was published in Wygnanski[52]. This solution was completed with an equation describing the temperature field and with parts representing viscosity dependence on temperature.

3.4 Numerical calculation using Finite volume methods

The Finite-Volume methods have become popular in CFD owing to two advantages. First, they ensure that the discretization is conservative. Second, the finite volume methods do not require a coordinate transformation in order to be applied on an irregular mesh. The advantage in generating grids about arbitrary geometries increases the flexibility of this method. Finite volume methods are applied to the integral form of the governing equations in the form of equation (2.1):

$$\frac{d}{dt}\int_V \phi dV + \oint_{\partial V} j^k(\Phi) da_k = \int_V \sigma(\Phi) dV \tag{3.17}$$

The basic idea of the finite-volume method is to satisfy the integral form of the conservation law to some degree of approximation for each of many contiguous control volumes which cover the domain of interest. Thus the volume V in the equation (3.17) is that of the control volume whose shape is dependent on the nature of the grid.

The flux j^k is required at the boundary δV of the control volume. This flux must be integrated to find the net flux through the boundary. Similarly, the source term σ must be integrated over the control volume.

The average value of φ in a cell with the volume V is

$$\bar{\varphi} = \frac{1}{V}\int_V \varphi dV \tag{3.18}$$

In order to evaluate the fluxes, which are a function of φ, φ can be represented within the cell by some piecewise approximation which produces the correct value of $\bar{\varphi}$. This is a form of interpolation often referred to as a reconstruction. This interpolation will produce different approximations to the flux at the boundary, between two control volumes, so that the flux will be discontinuous. A non dissipative scheme analogous to centered differencing is obtained by taking the average of these two fluxes.

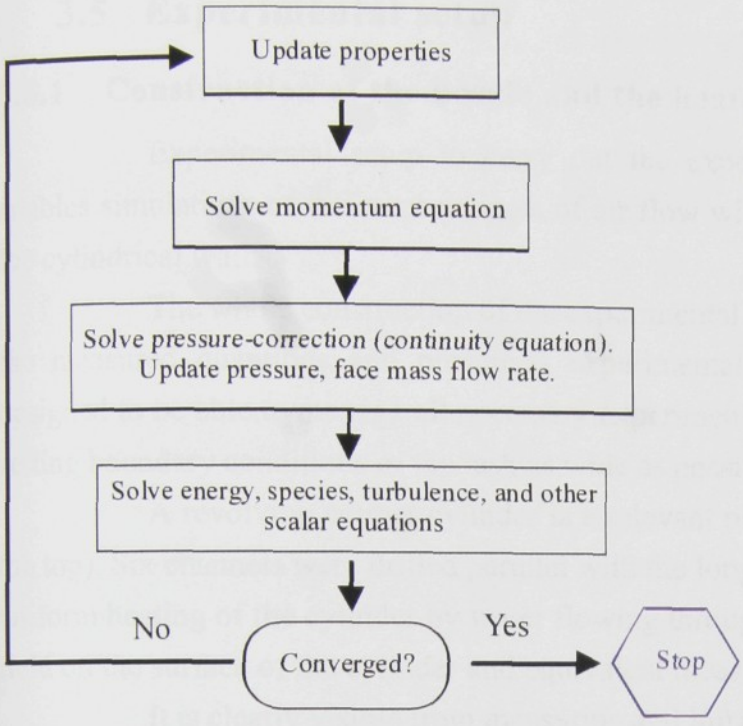

Fig.3.10 Overview of the segregated solution method of FVM

Fluxes are integrated to find the net flux through the control volume boundary and new values of $\bar{\varphi}$ are obtained.

There are two numerical methods to solve the governing integral equations:

1. segregated solver
2. coupled solver

allowed by FLUENT. Let's briefly describe the process of solving used in the segregated solver. Using this approach, the governing equations are solved sequentially. As the governing equations are non-linear and coupled, several iterations of the solution loop must be performed before a converged solution is obtained. Each iteration consists of the steps illustrated in Fig.3.10.

In addition to the selection of the solver, FLUENT enables to adjust a great number of solver parameters that enable optimal adjustment of calculation for the given problem. To the most important parameters belongs selection of linearization method of governing equations (implicit vs. explicit), method of reconstruction (First-Order Upwind scheme, Power-Law scheme, Second-Order Upwind scheme etc.)

Only the model for laminar flow from the library of offered viscosity models was used. Viscosity for calculation of laminar isothermal flow was considered as constant (ν=1.789 10^{-5} m^2s^{-1}). Viscosity for calculation of laminar non-isothermal flow was considered as function of temperature according to the relation (2.58).

The van Driest model of eddy viscosity (2.88) for inner section of the wall jet and the Clausier model (2.90) for outer section of the wall jet were used for calculation of turbulent flow (flow at high values of *Re*). Correction for flow along the curved wall in the form described in the (2.96) was used for both of the models

3.5 Experimental setup

.5.1 Construction of the nozzle and the heated cylinder

Experimental setup to carry out the experiment was designed and assembled. It nables simulations of different regimes of air flow with the possibility to heat up or cool down he cylindrical wall.

The whole construction of the experimental setup was affected by the requirements on he measured quantities and presumed experimental methods. The experimental setup was lesigned to be able to manage all necessary experiments and with the respect to the necessity of setting boundary conditions of the task as wide as possible (see Fig.3.11 and Fig.3.12)

A revolving copper cylinder is a relevant part of the setup (for detail see Fig.3.12 on he top). Six channels were drilled parallel with the longitudinal axis of the cylinder. They ensure niform heating of the cylinder by water flowing through them. There is a picture of temperature ield on the surface of the cylinder and equivalent measured temperatures illustrated in Fig.3.13.

It is clearly visible from measuring and infrared photography that it is possible to consider temperature field as uniform and in this way boundary conditions correspond to the constant

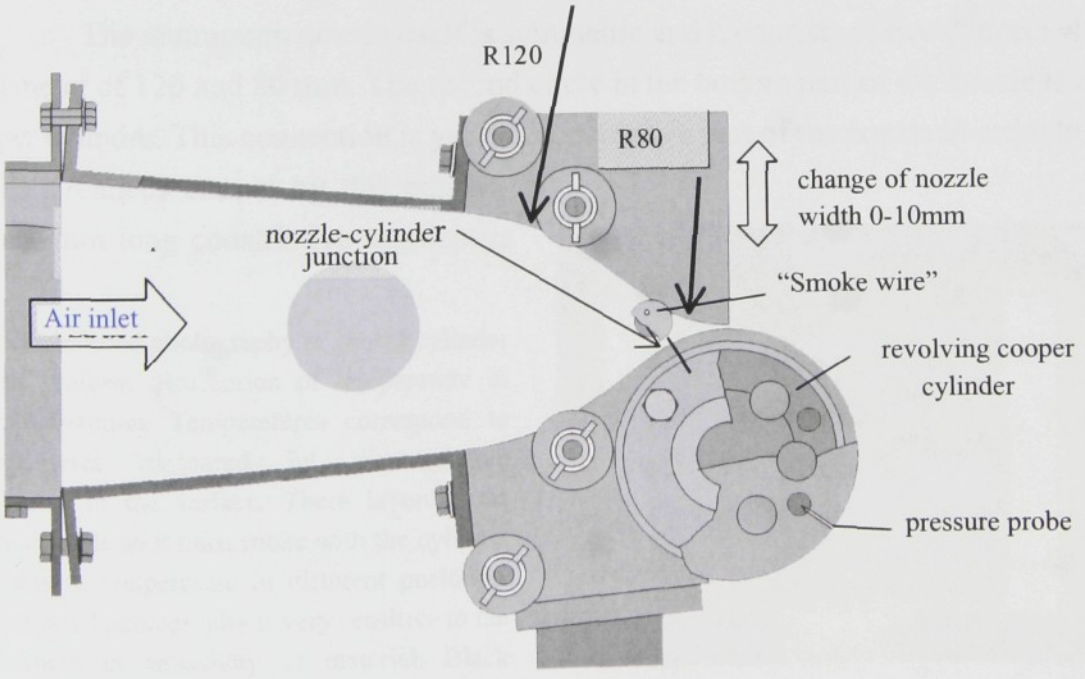

Fig.3.11 Construction of the equipment for experiments

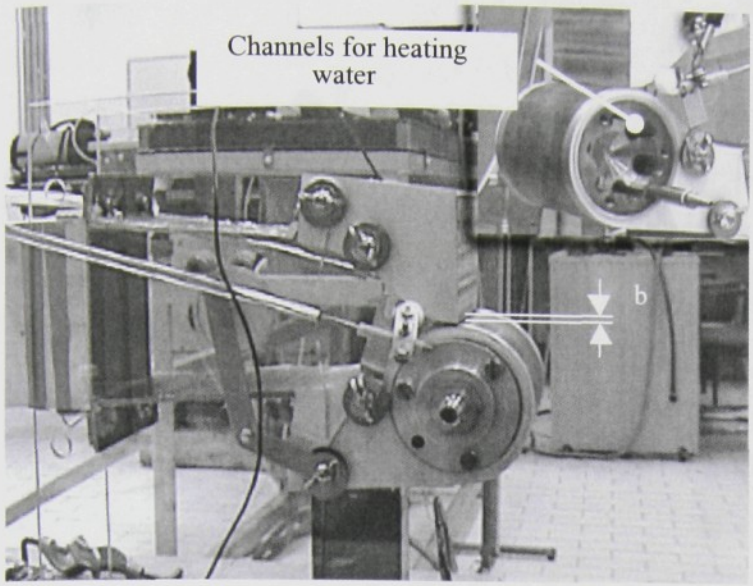

Fig.3.12 Experimental setup. See detail of heating on the top of the picture

temperature. Heating of water is carried out in a heating circulator, where the temperature with the deviation of ±0.5 °C can be set.

In similar experiments (see Tesař[44]), electrical heating is used more often. However this method cannot ensure constant temperature of the surface of the cylinder.

An original setup was designed for the temperature range up to 150 °C. The first experiments showed that the sufficient temperature range is from 20 to 70 °C to describe the studied phenomenon.

There is a small hole with a sensor to measure static pressure and a hole for thermocouples on the surface of the cylinder. A rotative cylinder is placed in the sideboards.

The aluminium nozzle itself is symmetric and it consists of two connected circles with the diameter of 120 and 80 mm. The second circle in the bottom part of the nozzle is connected to a copper cylinder. This connection is yet in a constrictive part of the nozzle in order to reduce possible disturbances caused by this connection. 150 mm long constrictive segment is

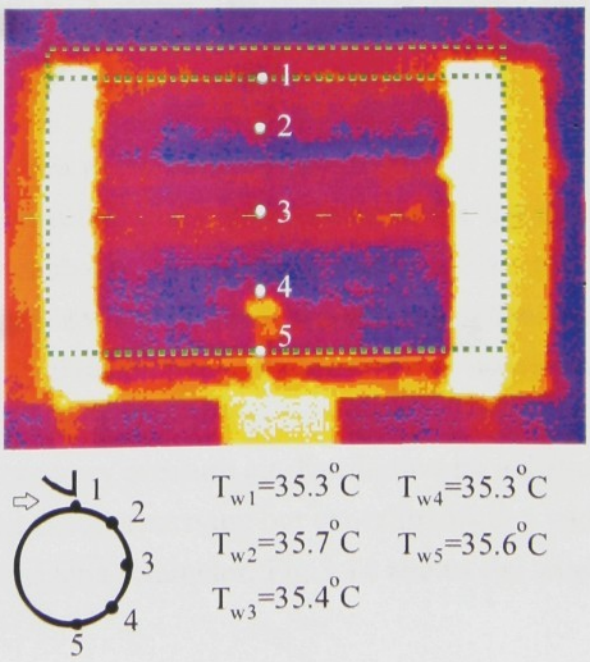

Fig.3.13 Infrared photography of heated cylinder shows uniform distribution of temperature in lateral direction. Temperatures correspond to temperatures measured by thermocouple integrated in the surface. There is only one thermocouple so it must rotate with the cylinder to measure temperature in different positions. The infrared photography is very sensitive to the differences in emissivity of material. Black painted parts of cylinder (ends) seem to have the highest temperature which is not true. Green dotted lines are added to mark the cylinder and the nozzle.

Fig.3.14 Laboratory equipment for our experiments: 1. Nozzle and heated cylinder; 2/ Power supply for "Smoke Wire experiments"; 3/ Rotameter; 4/ Heating circulator; 5/ Computer; 6/ Velocity calibr. unit; 7/ Temperature calibr. unit; 8/ Oscilloscope; 9/ CCA bridge; 10/ CTA bridge; 11/ Voltmeter to measure signal from thermocouples (on the cylinder surface and in the nozzle); 12/ Tripod for camera

in front of the nozzle in order to achieve the highest compression of air flow.

Side plates made of 5 mm thick anti-reflex glass are screwed to the top and bottom parts of the nozzle. This glass should not only enable to obtain proper pictures from the "Smoke Wire" visualization but it should also have sufficiently stable mechanical and optical properties for the presumed temperature range. Holes in the glass endplates enable to move upper side of the nozzle and so the width of the nozzle in the range from 0 to 10mm can be set.

The whole setup is connected to laboratory pressure air distribution by a diffuser containing grids and filters. Pressure air distribution ensures carrying out experiments in a wide range of velocities. Flow rate of air is measured and set by a rotameter. Fig.3.14 shows the whole laboratory equipment used for our experiments.

3.5.2 Equipment for the "Smoke wire" experiments

The construction of the setup is affected by the choice of used experimental methods. The wire used for the "Smoke wire" visualization method is placed eccentrically in "plugs" which are in the endplates. This arrangement enables to choose the position of the smoke wire in dependence on the width of the nozzle and flow velocity.

It is possible to set the intensity of "smoke" by changing amperage on a connected power supply. Relatively long (cca 5 sec.) period of smoke generation can be achieved for low amperage. This is suitable for observation of flow structure and for setting the parameters of the experiment. It is necessary to use more intensive smoke for photography. If the smoke is intensive the period of smoke generation shortens. Several kinds of oil were used during the experiments. The use of ricin oil seems to be the best choice.

Each experiment was photographed by digital cameras Canon G2 and Olympus E10. Lamps placed parallel with the side plates below and above studied area were used for lighting.

3.5.3 Equipment for HWA

Traversing bridge fixed to the cylinder was designed to carry out experiments by HWA method (see. Fig.3.15). This arrangement enables the exact measuring of tangential velocity, intensity of turbulence and temperature in the whole boundary layer. The probe remains stable with regard to coordinates connected to cylinder with the use of this setup. Only the shift in radial direction, which is set by a micrometer is possible. The micrometer enables to set the position of the probe with an accuracy of 0.01mm. The arrangement of setup for HWA method is shown in Fig.3.14 and Fig.3.15. The hot wire probe DANTEC 55P11 is connected to the DANTEC 56C17 CTA bridge (See "HWA principles" on page 48. for details) to measure velocity. An output signal from CTA bridge is amplified and offset is applied. This signal is sent to the computer for further processing through A/D 12bit converter.

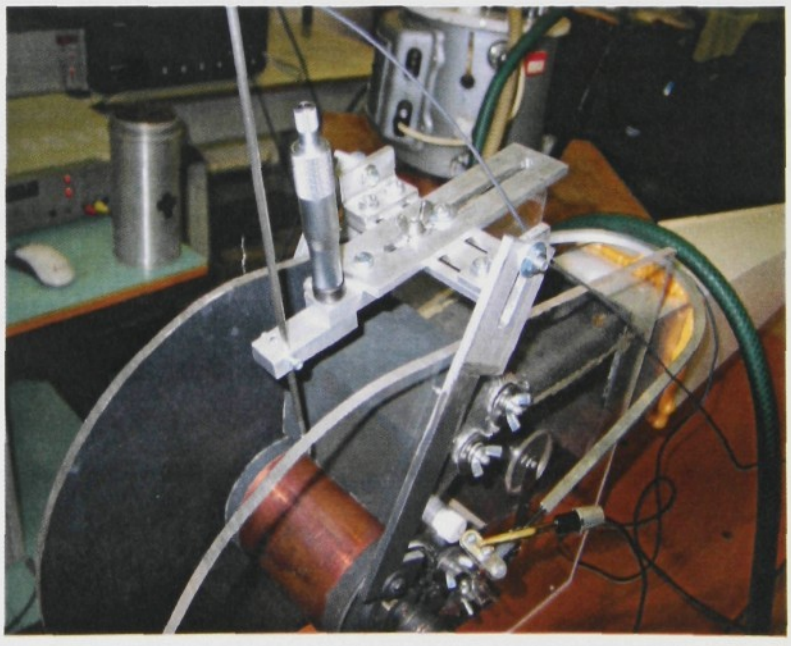

Fig.3.15 Traversing bridge for Hot wire probe

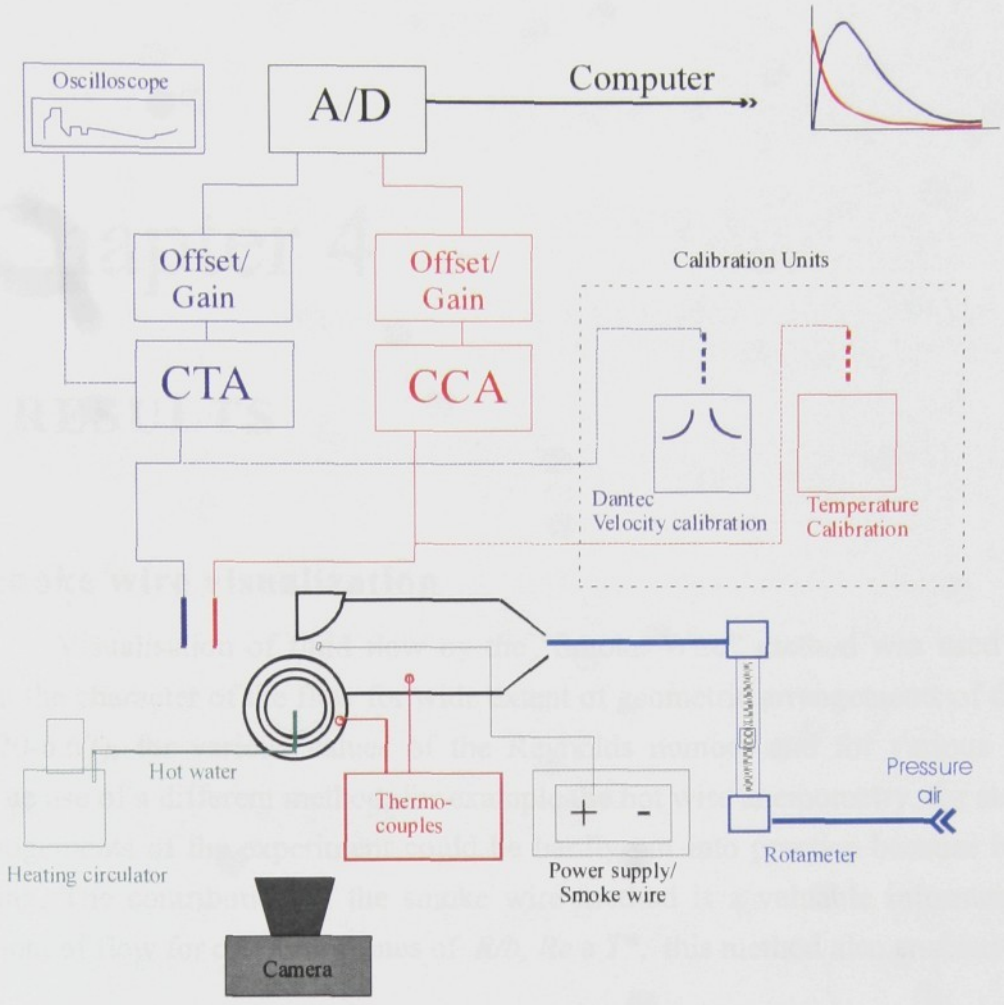

Fig.3.16 Schema of connection of experimental equipment

Temperature measuring is carried out by the same probe which was connected to the DANTEC 90P20 CCA module. Offset and gain are set there and signal is sent to the computer through A/D 12bit converter for further processing.

DANTEC 90H02 Flow unit was used for velocity calibration. A calibration oven was used for temperature calibration. Stability of CTA bridge is necessary for measuring. An oscilloscope was used to analyze the response of the square wave test.

Chapter 4

RESULTS

4.1 Smoke wire visualization

Visualisation of fluid flow by the "Smoke Wire" method was used to obtain the idea about the character of the flow for wide extent of geometric arrangements of the experiment (R/b = 20-6.67), for various values of the Reynolds number and for various values of $T^* = T_w/T_\infty$. The use of a different method, for example the hot wire anemometry, for such a wide extent of arrangements of the experiment could be hardly put into practice because it is rather time-consuming. The contribution of the smoke wire method is a valuable information about the development of flow for different values of R/b, Re a T^*, this method also enabled to formu-

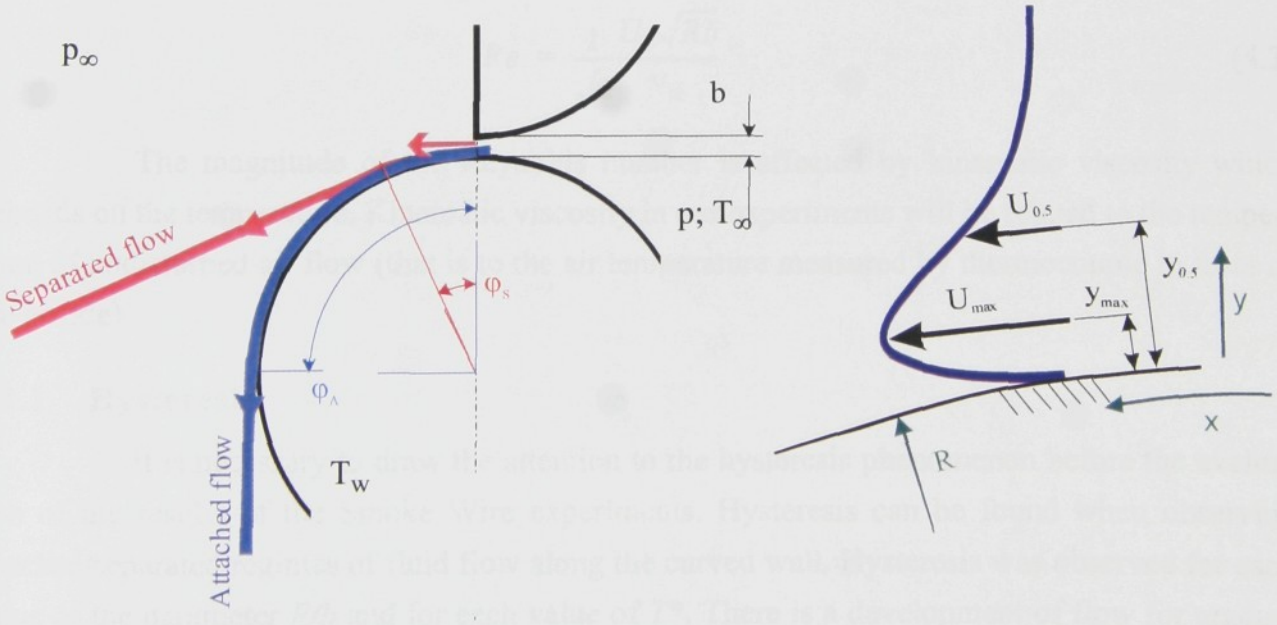

Fig.4.1 Schema of the heated Coanda jet experiments and used terminology

late the first hypothesis about the effect of particular parameters and last but not least it enabled to specify certain areas that were later studied in detail with the use of the HWA method. Quantification and significance of particular quantities which were used to process the results of the "Smoke Wire" experiments are shown in Fig.4.1.

There is not a uniformly established form of the Reynolds number characterizing the presented experiment for geometric arrangements chosen by us in the references. Most often we can come out from the Reynolds number (Re_b), which is in relation to the parameters of fluid and flow field

$$Re_b = \frac{U_b b}{\nu_\infty}. \tag{4.1}$$

In Newman[28] we can come across the form of the Reynolds number which also includes the parameters of cylindrical surface. This form of the Reynolds number can be defined with the use of pressure gradient $p\text{-}p_\infty$:

$$Re = \left[\frac{(p - p_\infty)Rb}{\rho \nu_\infty^2}\right]^{1/2} \tag{4.2}$$

If we presume square velocity profile in the nozzle then $p - p_\infty = \frac{1}{2}\rho U_b^2$ and the Reynolds number can be in the form

$$Re = \frac{1}{\sqrt{2}} \frac{U_b \sqrt{Rb}}{\nu_\infty} \tag{4.3}$$

The magnitude of the Reynolds number is affected by kinematic viscosity which depends on the temperature. Kinematic viscosity in our experiments will be related to the temperature of undisturbed air flow (that is to the air temperature measured by thermocouple in front of the nozzle).

4.1.1 Hysteresis

It is necessary to draw the attention to the hysteresis phenomenon before the evaluation of the results of the Smoke Wire experiments. Hysteresis can be found when observing attached/separated regimes of fluid flow along the curved wall. Hysteresis was observed for each value of the parameter R/b and for each value of T^*. There is a development of flow for gradual increase and sequential decrease of the Reynolds number presented in Fig.4.2. It is clear that the Re value in which the transition of flow from separated flow to attached flow occurs, depends on

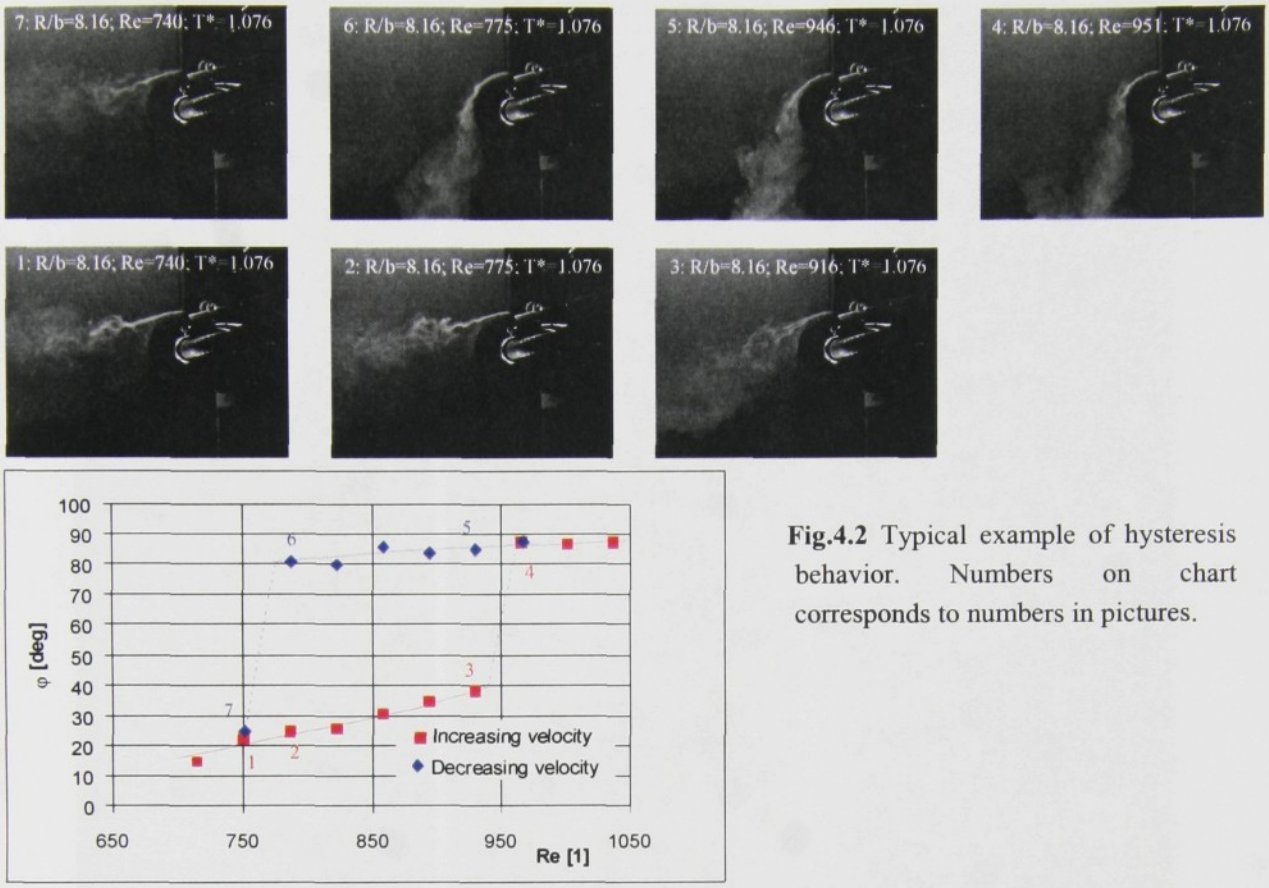

Fig.4.2 Typical example of hysteresis behavior. Numbers on chart corresponds to numbers in pictures.

the situation whether the Reynolds number was increased or decreased before the experiment itself. The Reynolds number was increased (that is to follow the red line in experiments in Fig.4.2.) so that the experiments could be comparable.

The change of velocity flow has similar a effect as the change of the temperature of the cylindrical wall. Even here it is possible to observe different behaviour of flow when heating and cooling down the wall. This phenomenon has not been observed in detail yet. The phenomenon of hysteresis has a great effect on non-isothermal experiments carried out for those *Re* that are close to Re_c. When observing the separated flow close to Re_c, even a small decrease of the wall temperature (approximately 0.1°C) leads to the attachment of the fluid flow to the wall. Separation of the flow occurs again when the wall is heated by approximately 1 °C.

4.1.2 Position of separation

The main aim of the Smoke Wire experiments was to define dependencies of the transition of flow from separated flow to attached one on the geometrical parameter *R/b* ($R/b \in \{20.00; 12.12; 10.00; 8.16; 6.78\}$) the Reynolds number and on the temperature ratio $T^* = T_w/T_\infty$ ($T^* \in \{1.000; 1.024; 1.041; 1.057; 1.074; 1.091; 1.108\}$). The Reynolds number was calculated from the inflow rate of air ($\dot{V} \in \langle 1000; 5000 \rangle$ liter/h). The flow rate was being changed after

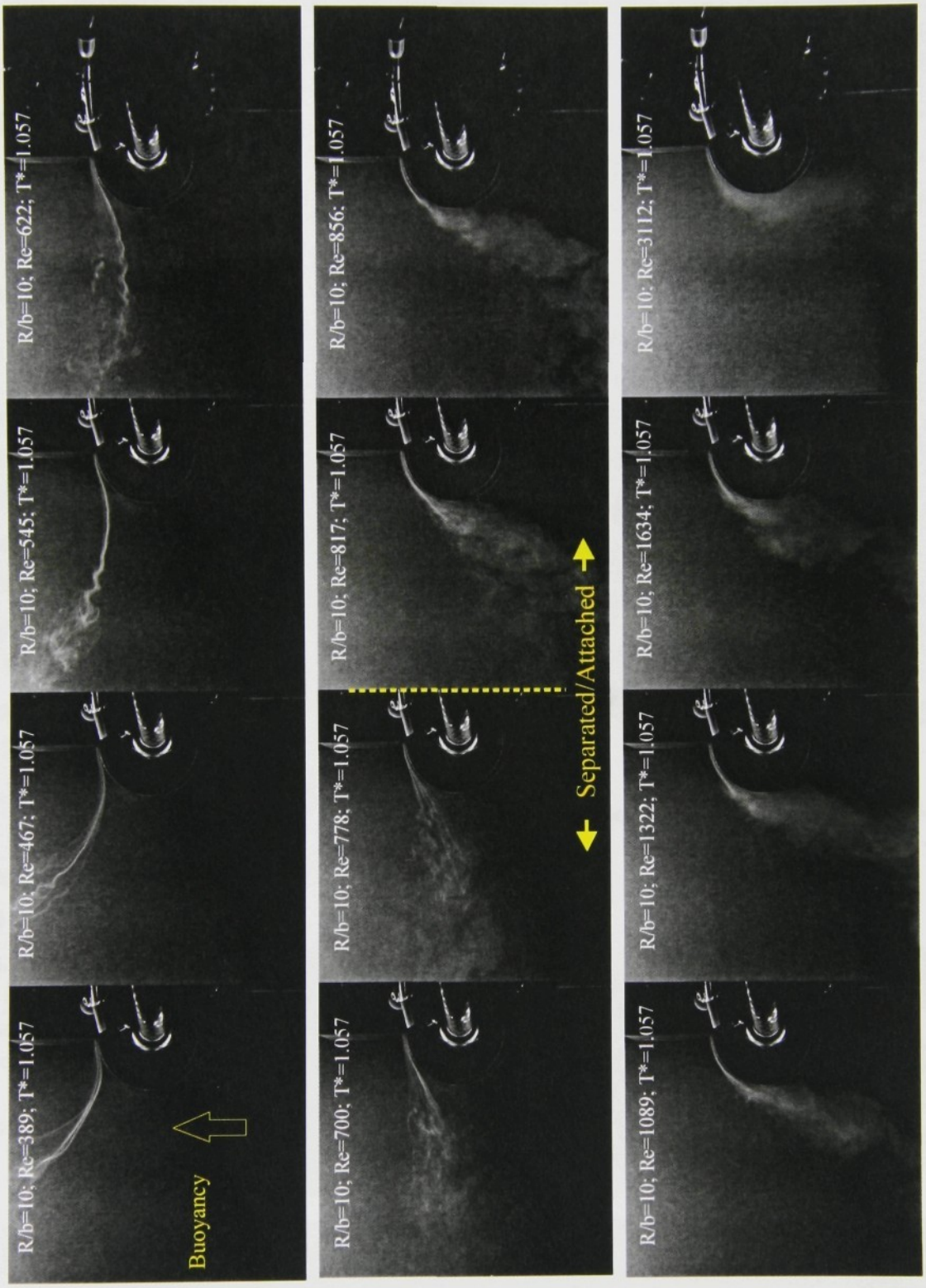

Fig.4.3 Development of flow

100 liter/h actually after 50 liter/h around the point of presumed transition. A photograph of each experiment was taken.

Approximately 1500 different states of fluid flows around the curved heated wall was observed during this stage of experiment. These series of photographs enabled a detailed analysis of the character of flow and the effects of particular factors. Out of this amount of obtained data it is possible to deduce a typical example of the development of flow for various values of the Reynolds number for: $R/b = 10$, $T^* = 1.057$, which is shown in Fig.4.3.

There is a clear buoyancy effect in the first pho-

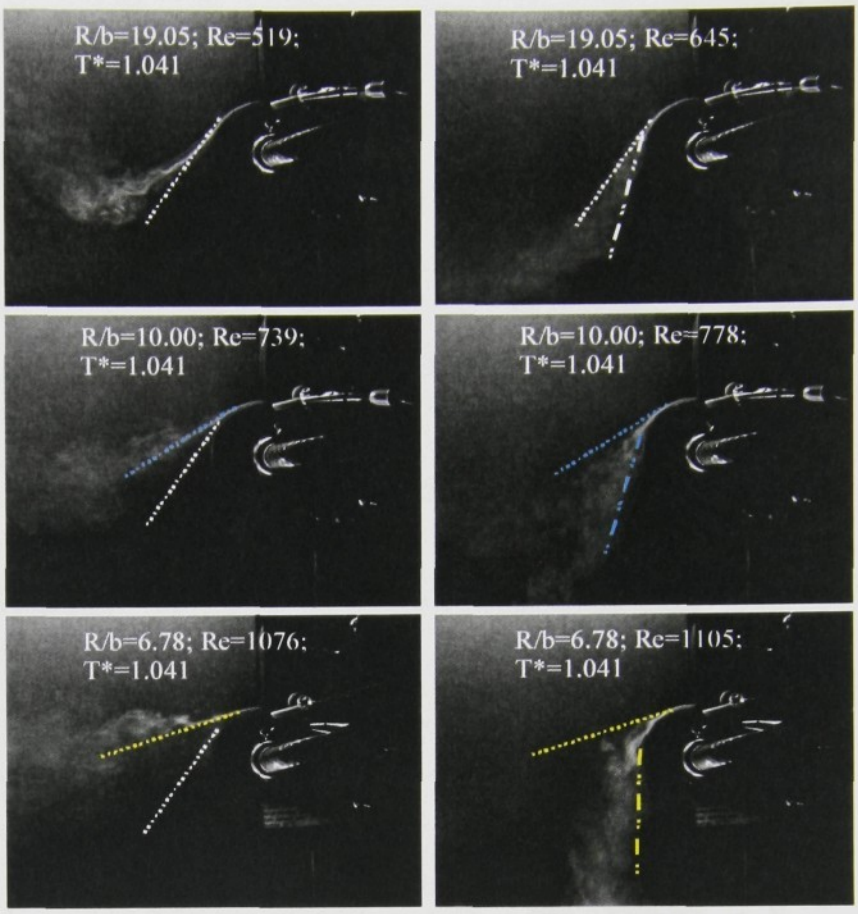

Fig.4.4 Change of separation angle with *R/b*. Separated flow on the left side, attached flow is shown on the right side. The curves that correspond to characteristic angles are plotted in pictures.

Fig.4.5 Influence of the buoyancy on the separation angle. Yellow line indicates the position of transition.

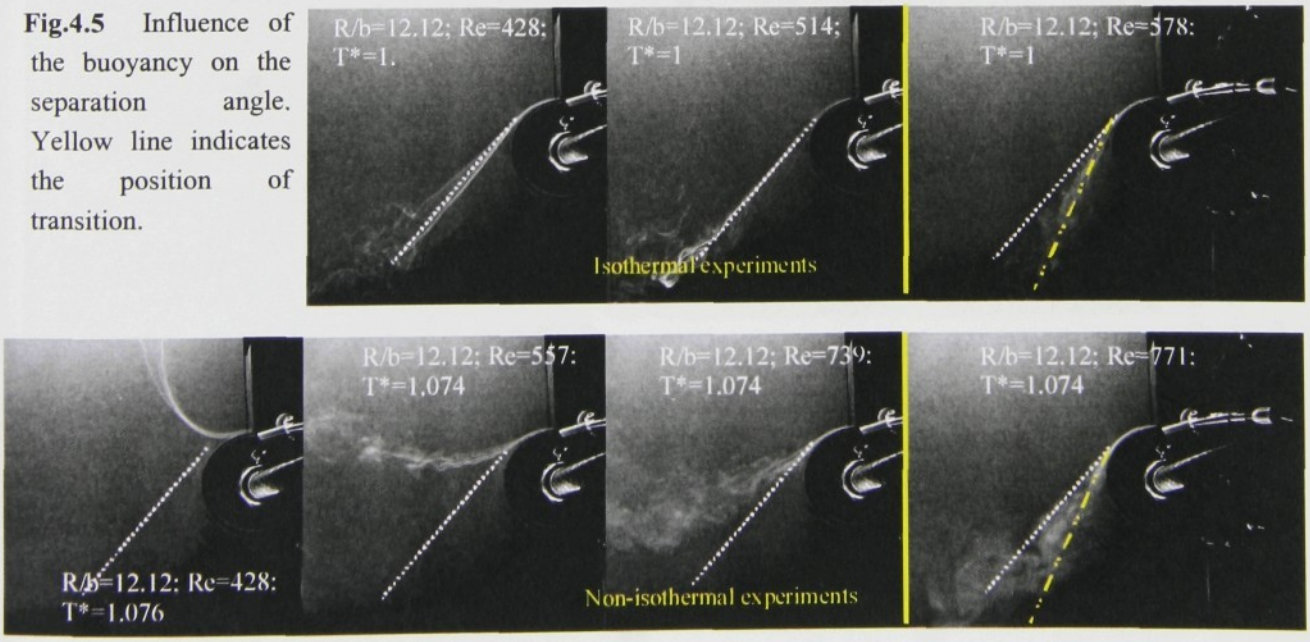

Fig.4.6 Variation of flow pattern with temperature. Upper pictures in the first and the second line show the flow pattern at $T^*=1$. Bottom pictures show flow pattern at $T^*=1.074$. The corresponding pictures are made at the same Reynolds numbers. The position of transition is marked by yellow line.

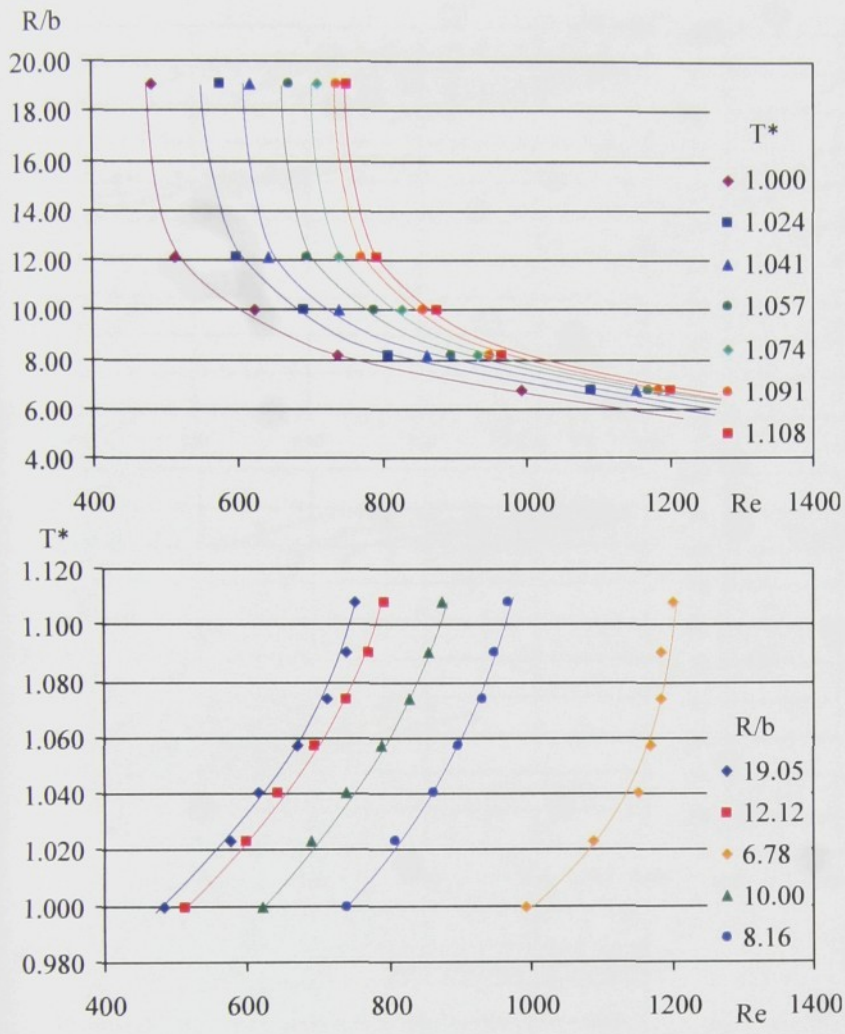

Fig.4.7 The dependence of critical Reynolds number on *R/b* ratio and on temperature ratio.

tographs which present the state of flow for small values of the Reynolds number as it is the question of flow around the heated wall. When the Reynolds number increases the buoyancy effect decreases and the laminar boundary layer follows the surface of the cylinder from which it separates at the angle of $\varphi \approx 20°$. Laminar flow remains almost unchanged up to the point of transition where a sudden change of flow occurs. The angles where the flow separates from the wall changes from the values of approximately $\varphi_s = 20°$ to values of approximately $\varphi_a = 80°$[1]. The striking increase of intensity of air entrainment is also clear after the transition and the increase of the thickness of the boundary layer is in connection to it. The limits of the use of the "Smoke wire" are clear from the last picture. Insufficient saturation of the air flow occurs at the high velocity speed.

The flow separates at the angles of about 20° for low values of *R/b*. The angles of separation of laminar flow for various values of *R/b* are shown in Fig.4.4. The accuracy of the recognition of the point of transition is affected by its position. The point of transition is prominent for low values of *R/b*, it is a sudden change of about 70°. On the other hand the transition is less evident (approximately 20°) for high values of *R/b* and precise measuring and slow incrementation of the Reynolds number were necessary to define the accurate point of the transition. Velocity of flow coming out of the nozzle has only a small effect on the angle of laminar separation.

1. The highest obtained values of φ around 100° are affected by unsuitable construction of the experimental setup in its lower part. Air flow would probably reach higher values of φ if the construction of attachment of experimental setup made it possible. Nevertheless, the aim of the experiment was not to study the character of the attached turbulent flow.

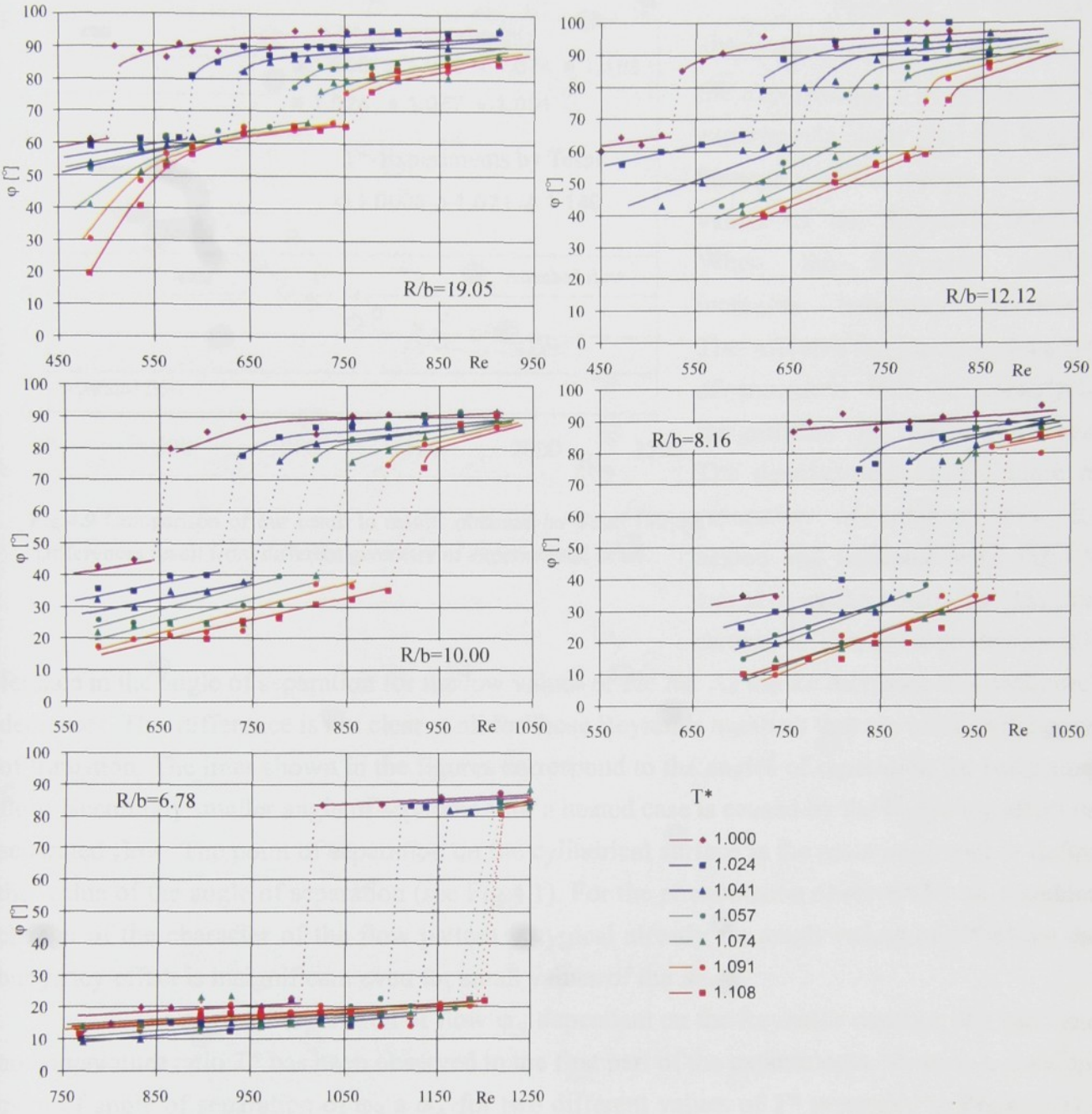

Fig.4.8 Variation of the angle of fluid separation φ on *R/b* ratio and temperature ratio. Dotted lines show expected transition from "separated" to "attached" flow.

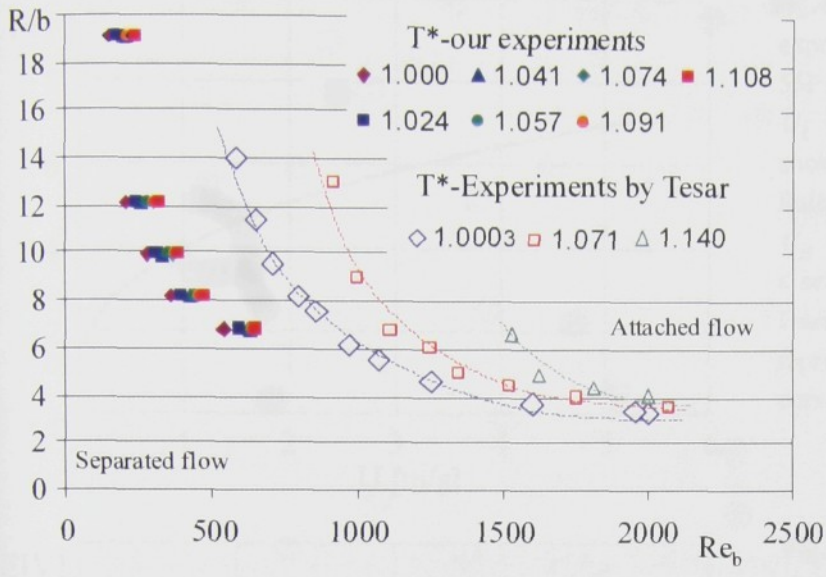

Fig.4.9 Comparison of our result to results obtained by Tesař [40]. Differences result from different geometry of experimental setup.

Presence of buoyancy affects the course and the results of the experiments. The results of the experiments show that the biggest buoyancy effect occurs for small values of the Reynolds number. When the Reynolds number increases buoyancy decreases. The effect of buoyancy in the point of transition will be considered insignificant in our experiments. The development of the angle of separation of laminar flow for heated and unheated wall Fig.4.5. can give us the reason for this presumption. There is a prominent difference in the angle of separation for the low values of the *Re*. As the Re increases this difference decreases. This difference is not clear at all for those Reynolds numbers that are close to the point of transition. The lines shown in the figures correspond to the angles of separation for isothermal flow. Seemingly smaller angle of separation for a heated case is caused by the buoyancy effect on separated flow. The point of separation on the cylindrical surface is the most important to define the value of the angle of separation (see Fig.4.1). For the phenomenon observed by us, a sudden change of the character of the flow pattern is typical already for small values of T^*,where the buoyancy effect is insignificant even for small values of the *Re*.

The angle of separation of flow φ_S dependant on the Reynolds number, *R/b* ratio and on temperature ratio T^* has been observed in the first part of the experiments. There is a development of angle of separation of φ_S a φ_A for two different values of T^* presented in Fig.4.5. The tendency which has already been described above is evident from the graphs. The decrease of buoyancy effect with the increase of the Reynolds number for the heated cases of the experiment are clearly evident here.

We get the clear idea about the development of flow if we plot the data into the graphs in Fig.4.8, where the change of the angle of fluid flow dependent on the temperature ratio T^* and Reynolds number is presented. The Reynolds number has been defined according to the relation (4.3) as in the previous figures. The Curves presented in the graphs are plotted here to make easy the orientation among the results and to represent the presumed development of flow.

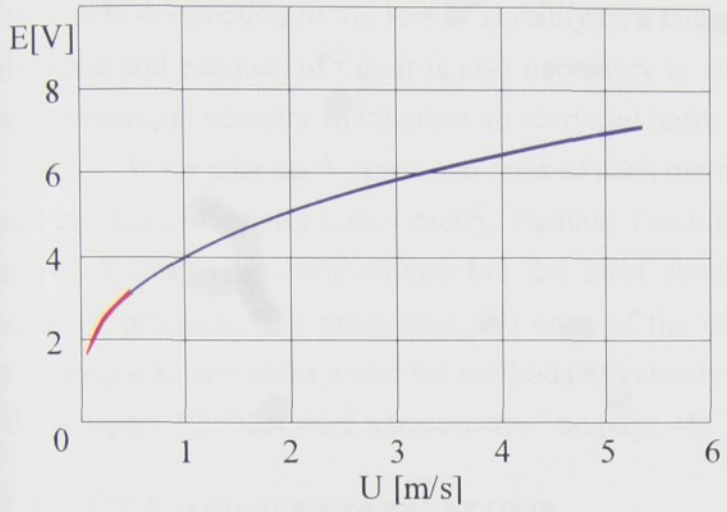

Fig.4.10 Calibration curve of velocity for experiments carried out by CTA (DANTEC 55P11) probe. Calibration curve $U_L = 0.114E^3 - 0.18E^2 + 0.33E + 0.057$ was chosen for velocity range $U_L \in (0.05,0.5)\,\mathrm{ms}^{-1}$ Suitable calibration curve $U_H = 0.003E^4 - 0.03E^3 + 0.25E^2 - 0.20E + 0.39$ was selected for velocity range $U_H \in (0.5,5)\,\mathrm{ms}^{-1}$ During the experiments calibration was reproduced several times, the final calibration curves were almost identical

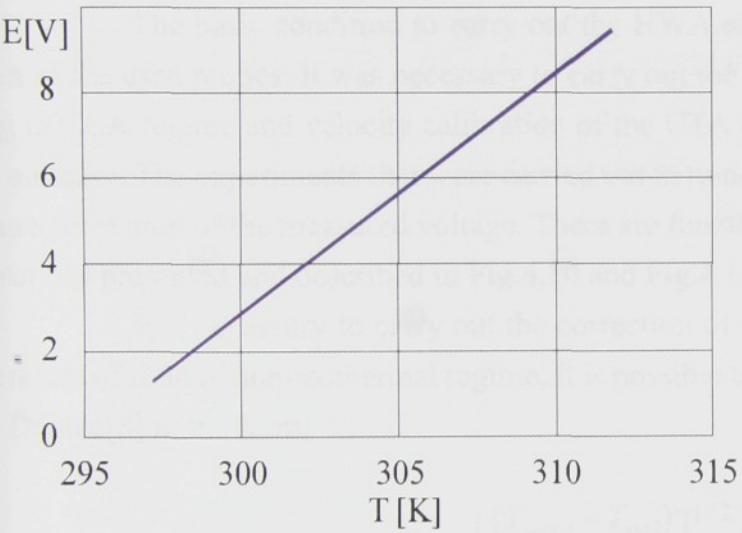

Fig.4.11 Calibration curve of temperature for CCA probe measuring (DANTEC 55P11). Linear function is described by the equation $T = 1.79E + 21.74$. Here the calibration was reproduced during the experiments several times as well and the results were also almost identical

The position of critical Reynolds number dependence on the temperature and *R/b* ratio is plotted in Fig.4.7. The slowing down of the increase of the critical Re value with the increase of the temperature gradient is evident here. The dependency measured by us is compared to the values published in Tesař[44] plotted in Fig.4.9. Our results are different from those published earlier which can probably be caused by a different geometric setup. It is clear from Fig.4.9 that the observed dependencies *Re* on *T** and *R/b* are identical in the case of both experiments. Unfortunately, the results according to Tesař[44] do not show results for many temperature gradients.

4.2 HWA measurements

The Smoke Wire experiments give us good idea about the behavior of flow with the changing temperature gradient. But if we want to try to understand the observed phenomenon more closely we have to get a more detailed information about the form and the development of the velocity profile. According to the Smoke Wire experiments we can presume that the transition

of flow is in connection to the loss of stability of a laminar boundary layer and to the transition to turbulence and because of this it is also necessary to study the development of turbulent quantities, for example velocity fluctuation, to carry out more complex conclusions.

If we take all the pros and cons of each method used nowadays into consideration, we could use Laser-Doppler anemometry, Particle Tracking Velocimetry, Particle Imaging Velocimetry and Hot Wire Anemometry but the most suitable method for us seemed to be HWA. The basic principle, the main pros and cons of the use of HWA method for fluid flow along the heated wall and notes about the methods of velocity and temperature calibration are presented in the Chapter 3.2 "Hot wire anemometry" on page 48.

4.2.1 CTA temperature calibration

The basic condition to carry out the HWA experiments properly is a precise calibration of the used probes. It was necessary to carry out the temperature calibration of probe operating in CCA regime and velocity calibration of the CTA probe operating in isothermal fluid flow in our case. The experiments that were carried out in non-isothermal regime also required temperature correction of the measured voltage. There are functions for the temperature and velocity calibrations presented and described in Fig.4.10 and Fig.4.11.

It is necessary to carry out the correction of the output voltage according to the temperature of fluid in non-isothermal regime. It is possible to derive the voltage correction according to Dantec[8] in the form:

$$E = \left[\frac{(T_{wire} - T_{cal})}{(T_{wire} - T)}\right]^{1/2} E_{acq} \tag{4.4}$$

where E_{acq} is the voltage measured at temperature of fluid T. T is temperature which is measured by the CCA probe. T_{cal} is air temperature measured during the calibration of the velocity probe and T_{wire} is the temperature of the wire. The temperature of the wire is usually not known exactly so it is more suitable to use the relation with the overheat ratio a_h instead of T_w:

$$E = \left[a_h / \left(a_h + \frac{\alpha_{20}}{1 + \alpha_{20}(T_{cal} - 293)}\right)\right](T - T_{cal})^{1/2} E_{CC} \tag{4.5}$$

where α_{20} is sensor temperature coefficient of resistance at 20°C.

Temperature difference $(T - T_{cal})$ reaches maximally 15°C in our experiments. It is evident, on the basis of the forms mentioned above, that the maximum error which can be made by neglecting the temperature correction is approximately about 2%. It would be possible to neglect such an error mainly if it is of the same order as the calibration error (cca. 1%) but because

the temperature was recorded during the experiment, the temperature correction was carried out during the evaluation as well.

4.2.2 Unheated regime

The first aim during HWA experiments was to measure velocity profiles and turbulent quantities for unheated regime. For obvious reasons it was not possible to carry out the experiments for a wide range of parameters, not as wide as in the Smoke Wire Experiments. That is why the experiments were limited to measuring the velocity profiles only in particular selected states. Except several sets of experiments, the aim of which was to measure the development of the velocity profiles along the whole cylindrical wall Fig.4.12, mostly velocity profiles at the positions before the separation of flow and at the positions after separation of flow in the case of attached flow were measured. With regard to the magnitude of the critical Reynolds number, the flow rate of air was set. It was found out from the results of the Smoke Wire experiments that if the R/b ratio is rather small, the transition to attached flow is significant and the decrease of buoyancy effect occurs. For this reason R/b ratio for the HWA experiments was selected as $R/b = 8$ in most experiments.

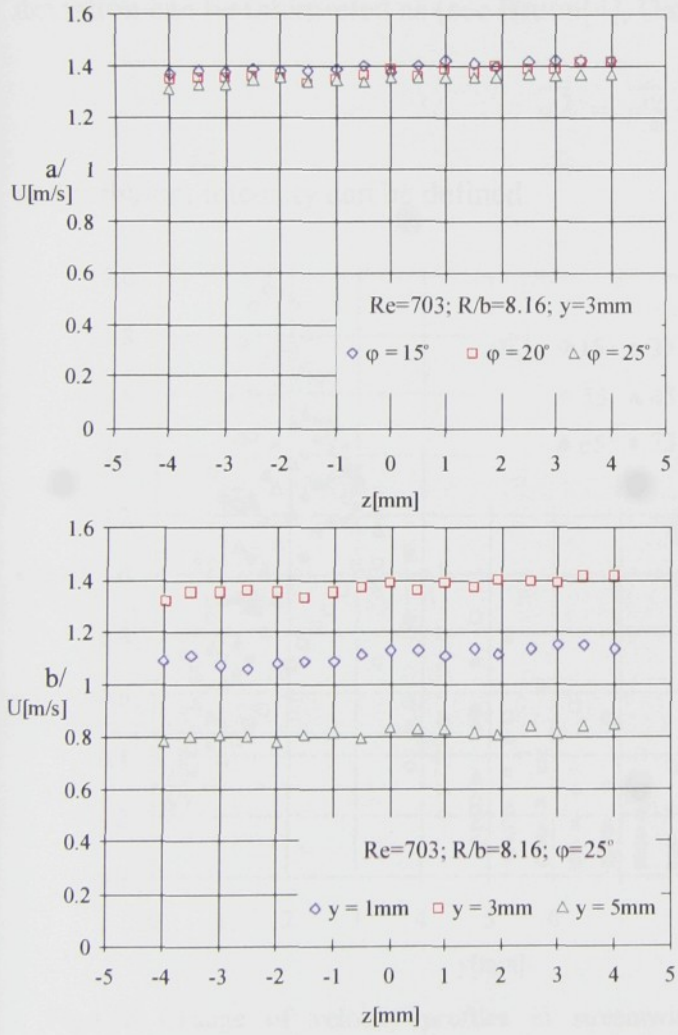

Single wire probes were used during the experiments and it was not possible to measure two components of velocity[1]. Owing to the used attachment of the probe and on condition that the magnitude of the radial component of velocity $U_r \approx 0$ (it is not valid in

Fig.4.12 Measured values of velocity in lengthwise direction a/ *U[m/s]* measured 3mm from the wall in the positions φ=15;20;25°. b/ *U* measured in positions φ=20° 1;3;5 mm from the wall.

1. Possible use of an inclined single wire probe to measure two components of velocity is limited by the size of the probes in our setup

the positions close to the point of separation), the component of the velocity vector measured by us will be interpreted as the tangential component of the velocity U_φ

The method of measuring the fluctuating part of the velocity is more questionable. A standard deviation from the recorded velocity

$$\sigma^2 = \frac{\sum (U_i - \bar{U})^2}{n-1} \tag{4.6}$$

is usually interpreted as the magnitude of the mean square value of the fluctuating part of velocity u'. In our case the probe is affected both by u_φ' fluctuations and by the radial component of fluctuations u_r' which are more important for the development of flow. With a certain inaccuracy the sensitivity of the probe can be considered almost the same for velocity range selected by us both in radial as well as in tangential directions. According to the relation (4.6) the calculated standard deviation can be interpreted as (see Bruun[4], Dantec[8])

$$\overline{u'^2} = \overline{u'^2_\varphi} + \overline{u'^2_r} \tag{4.7}$$

and turbulent intensity can be defined

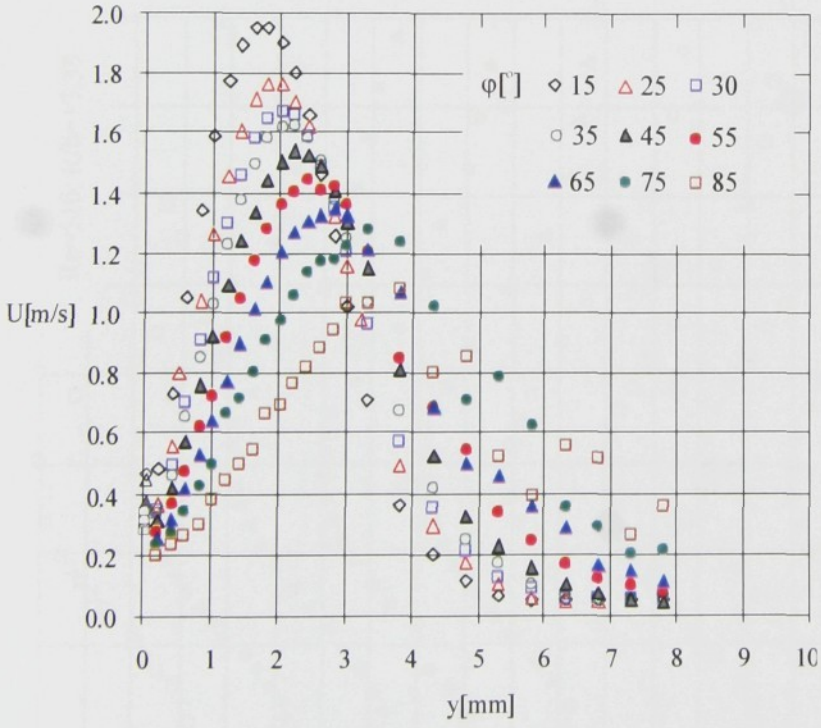

Fig.4.13 Change of velocity profiles in streamwise direction. *Re*=510; *R/b*= 13.33.

$$TI = \frac{\overline{u'^2}}{U^2} \tag{4.8}$$

The concept of the magnitude of the individual components of velocity fluctuations can be obtained from the experiments published in literature (see Guitton[14]).

Sensitivity of a hot wire probe in lengthwise (z) direction is very small and that is why it is possible to neglect the effect of u_w' component.

It was considered appropriate to carry out the measuring that would verify two-dimensionality of flow during the first

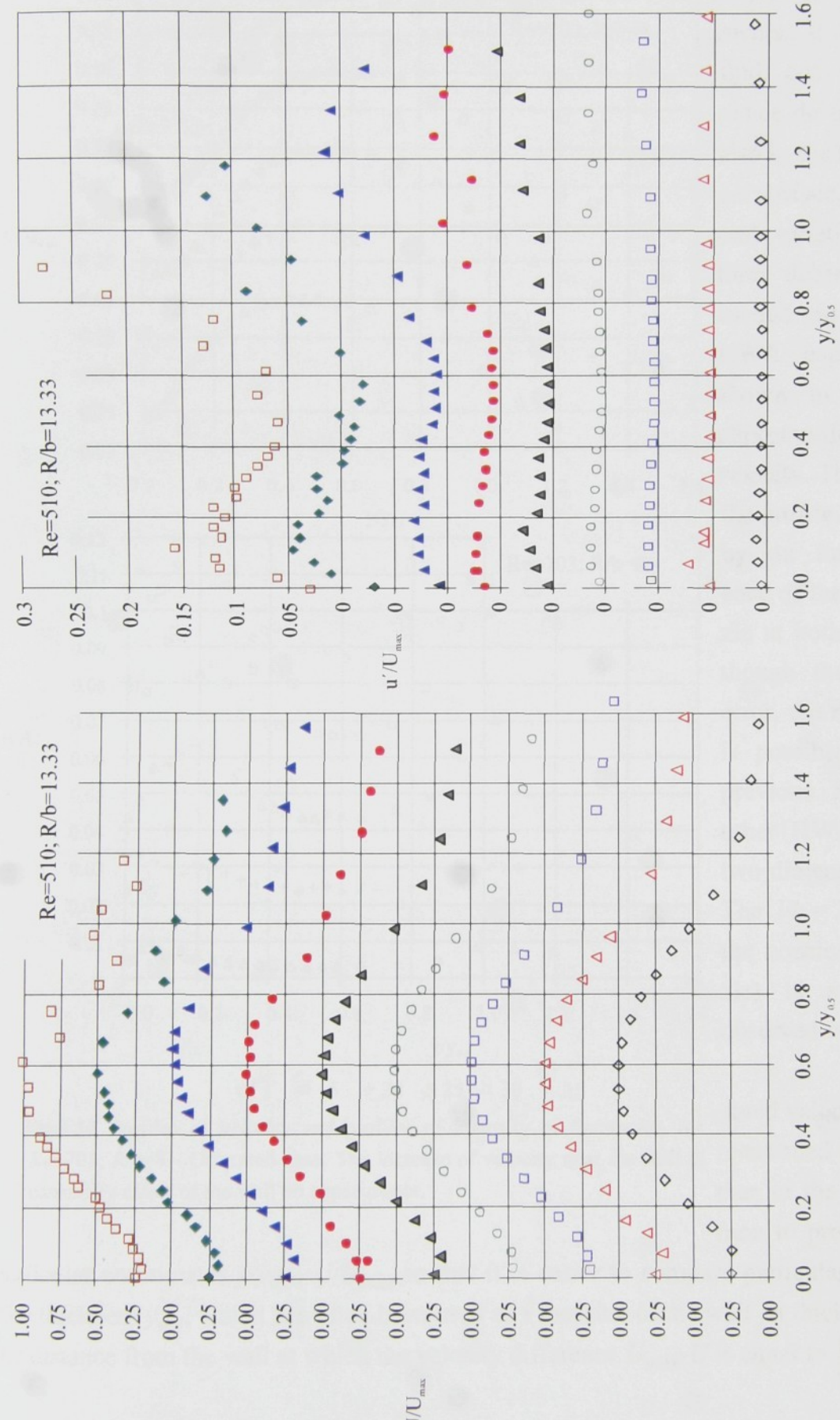

Fig.4.14 Profiles of velocity and profiles of intensity of fluctuation for *Re*=510; *R/b*=13.33 - Unheated case.

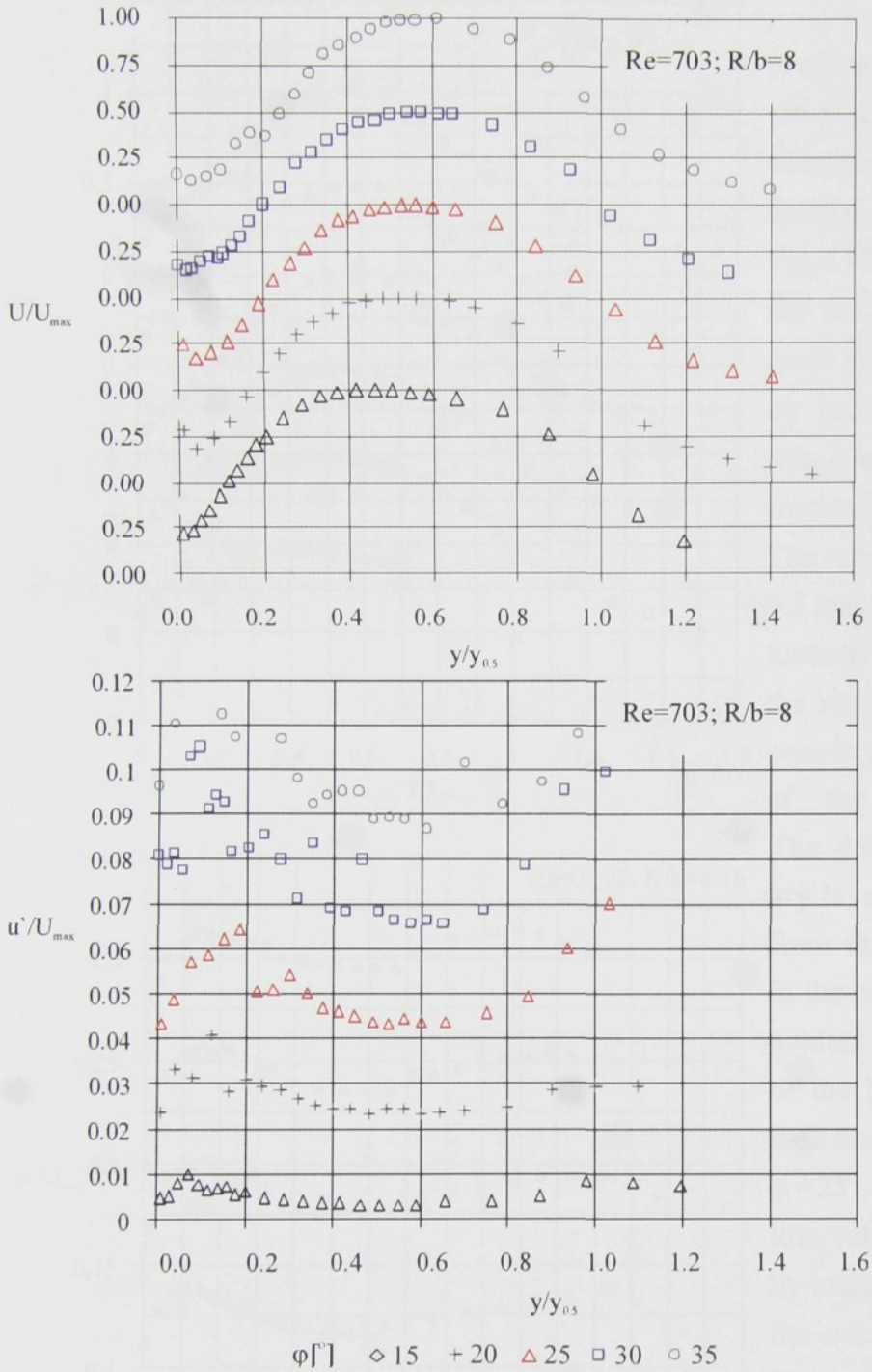

Fig.4.15 Profiles of velocity and profiles of intensity of fluctuation for *Re*=703; *R/b*=8 - Unheated case. The increase of velocity near the wall is caused by effect of the wall on experiments.

phase of the HWA experiments. It was necessary to find out whether the end plates do not effect the flow also in the middle of cylindrical surface. Measuring of lateral variation of velocity in three different positions was carried out in the first of the HWA experiments. Results shown in Fig.4.12 present almost uniform distribution of velocity. The evident slope of the profile is probably caused by an insignificant difference of the width of the nozzle at both end plates. Even though there is this minor error, the results show that it is possible to consider the previous Smoke Wire and other HWA experiments as two-dimensional ones. The $l/b = 20$ ratio (length of the nozzle/width of the nozzle) is sufficient for the observed velocity range

Some of the measured velocity profiles will be mentioned and described further in the thesis. It is common to present the results in particular coordinates $y/y_{0.5}$, U/U_{max} so that it is easier to compare particular velocity profiles. The thickness $y_{0.5}$, which has often been used as a measure of the wall jet thickness, is defined as the distance from the wall at which the velocity difference U_{max}-U is equal to $\frac{1}{2} U_{max}$.

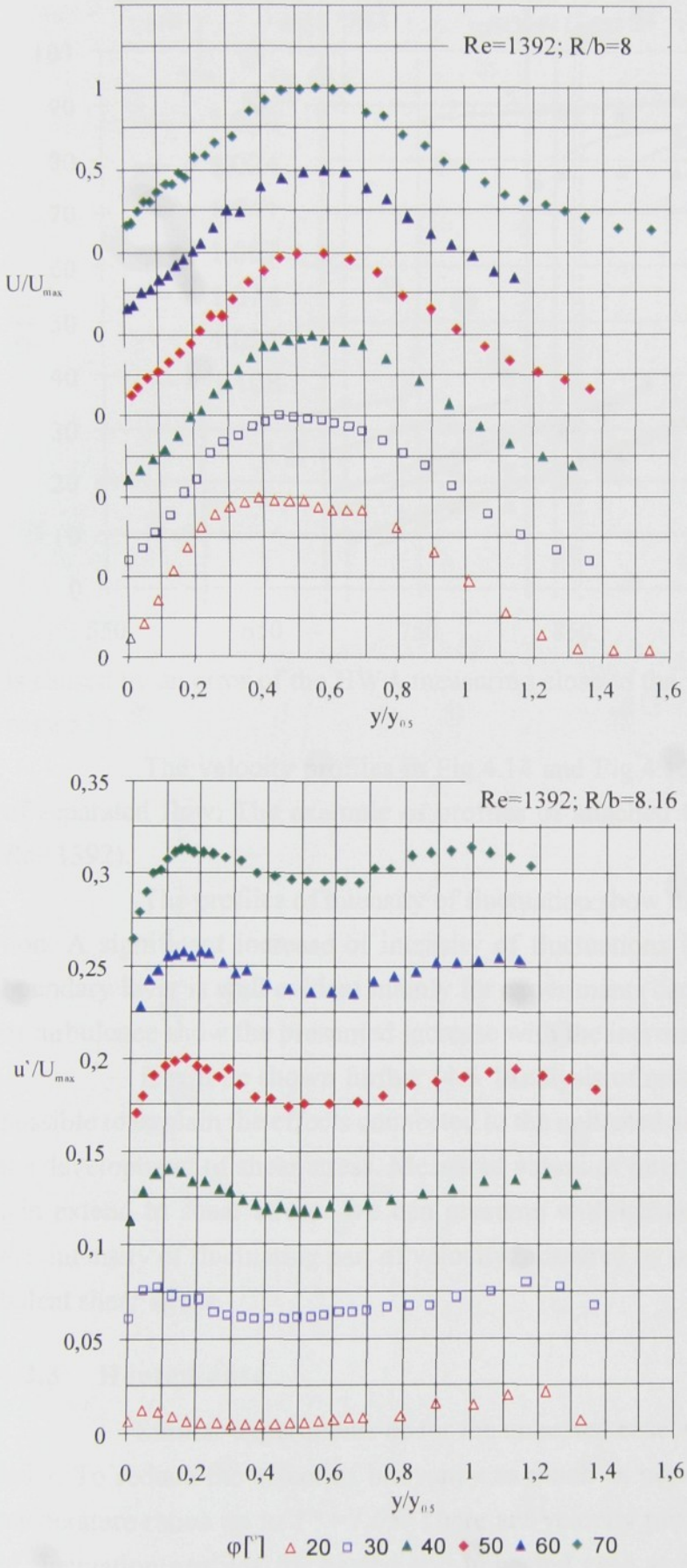

The measured velocity profiles for $Re = 674$ and $R/b = 13.33$ ratios are presented in Fig.4.14. The comparison of the measured and calculated values is carried out in Fig.4.32. The correspondence of the measured and calculated values is quite good. There are measured velocity profiles (in coordinates U/U_{max} - $y/y_{0.5}$) and corresponding intensities of fluctuations presented in Fig.4.15. The velocity profiles were shifted by 0.5 and the profiles of intensity of fluctuations were shifted by 0.05 to make the results clearer. A similar shift of axes in graphs was carried out in most of the further published graphs. The development of a laminar boundary layer in the stream-wise direction from the nozzle is well distinguished in the presented velocity profiles. It is evident for $R/b = 8$ that the inner part of the boundary layer is affected by the nozzle even for the position $\varphi = 25^{o}$. Earlier separation of flow for low values of R/b is probably caused by under developed velocity profile in the outer part of the boundary layer. The velocity near the wall does not decrease to the presumed zero value. It

Fig.4.16 Profiles of attached flow. Re=1392; R/b=8. For this value of Re the flow remains attached up to 90^{o}

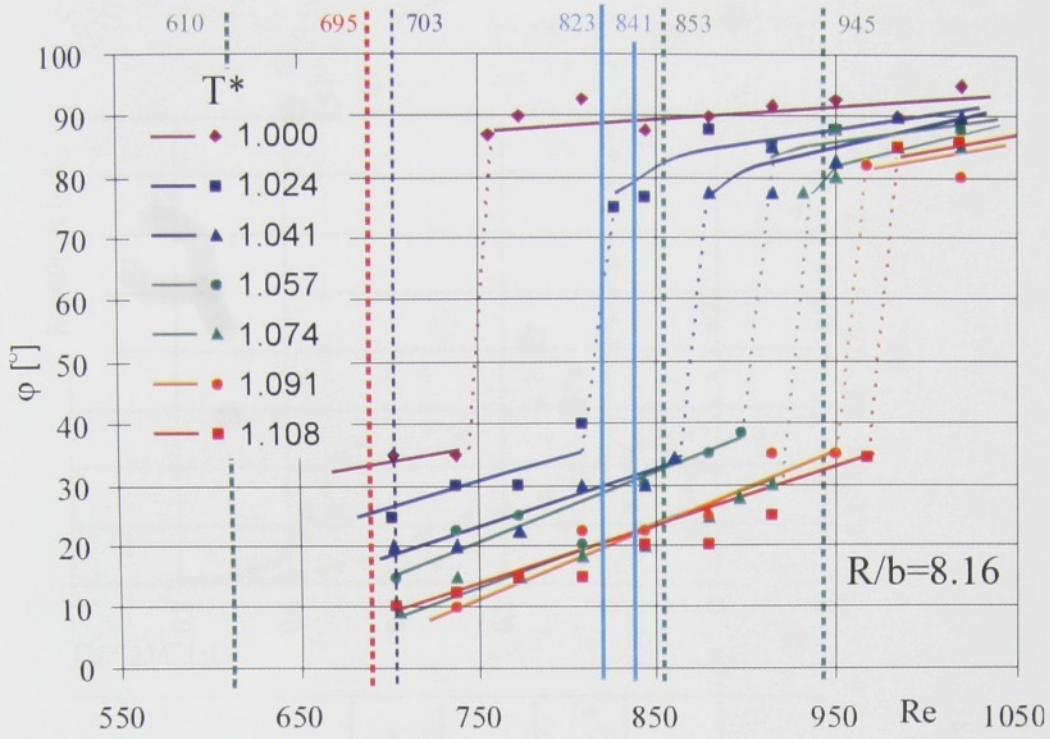

Fig.4.17 Comparison of "Smoke-Wire" and CTA results. Lines with numbers shows Re from next pictures: Dark blue line Fig.4.15; Red line Fig.4.18; Blue line Fig.4.19; Green line Fig.4.22;

is caused by an error of the HWA measuring close to the wall (See "Measuring near the wall" on page 53.)

The velocity profiles in Fig.4.14 and Fig.4.15 represent typical examples of profiles of separated flow. The example of profiles of attached flow are presented in Fig.4.16 (R/b=8, Re=1392).

The profiles of intensity of fluctuation show that it is closely up to the point of separation. A significant increase of intensity of fluctuations in the point of separation of a laminar boundary layer is well evident mainly for experiments carried out at R/b=8. Measured intensities of turbulence show the presumed increase with the increase of the Reynolds number.

It will be shown further (4.6 "Analysis of results" on page 103) in the thesis that it is possible to explain the effects connected to the unheated and heated curved wall jet on the basis of the development of shear stress. Measured values of intensity of fluctuations correspond to a certain extend to shear stress. We can presume with certain inaccuracy that the higher values of the intensity of fluctuating part of velocity measured by us correspond to the higher values of turbulent shear stress.

4.2.3 Heated case

Similar experiments as for the unheated case were carried out even for the heated cylinder. To reduce the effect of buoyancy as much as possible we carried out the experiments at temperature ratios up to $T^*=1.05$. There are velocity profiles, temperature profiles and intensity of fluctuation profiles for heated and unheated case at $Re=701$ in Fig.4.18. The difference of

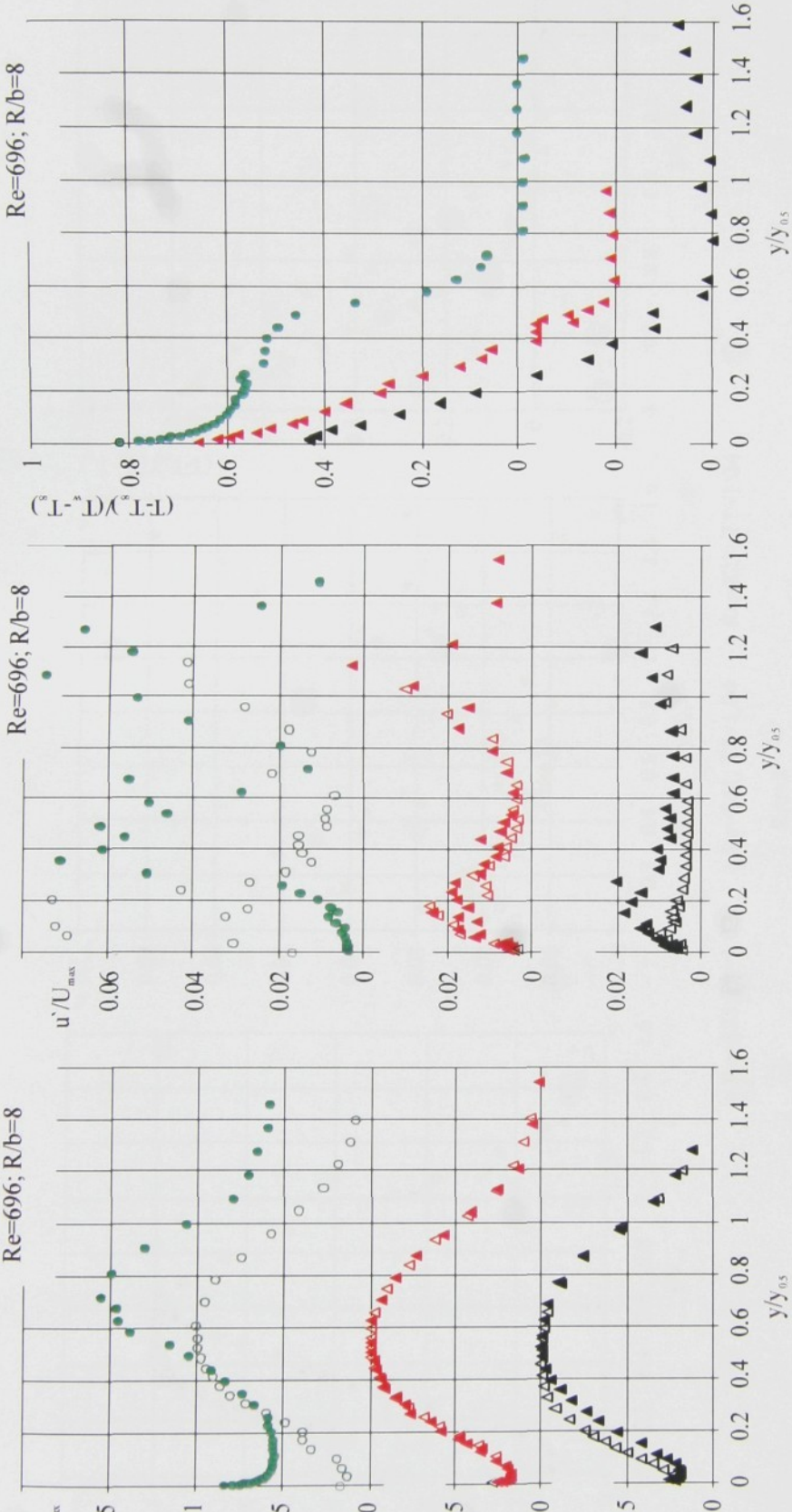

Fig.4.18 Variation of velocity profiles with change of temperature ratio.

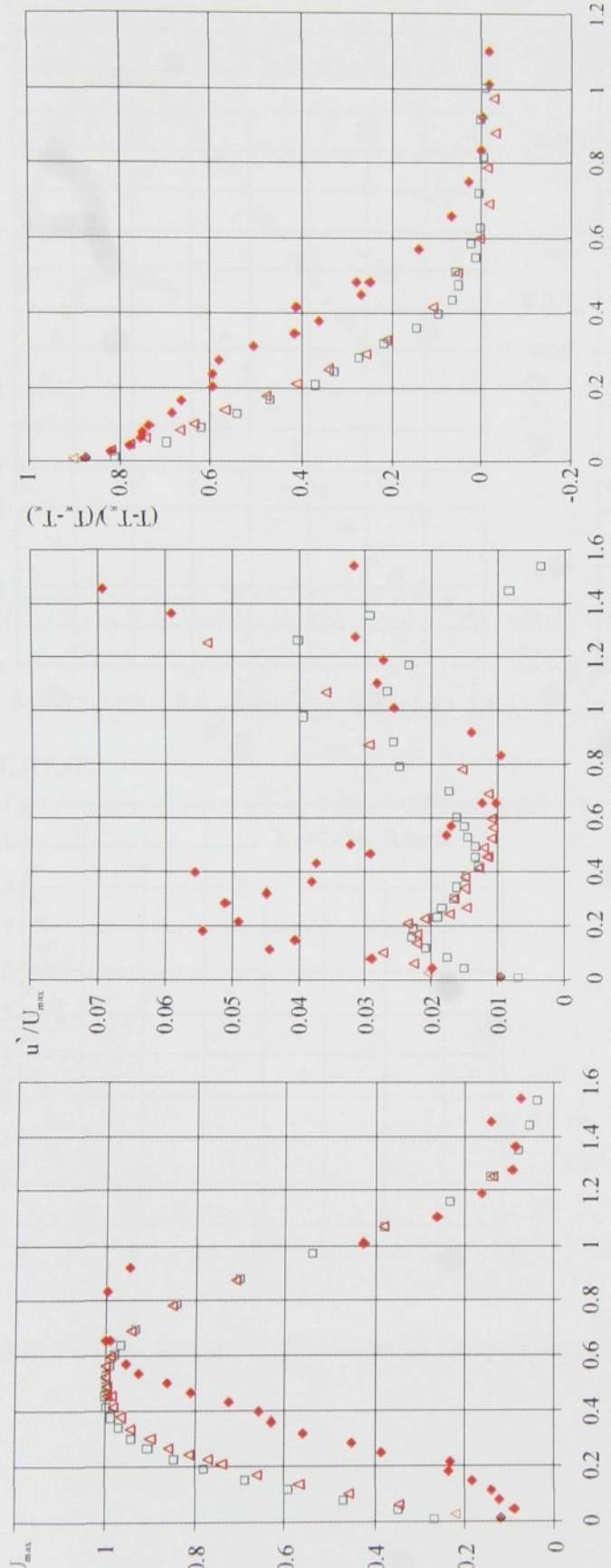

Fig.4.19 Effect of temperature ratio and of Reynolds number on character of flow. It is clear, that small increase of temperature ratio and decrease of velocity lead to change of flow pattern from atached to separated state.

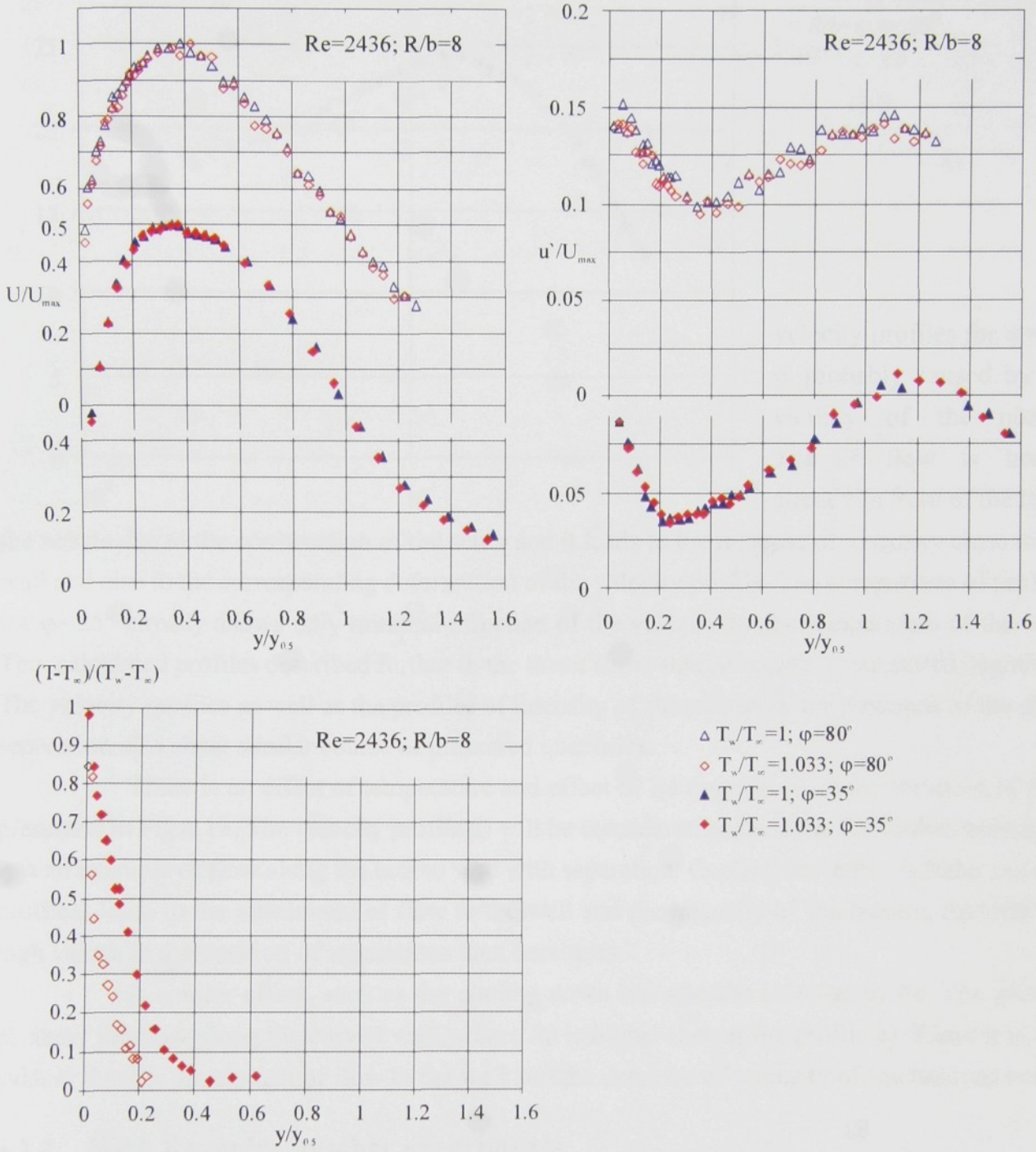

Fig.4.20 Velocity, intensity of fluctuations and temperature profiles measured at high *Re* (*Re*=2436).

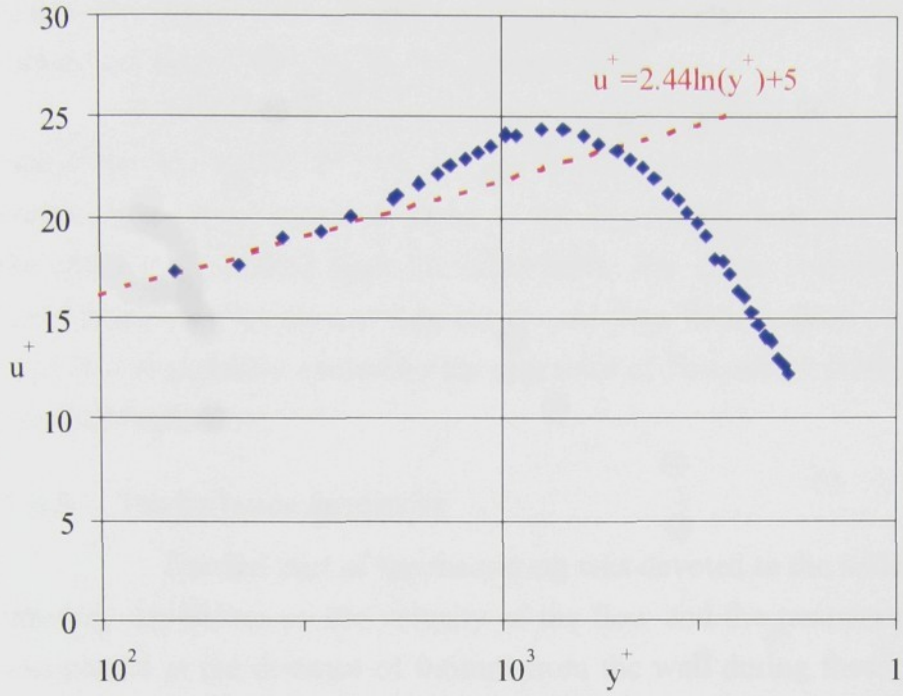

Fig.4.21 Velocity profiles in wall coordinates Re=2436; R/b=8; φ=80°

velocity profiles for φ=15° is probably caused by the vicinity of the nozzle. The air flow is heated already in front of the lip of the nozzle due to the construction of the setup and it leads to the increase of viscosity close to the wall and also to the corresponding deformation of the velocity profile. The comparison of profiles for φ=25° already shows only minimal affection of the velocity by the temperature of the wall. The calculated profiles described further in the thesis show similar course of measured quantities. The velocity profiles as well as the profiles of intensity of fluctuation in the positions of the flow separation also show similar course of measured quantities.

There is an effect of temperature and effect of Re magnitude on the variation of flow presented in Fig.4.19. The velocity profile a) will be considered as the basis for further deduction. It is an example of flow along the heated wall with separation. Cooling down the cylinder wall (b) profiles) leads to the attachment of flow to the wall and the intensity of fluctuation, that reached high values in the position of separations then decreases.

A similar effect, such as the cooling down has also the increase of *Re*. The profiles c) show the flow along the curved wall, where *Re* is higher than at the profile a). There it is also evident that the attachment of flow to the wall and the decrease of intensity of fluctuations occur.

4.2.4 High Reynolds number experiments

There are the results of experiments carried out for rather high values of the Reynolds number which corresponds to the transition from separated to the attached flows presented in Fig.4.20.

The velocity profiles for high values of *Re* were also measured for various values of temperature ratio T^*. It is evident from the results of the experiments that the effect of tempera-

ture on the shape of the velocity profile as well as on the value of intensity of fluctuations is insignificant for high values of the Reynolds number.

Turbulent velocity profiles are usually expressed in coordinates $u+; y+$[1]. The velocity profile for $Re = 2436; T^* = 1; \varphi = 80^o$ is plotted in Fig.4.21. It can be observed that the velocity profile in an inner region is close to the logarithmic law of the wall which is represented by the red line. Deviation from the logarithmic law of the wall the validity of which was proven many times even for the curved wall jet case (See "Inner region - Models for a boundary layer" on page 39.) is probably caused by the character of flow which cannot be considered as fully developed turbulent flow.

4.2.5 Turbulence intensity

The last part of the measuring was devoted to the detection of variation of turbulence intensity dependent on the velocity of the flow and the temperature ratio (Fig.4.22). The probe was placed at the distance of 0.6mm from the wall during these measurements ($R/b = 8$) and it was rotated around the center of rotation of the cylindrical surface during the measurements. Velocity and turbulence intensities were measured for various magnitudes of angle φ. The measurement carried out in a position corresponding to some of the characteristic points of the velocity profiles would be more accurate because the development of the velocity profile occurs in the streamline direction along the circumfluenced wall. It is evident from Fig.4.14 that the good choice would be, for example, the position $y_{0.1}$, which corresponds to the proximity from wall in which the magnitude of velocity reaches $0.1\,U_{max}$ and where the intensity of fluctuations reaches the highest values. The certain difficulties in comparing the results are compensated by the simplicity and relatively high applicability of this method.

The measured results of the turbulence intensity show the development of the flow character along the circumfluenced wall. A laminar character of the flow is evident close to the nozzle and the measured fluctuations do not exceed the values corresponding to the inaccuracy of measuring. A significant increase of the turbulence intensity starts to occur at the angle of approximately 40° and for the angles exceeding 80° it is already possible, owing to the magnitude of the measured turbulence intensity, to consider the flow as turbulent. The effect of heating the wall on the development of the velocity profile is also evident from Fig.4.22. The effect of heating the wall on the values of the turbulence intensity is neglected for the observed ratio T^* and Re.

The results of experiments, where the separation of flow occurs, show a laminar character up to the position close to the point of separation where a sharp increase of the turbulence

1. See footnote *1* on page 39

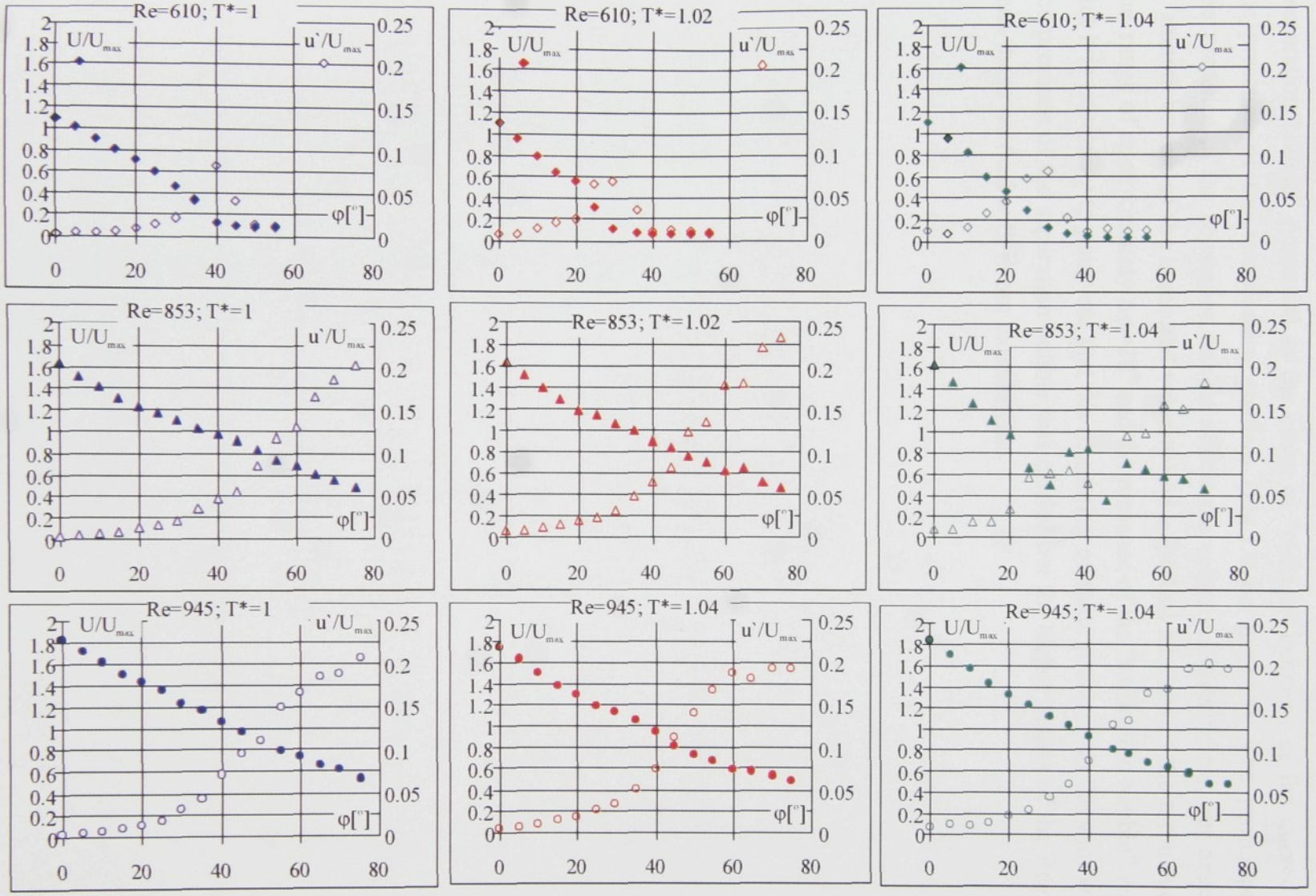

Fig.4.22 Variation of velocity and intensity of fluctuations in streamvice direction with the change of *Re* (from top to bottom) and temperature ratio (from left to right). The positions of separation and region of transition to turbulence is clearly visible.

intensity occurs. It corresponds to a gradual increase of radial components of the velocity fluctuations after the separation of the flow and to the loss of a dumping effect of the wall.

These experiments should originally have helped to define the position of a so called "separation bubble" presented as the cause of "strange" behavior of the curved wall jet with the presence of the temperature gradient (Fig.1.9 on page 13). The presumption was that the presence of the separation bubble affects the velocity. Nevertheless, our experiments show a smooth course of the measured velocity and a gradual increase of the turbulence intensity at the range of approximately $\Delta\varphi=20^{o}$ and the presence of the "separation bubble" was not proven. But it is necessary to point out that the measuring of static pressure on the wall which indicates the presence of the separation bubble was carried out for higher values of the Reynolds number than those we deal with in our experiments.

4.3 Similarity solution

The derivation of the similarity solution for a laminar heated curved wall jet is presented in this chapter. The derivation of this solution for an unheated case was published in Wygnanski[52]. The solution presented there will be extended so it could be used for the flow along the heated or cooled wall.

If we take into consideration only a thin boundary layer the momentum equation for two-dimensional fluid along the curved wall with the constant curvature R can be in curvilinear orthogonal coordinates written in the form as (Goldstein[13]):

For longitudial direction x:

$$v_x\frac{\partial v_x}{\partial x}+\left(1+\frac{y}{R}\right)v_y\frac{\partial v_x}{\partial y}+\frac{v_x v_y}{R}=-\frac{1}{\rho}\frac{\partial p}{\partial x}+\nu(T)\left[\frac{1}{\left(1+\frac{y}{R}\right)}\frac{\partial^2 v_x}{\partial x^2}+\left(1+\frac{y}{R}\right)\frac{\partial^2 v_x}{\partial y^2}\right. \tag{4.9}$$

$$\left.+\frac{1}{R}\frac{\partial v_x}{\partial y}-\frac{v_x}{R^2\left(1+\frac{y}{R}\right)}+\frac{2}{R\left(1+\frac{y}{R}\right)}\frac{\partial v_y}{\partial y}\right]+\frac{d\nu}{dy}\left[\left(1+\frac{y}{R}\right)\frac{\partial v_x}{\partial y}-\frac{v_x}{R}+\frac{\partial v_y}{\partial x}\right]$$

For normal direction y:

$$v_x\frac{\partial v_y}{\partial x}+\left(1+\frac{y}{R}\right)v_y\frac{\partial v_y}{\partial y}+\frac{v_x v_x}{R}=-\left(1+\frac{y}{R}\right)\frac{1}{\rho}\frac{\partial p}{\partial y}+\nu(T)\left[\left(1+\frac{y}{R}\right)\frac{\partial^2 v_y}{\partial y^2}-\frac{v_y}{R^2\left(1+\frac{y}{R}\right)}\right. \tag{4.10}$$

$$\left.+\frac{1}{R}\frac{\partial v_y}{\partial y}+\frac{1}{\left(1+\frac{y}{R}\right)}\frac{\partial^2 v_y}{\partial x^2}-\frac{2}{R\left(1+\frac{y}{R}\right)}\frac{\partial v_x}{\partial x}\right]+\frac{d\nu}{dy}\left[\left(1+\frac{y}{R}\right)\frac{\partial v_y}{\partial y}\right]$$

In a similar system of coordinates the continuity equation can be written in the form

$$\frac{\partial v_x}{\partial x}+\frac{\partial}{\partial y}\left[\left(1+\frac{y}{R}\right)v_y\right]=0 \tag{4.11}$$

We also have to solve the equation for heat transfer together with the equations mentioned above. For curvilinear system of coordinates this equation can be in the form

$$v_x \frac{\partial T}{\partial x} + \left(1 + \frac{y}{R}\right) v_y \frac{\partial T}{\partial y} = \frac{\lambda(T)}{c_p(T)\rho(T)} \left[\left(1 + \frac{y}{R}\right) \frac{\partial^2 T}{\partial y^2} + \frac{1}{R} \frac{\partial T}{\partial y} \right] \tag{4.12}$$

There is $R>0$ for convex curvature of the wall and $R<0$ for concave curvature of the wall in the equations mentioned above. If we presume a characteristic jet width b small in comparison with R, the above equations may be simplified by retaining terms to order b in the equation (4.9) and (4.11) and to order unity in the equation (4.10).

Non-dimensional quantities can be defined (similar as in Wygnanski[52])

$$\tilde{v}_x = \frac{v_x}{U_{Ref}}, \tilde{v}_y = \frac{v_y}{U_{Ref}}, \tilde{x} = \frac{x U_{Ref}}{\nu_{20}}, \tilde{y} = \frac{y U_{Ref}}{\nu_{20}}, \tilde{R} = \frac{R U_{Ref}}{\nu_{20}}, \tilde{p} = \frac{p}{\rho U_{Ref}^2},$$

$$\Theta = \frac{T - T_w}{T_\infty - T_w} \tag{4.13}$$

where ν_{20} corresponds to kinematic viscosity at 20°C and U_{Ref} is a reference velocity.

The equations (4.9) - (4.12)can be written in the form

$$\tilde{v}_x \frac{\partial \tilde{v}_x}{\partial \tilde{x}} + \left(1 + \frac{\tilde{y}}{\tilde{R}}\right) \tilde{v}_y \frac{\partial \tilde{v}_x}{\partial \tilde{y}} + \frac{\tilde{v}_x \tilde{v}_y}{\tilde{R}} = -\frac{1}{\rho} \frac{\partial \tilde{p}}{\partial \tilde{x}} + \frac{\nu}{\nu_{20}} \left[\left(1 + \frac{\tilde{y}}{\tilde{R}}\right) \frac{\partial^2 \tilde{v}_x}{\partial \tilde{y}^2} + \frac{1}{\tilde{R}} \frac{\partial \tilde{v}_x}{\partial \tilde{y}} \right] + \frac{1}{\nu_{20}} \frac{d\nu}{d\tilde{y}} \left[\left(1 + \frac{\tilde{y}}{\tilde{R}}\right) \frac{\partial \tilde{v}_x}{\partial \tilde{y}} \right] \tag{4.14}$$

$$\frac{\tilde{v}_x \tilde{v}_x}{\tilde{R}} = \frac{\partial \tilde{p}}{\partial \tilde{y}} \tag{4.15}$$

$$\frac{\partial \tilde{v}_x}{\partial \tilde{x}} + \frac{\partial}{\partial \tilde{y}} \left[\left(1 + \frac{\tilde{y}}{\tilde{R}}\right) \tilde{v}_y \right] = 0, \tag{4.16}$$

$$\tilde{v}_x \frac{\partial \Theta}{\partial \tilde{x}} + \left(1 + \frac{\tilde{y}}{\tilde{R}}\right) \tilde{v}_y \frac{\partial \Theta}{\partial \tilde{y}} = \frac{\lambda}{c_p \rho \nu_{20}} \left[\left(1 + \frac{\tilde{y}}{\tilde{R}}\right) \frac{\partial^2 \Theta}{\partial \tilde{y}^2} + \frac{1}{\tilde{R}} \frac{\partial \Theta}{\partial \tilde{y}} \right] \tag{4.17}$$

The boundary conditions corresponding to the wall jet can be in the form

$$\tilde{y} = 0: \ \tilde{v}_x = \tilde{v}_y = 0, \ \Theta = 1 \tag{4.18}$$

$$\tilde{y} \to 0: \ \tilde{v}_x = 0, \ \Theta = 0. \tag{4.19}$$

The stream function ψ, non-dimensional distance from the wall η and higher velocity and temperature derivations can be according to the wanted similarity solution written in the forms:

$$\tilde{v}_x = \frac{\partial \psi}{\partial \tilde{y}}, \left(1 + \frac{\tilde{y}}{\tilde{R}}\right)\tilde{v}_y = -\frac{\partial \psi}{\partial \tilde{x}}, \tag{4.20}$$

$$\psi = \tilde{x}^m f(\eta), \eta = \frac{c\tilde{y}}{\tilde{x}^n}, \tilde{R} = \alpha \tilde{x}^n, \tag{4.21}$$

$$\tilde{v}_x = c\tilde{x}^{m-n}\frac{\partial f}{\partial \eta}, \left(1 + \frac{\tilde{y}}{\tilde{R}}\right)\tilde{v}_y = m\tilde{x}^{m-1} f - n\tilde{x}^{m-1}\frac{\partial f}{\partial \eta}\eta, \tag{4.22}$$

$$\frac{\partial \tilde{v}_x}{\partial \tilde{x}} = c\tilde{x}^{m-n-1}\left((m-n)\frac{\partial f}{\partial \eta} - n\frac{\partial^2 f}{\partial \eta^2}\eta\right), \frac{\partial \tilde{v}_x}{\partial \tilde{y}} = c^2\tilde{x}^{m-2n}\frac{\partial^2 f}{\partial \eta^2}, \tag{4.23}$$

$$\frac{\partial^2 \tilde{v}_x}{\partial \tilde{y}^2} = c^3\tilde{x}^{m-3n}\frac{\partial^3 f}{\partial \eta^3}, \tag{4.24}$$

$$\frac{\partial \Theta}{\partial \tilde{y}} = c\tilde{x}^{-n}\frac{\partial \Theta}{\partial \eta}\ \frac{\partial \Theta}{\partial \tilde{x}} = -n\eta\tilde{x}^{-1}\frac{\partial \Theta}{\partial \eta}, \tag{4.25}$$

$$\frac{\partial^2 \Theta}{\partial \tilde{y}^2} = c^2\tilde{x}^{-2n}\frac{\partial^2 \Theta}{\partial \eta^2}. \tag{4.26}$$

Applying the transformations mentioned above into the equation (4.14) and using (4.17), we obtain the following ordinary differential equation for the unknown functions $f(\eta)$ and $\Theta(\eta)$

$$\begin{aligned}&\tilde{x}^{2m-2n-1}\left[c(m-n)(f')^2 - cmff'' + \frac{1}{(\alpha + \eta/c)}[n\eta(f')^2 - mff']\right. \\ &\left.-\frac{1}{\alpha}\int_\eta^\infty [(2m-3n)(f')^2 - 2n\eta f'f'']d\eta\right] - \frac{\nu}{\nu_{20}}c\tilde{x}^{m-3n}\left[c\left(1 + \frac{\eta}{\alpha c}\right)f''' + \frac{1}{\alpha}f'\right] \\ &-\frac{d\nu}{d\eta}\frac{1}{\nu_{20}}c\tilde{x}^{m-3n}\left[c\left(1 + \frac{\eta}{\alpha c}\right)f'''\right] = 0\end{aligned} \tag{4.27}$$

where $f' = \frac{df}{d\eta}, f'' = \frac{d^2 f}{d\eta^2}, f''' = \frac{d^3 f}{d\eta^3}$.

The similarity solution is obtained, when it does not depend on the stream-vice coordinate $\tilde{x}$, so $m + n = 1$ must be valid.

Obtaining the second necessary relation to define the parameters m a n is quite complicated for non-isothermal flow and a correct solution has not been found yet. If the temperature gradient in a boundary layer is small we can neglect the effect of buoyancy in the calculations, moreover we can presume that neither the width of the boundary layer, nor the magnitude of the maximum

velocity in the velocity profile, which are defined by the magnitudes of the exponents m and n, are dependant on the temperature ratio. Methods presented in Glauert[12] and Wygnanski[52] can be used to estimate the magnitude of m and n.

For the case of a wall jet over an infinite flat wall, Glauert derived an integral invariant by considering the exterior momentum flux and this invariant gave us the second relation between the similarity exponents. An analogous procedure for the curved wall jet is adopted in Wygnanski[52].

Considering in the integral of (4.14) with respect to $\tilde{y}$ between the limits of $\tilde{y}$ and ∞ and using the condition that $\tilde{v}_x \to 0$ as $\tilde{y} \to \infty$. Then, using the continuity equation, one obtains

$$\frac{\partial}{\partial \tilde{x}}\int_{\tilde{y}}^{\infty}\tilde{v}_x^2 d\tilde{y} - \left(1+\frac{\tilde{y}}{\tilde{R}}\right)\tilde{v}_x\tilde{v}_y + \frac{1}{\tilde{R}}\int_{\tilde{y}}^{\infty}\tilde{v}_x\tilde{v}_y d\tilde{y} = \int_{\tilde{y}}^{\infty}\frac{\partial}{\partial \tilde{x}}\left(\frac{1}{\tilde{R}}\int_{\tilde{y}}^{\infty}\tilde{v}_x^2 d\tilde{y}\right)d\tilde{y} - \left(1+\frac{\tilde{y}}{\tilde{R}}\right)\frac{\partial \tilde{v}_x}{\partial \tilde{y}} \tag{4.28}$$

Multiplying by $\tilde{v}_x$, integrating with respect to $\tilde{y}$ from 0 to ∞, and simplifying gives

$$\begin{aligned}&\frac{\partial}{\partial \tilde{x}}\int_0^{\infty}\tilde{v}_x\left[\left(1+\frac{\tilde{y}}{\tilde{R}}\right)\left(\int_{\tilde{y}}^{\infty}\tilde{v}_x^2 d\tilde{y}\right) - \int_{\tilde{y}}^{\infty}\frac{\tilde{y}}{\tilde{R}}\tilde{v}_x^2 d\tilde{y}\right]d\tilde{y} - \int_0^{\infty}\left(1+\frac{\tilde{y}}{\tilde{R}}\right)\frac{\tilde{v}_y}{\tilde{R}}\left(\int_{\tilde{y}}^{\infty}\tilde{v}_x^2 d\tilde{y}\right)d\tilde{y} \\ &+\frac{1}{\tilde{R}}\int_0^{\infty}\tilde{v}_x\left(\int_{\tilde{y}}^{\infty}\tilde{v}_x\tilde{v}_y d\tilde{y}\right)d\tilde{y} - \frac{1}{2\tilde{R}}\int_0^{\infty}\tilde{v}_x^2 d\tilde{y} = 0\end{aligned} \tag{4.29}$$

An invariant is obtained if

$$\int_0^{\infty}\left(1+\frac{\tilde{y}}{\tilde{R}}\right)\tilde{v}_y\left(\int_{\tilde{y}}^{\infty}\tilde{v}_x^2 d\tilde{y}\right)d\tilde{y} + \frac{1}{2}\int_0^{\infty}\tilde{v}_x^2 d\tilde{y} - \int_0^{\infty}\tilde{v}_x\left(\int_{\tilde{y}}^{\infty}\tilde{v}_x\tilde{v}_y d\tilde{y}\right)d\tilde{y} = 0, \tag{4.30}$$

in terms of the similarity variables if

$$\int_0^{\infty}\frac{ff'(1-n)f - n\eta f'}{\left(1+\frac{\eta}{\alpha c}\right)}d\eta + \frac{1}{2}c\int_0^{\infty}(f')^2 d\eta + n\int_0^{\infty}nf(f')^2 d\eta - \int_0^{\infty}f\left(\int_{\eta}^{\infty}(f')^2 d\eta\right)d\eta = 0, \tag{4.31}$$

where α is the curvature parameter defined by the equation (4.21). Provided (4.31) is satisfied, then

$$\frac{\partial}{\partial \tilde{x}}\int_0^{\infty}\tilde{v}_x\left[\left(1+\frac{\tilde{y}}{\tilde{R}}\right)\tilde{v}_x\int_{\tilde{y}}^{\infty}\tilde{v}_x^2 d\tilde{y} - \frac{1}{\tilde{R}}\int_0^{\infty}\tilde{y}\tilde{v}_x{}^2 d\tilde{y}\right]d\tilde{y} = 0 \tag{4.32}$$

In the case of the similarity solution, (4.32) shows that $3m - n = 0$ and the second relation between the similarity exponents has been obtained. Thus $m = \frac{1}{4}$ and $n = \frac{3}{4}$.

If one multiplies (4.31) by $16/\alpha$, uses the derived values of c and n, and substitutes for double integral term from (4.25), the (4.31) takes the form

$$\int_0^\infty f\left[f'''\left(1+\frac{4\eta}{\alpha}\right)+f''\left(f+\frac{4}{\alpha}\right)2(f')^2\left(1-\frac{1}{\alpha f}\right)\right]d\eta, \tag{4.33}$$

which, as can be shown, has to be identically zero. Therefore (4.27) satisfies the restriction and the invariant is obtained in the following dimensional form

$$F = \nu^2 U_{Ref}\int_0^\infty f\left[\left(1+\frac{4\eta}{\alpha}\right)\int_\eta^\infty \frac{1}{4}(f')^2 d\eta - \frac{1}{\alpha}\int_\eta^\infty \eta(f')^2 d\eta\right]d\eta, \tag{4.34}$$

The constant value of F is strictly dependent on the velocity profiles being similar, whereas the existence of the corresponding invariant for flow over a flat surface is not dependent on this similarity. Although the similarity solution is self-consistent, the conditions under which F is invariant appear to be far more restrictive then those required for the invariants in classical similarity solutions such as the plane wall-jet or free jet.

The reference velocity U_{Ref} may be determined by using the invariant F from (4.34). The value of $F/(\nu^2 U_{Ref})$ as a function of the curvature parameter $4/\alpha$ was determined by evaluating the integral numerically and it is plotted in Fig.4.23. The value of F could be determined from the measured velocity profiles. The reference velocity U_{Ref} would then be determined and the results of the similarity solution could be used to predict the development of the flow or to calculate the stability criterion for non-isothermal flow.

Dependence of air viscosity on temperature in the temperature range 20-70°C will be replaced by a linear function in the form

$$\frac{\nu}{\nu_{20}} = aT + b \tag{4.35}$$

and differential of viscosity by the expression

$$\frac{d\nu}{d\eta}\frac{1}{\nu_{20}} = a\frac{dT}{d\eta}, \tag{4.36}$$

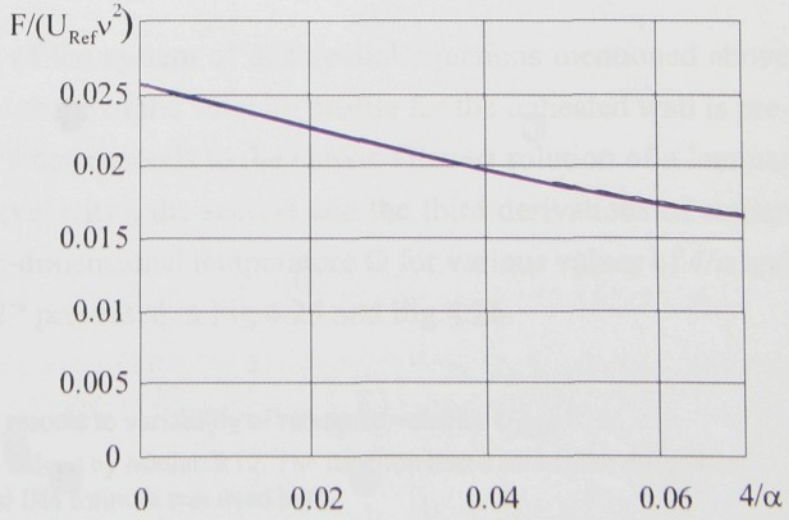

Fig.4.23 Variation of the invariant $F/(U_{Ref}\nu^2)$ with the curvature parameter $4/\alpha$

where the values of constants a and b are $a=0.0074$ and $b=1$ for air according to Hilsenrath[15]. It is not necessary to express the dependence of (ρ, λ, c_p) on temperature because these quantities are included in the Prandtl number, which remains nearly constant for a wide range of temperatures for air. Differentiating the equation (4.27) and substituting from (4.35) and (4.36) we get the differential equation for the boundary layer in the form

$$(aT+b)f^{iv}\left(1+\frac{4\eta}{\alpha}\right)+f'''\left[(4-4n)f+\frac{8}{\alpha}(aT+b)+a\left(1+\frac{8\eta}{\alpha}\right)T'\right] \tag{4.37}$$
$$+ff''\left[32n\frac{\eta}{\alpha}-(4-12n)\right]+(f')^2\frac{(5n-2)}{\alpha}+\frac{4}{\alpha}aT'f''$$
$$+\frac{4}{\alpha+4\eta}\left[(4-4n)f''f-4nf''f'\eta-(8n-4)(f')^2\right.$$
$$\left.-\frac{4}{\alpha+4\eta}((4-4n)f''f-4n(f')^2)\right]+aT'\left(\frac{4}{\alpha}f''+f'''\right)+aT''\left(1+\frac{4\eta}{\alpha}\right)f''=0$$

where $f^{iv}=\frac{d^4f}{d\eta^4}$. It is necessary to solve the equation for the boundary conditions

$$f(0)=f'(0)=f'(\infty)=0 \quad \text{and} \quad f(\infty)=1\ ^{1} \tag{4.38}$$

The differential equation for heat transfer must be solved with the equation (4.37). After applying the transformations (4.25) and (4.26) it has the form

$$(n-1)f\Theta=\frac{1}{Pr}\left[\left(\frac{1}{4}+\frac{\eta}{\alpha}\right)\Theta''+\frac{1}{\alpha}\Theta'\right] \tag{4.39}$$

and the boundary conditions

$$\Theta(0)=1 \text{ and } \Theta(1)=0. \tag{4.40}$$

The results of the solution[2] of the system of differential equations mentioned above are presented in Fig.4.24 - Fig.4.26. The shape of the velocity profile for the unheated wall is presented in Fig.4.24. The profile for $4/\alpha=0$ corresponds to the classic Glauert solution of a laminar wall jet. There are profiles of the first (velocity), the second and the third derivations of stream the function $f(\eta)$ and profiles of the non-dimensional temperature Θ for various values of $4/\alpha$ and for various values of temperature ratio T^* presented in Fig.4.25 and Fig.4.26.

1. Choice of $f(\infty)=1$ is possible with respect to variability of reference velocity U_{Ref}.
2. The system of differential equations was solved by Matlab R12. The function based on a finite difference code that implements the 3-stage Lobatto IIIa formula was used here.

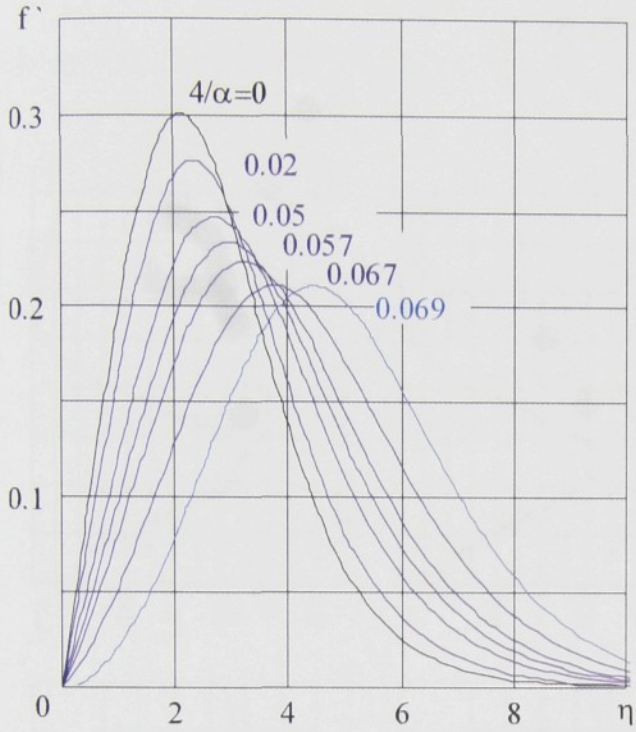

Fig.4.24 Variation of the velocity profile with the pressure gradient

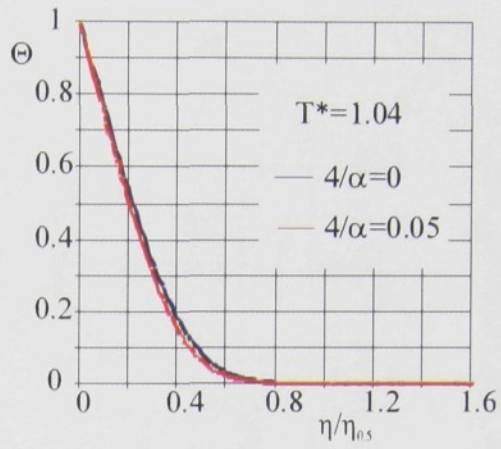

Fig.4.25 Example of the temperature profile in non-dimensional $\Theta(\eta)$ coordinates for various values of $4/\alpha$

4.4 Stability of curved laminar flow

The velocity and temperature profiles calculated above will be used for the analysis of flow from the point of view of stability criterion. First it will be necessary to transform a thermodynamic stability criterion (See "Stability criterion" on page 29.) to the curvilinear orthogonal coordinates

The stability criterion in the curvilinear orthogonal coordinates can be obtained by coordinate conversion of the equation (2.51). It is valid:

$$\vec{q} = -\lambda\frac{\partial T}{\partial r}\vec{r} - \lambda\frac{1}{r}\frac{\partial T}{\partial \varphi}\vec{\varphi} \tag{4.41}$$

$$\overrightarrow{\tau_{diss}} = 2\mu\begin{bmatrix} \dfrac{\partial v_x}{\partial r} & \dfrac{1}{2}\left(r\dfrac{\partial}{\partial r}\left(\dfrac{v_y}{r}\right) + \dfrac{1}{r}\dfrac{\partial v_x}{\partial \varphi}\right) \\ \dfrac{1}{2}\left(r\dfrac{\partial}{\partial r}\left(\dfrac{v_y}{r}\right) + \dfrac{1}{r}\dfrac{\partial v_x}{\partial \varphi}\right) & \dfrac{1}{r}\dfrac{\partial v_y}{\partial \varphi} + \dfrac{v_x}{r} \end{bmatrix} \tag{4.42}$$

in the curvilinear orthogonal coordinates. If we use a similar method as in the previous paragraph we obtain the thermodynamic stability criterion in the form:

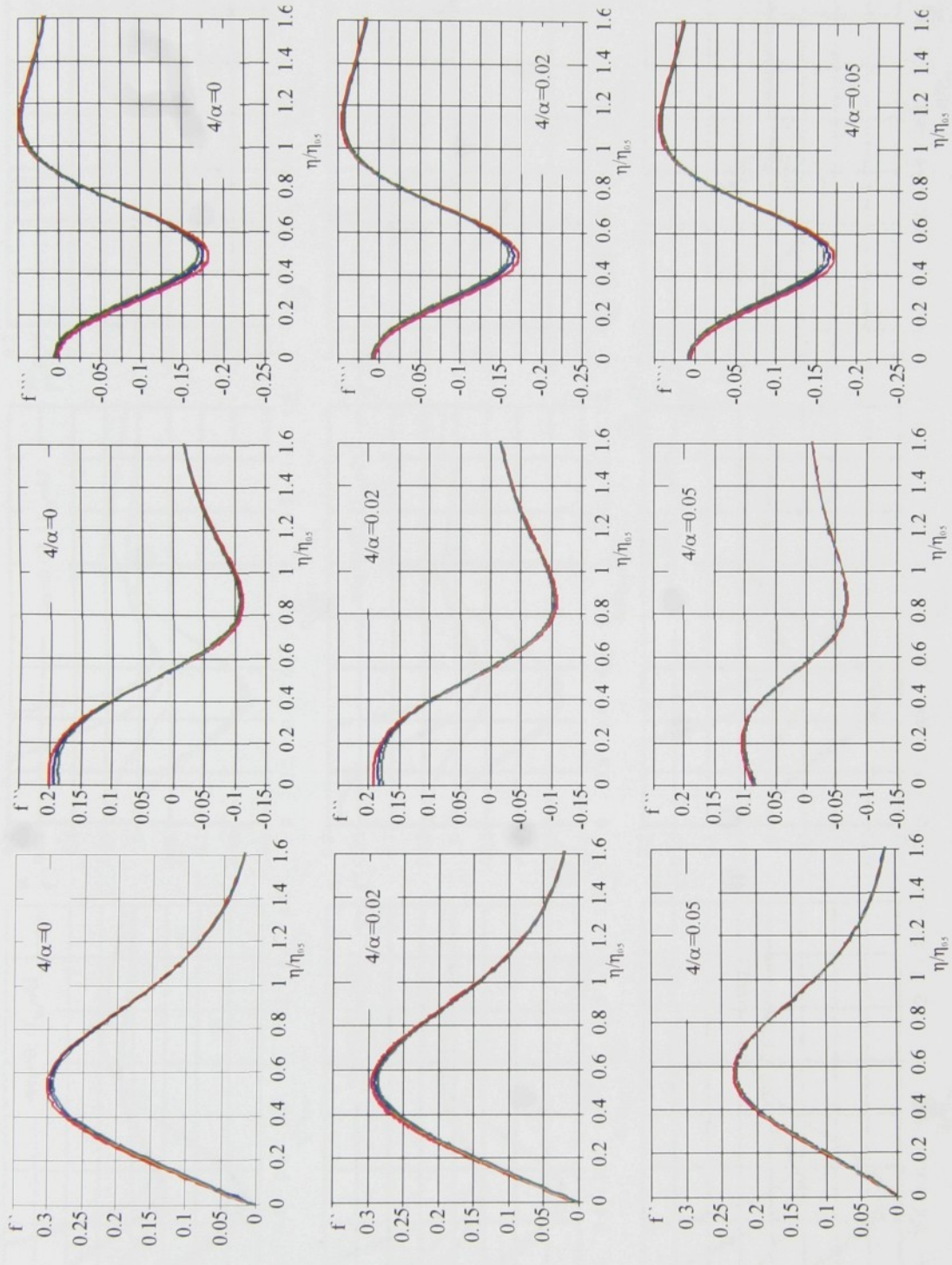

Fig.4.26 Variation of velocity profile with temperature ratio T^* and position on cylinder $4/\alpha$. The "real" profile and "real" position must be evaluated using the known reference velocity $U_{Ref.}$

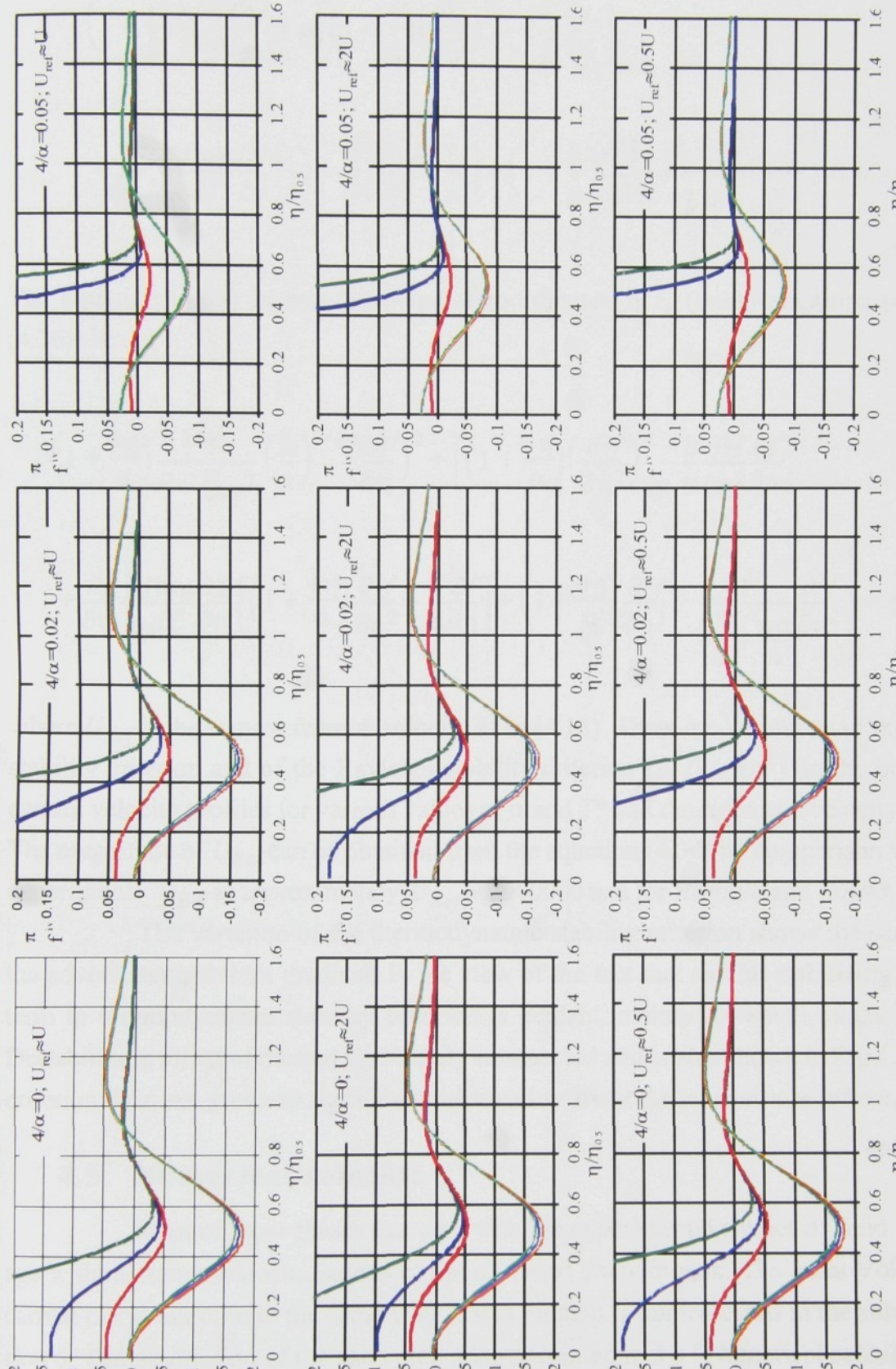

Fig.4.27 Variation of thermodynamic criterion of stability $\tilde{\pi}$ and Rayleigh criterion f^{iv} with temperature ratio T^* nondimensional curvature $4/\alpha$ and reference velocity U_{Ref} Stabilization of boundary layer by heating the wall is significant. from the picture

$$\left(1+\frac{\tilde{y}}{\tilde{R}}\right)\frac{\lambda}{T}\left(\frac{\partial T}{\partial \tilde{y}}\right)^2+\mu\left[\left(1+\frac{\tilde{y}}{\tilde{R}}\right)\left(\frac{\partial \tilde{v}_x}{\partial \tilde{y}}\right)^2-2\frac{\tilde{v}_x}{\tilde{R}}\frac{\partial \tilde{v}_x}{\partial \tilde{y}}\right] \tag{4.43}$$

$$+\mu\tilde{v}_x\left\{\frac{d\ln\mu}{dT}\frac{\partial T}{\partial \tilde{y}}\left[\left(1+\frac{\tilde{y}}{\tilde{R}}\right)\frac{\partial \tilde{v}_x}{\partial \tilde{y}}-\frac{\tilde{v}_x}{\tilde{R}}\right]+\left(1+\frac{\tilde{y}}{\tilde{R}}\right)\frac{\partial^2 \tilde{v}_x}{\partial \tilde{y}^2}+\frac{\tilde{v}_x}{\tilde{R}^2\left(1+\frac{\tilde{y}}{\tilde{R}}\right)}\right\}=\pi\geq 0$$

The equation (4.43) in non-dimensional coordinates η, ξ (transformations (4.13) and (4.20)-(4.26)) is:

$$\left(1+\frac{4\eta}{\alpha}\right)\frac{16c_p}{PrU_{Ref}^2T}\left(\frac{\tilde{R}}{\alpha}\right)^{4/3}\left(\frac{\partial T}{\partial \eta}\right)^2+\left[\left(1+\frac{4\eta}{\alpha}\right)\left(\frac{\partial^2 f}{\partial \eta^2}\right)^2-\frac{8}{\alpha}\frac{\partial^2 f}{\partial \eta^2}\frac{\partial f}{\partial \eta}\right] \tag{4.44}$$

$$+\frac{\partial f}{\partial \eta}\left\{\frac{d\ln\mu}{dT}\frac{\partial T}{\partial \eta}\left[\left(1+\frac{4\eta}{\alpha}\right)\frac{\partial^2 f}{\partial \eta^2}-\frac{4}{\alpha}\frac{\partial f}{\partial \eta}\right]+\left(1+\frac{4\eta}{\alpha}\right)\frac{\partial^3 f}{\partial \eta^3}+\frac{1}{\frac{\alpha^2}{16}+\frac{\eta\alpha}{4}}\frac{\partial^2 f}{\partial \eta^2}\right\}=\tilde{\pi}\geq 0$$

where U_{Ref} is the same reference velocity as in (4.13). There are variations of the thermodynamic stability criterion and of the Rayleigh stability criterion $(\delta^4 f)/(\delta\eta^4)$ in the boundary layer for certain velocity profiles for various values of α and T^* and the reference velocity U_{Ref} in Fig.4.27. The magnitude of U_{Ref} can be obtained from the equation (4.34) by comparison with the results of experiments. U_{Ref} is approximately $U_{Ref}\approx 2900000$ m/s for $Re=700$ and $R/b=8$.

The variation of the thermodynamic stability criterion shows the stabilizing effect of the adverse temperature gradient. In the view of the fact that similar stabilizing effect of the first term in thermodynamic stability criterion is evident, mainly for small magnitudes of velocity. Destabilizing effect of increasing velocity is expected and is also shown in Fig.4.27. The Rayleigh criterion does not give any significant information about the temperature influence.

4.5 Numerical solution

Most of those theses that deal with the experimental studies of fluid flow cannot manage without numerical simulations of the observed phenomenon. The Final Volume Method was carried out in our case in the same way as this method is implemented in the solver FLUENT version 6. The description of the used method is presented in 3.4 "Numerical calculation using Finite volume methods" on page 56. or in Pulliam[33].

In the view of the fact that geometric arrangement describing current wall jet is simple, the construction of mash of finite volumes and entering the boundary conditions to certain CFD codes such as FLUENT does not cause any problems and therefore it is not necessary to describe them in details. Two-dimensional quadrangular mesh fine near the wall was created.

Even though the geometric arrangement of the problem is simple from the point of view of the numerical simulation, the solution of the studied wall jet represents a complex problem, as it deals with both transition to turbulence and the separation of flow. And as it was presented in the Chapter 2.3.3 "Models of turbulence for complex flows" on page 42, the solution of such specific problems is at the limits of contemporary CFD solvers.

With respect to the aims mentioned above we limited our solution to two different cases of flow. Laminar flow for the case of separated flow was simulated in a special way. The influence of temperature of the wall on the shape of velocity profiles and variation of pressure on the wall were observed during the calculations. These profiles were compared with the results from CTA experiments and with the results from the similarity solution at the end of this chapter.

Turbulent flow was simulated in a different way. The Van Driest model of eddy viscosity for an inner region of the wall jet and the Prandtl model for an outer region of the wall jet were used for calculations. Correction for flow with curvature was also used in this model, which, with respect to the magnitude of velocity of flow and to the magnitude of curvature does not have a significant effect on the final magnitude of turbulent viscosity. Calculations with the used Spalar-Almaras model, which is implemented in FLUENT solver and described in detail in Fluent[9], were also carried out to make comparisons.

4.5.1 Calculations of laminar flow

There are the results of the numerical solution for laminar regime of current wall jet presented in Fig.4.30a and Fig.4.30b. These figures describe the velocity field, temperature field and velocity and non-dimensional temperature profiles. Distribution of static pressure on the wall in the case of laminar curved wall jet is presented in Fig.4.28.

4.5.2 Calculations of turbulent flow

The numerical simulation of turbulent flow along the curved wall was carried out on the basis of the model described above. Discrepancy between the experiment and the calculation could be expected in this case. It is caused by the fact that the used turbulent model was designed for developed turbulent flow. As the results of the CTA experiments show, there is not fully developed turbulent flow even for the Reynolds numbers of about Re=2000. Nevertheless, even these obtained results correctly show the trends of the development of flow. The tendency of tur-

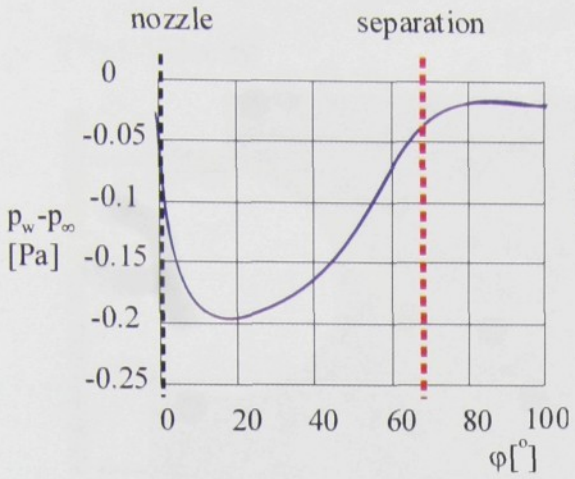

Fig.4.28 Distribution of subatmospheric pressure on the wall for laminar flow (*Re*=703;T*=1; *R/b*=8)

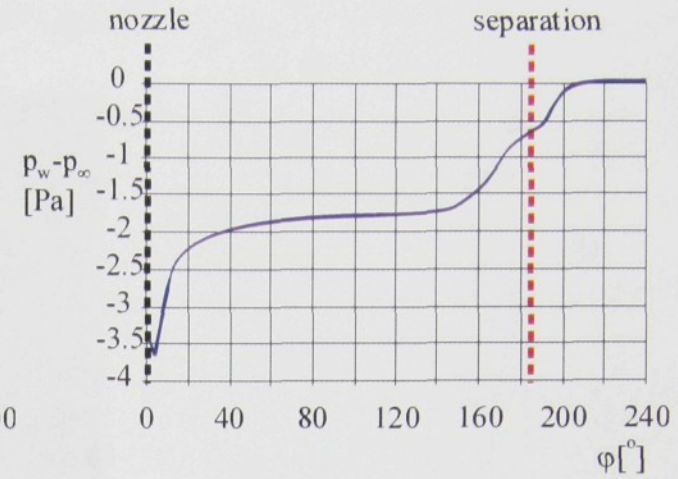

Fig.4.29 Distribution of subatmospheric pressure on the wall for turbulent flow (*Re*=2430;T*=1; *R/b*=8)

bulent flow to remain attached to the wall is well evident. There are contours of velocity and velocity profiles as well as profiles of viscid and total shear stress obtained from the calculated turbulent viscosity according to the relation:

$$\tau_{tot} = (\mu_t + \mu)\frac{\partial \overline{v_x}}{\partial y} \tag{4.45}$$

presented in Fig.4.31. Fig.4.29 shows stream-vice variation of the pressure on the wall.

The aim of the thesis was not to study the effect of the temperature of the wall on the turbulent flow. The model used by us does not accurately describe the transition from laminar to turbulent flow.

There is a comparison of the measured velocity and temperature profiles; profiles calculated numerically and profiles obtained on the basis of similarity solution (only laminar profiles) illustrated in Fig.4.32 and Fig.4.33.

When we compare the results of the experiments and the numerical simulation it is clear that none of the used numerical methods (numerical simulation and similarity solution) can describe the observed phenomenon precisely. The results of the numerical simulation accurately describe the flow close to the nozzle. Similar development of flow is clear both for the results of the experiments and for the numerical simulation. The correspondence of the numerical simulation with the experiment is not good when there is larger distance from the nozzle. It is possible that the results of the experiments are affected by such effects in the outer region (for example Görter vortexes), which laminar two dimensional model cannot describe.

T*=1-Velocity

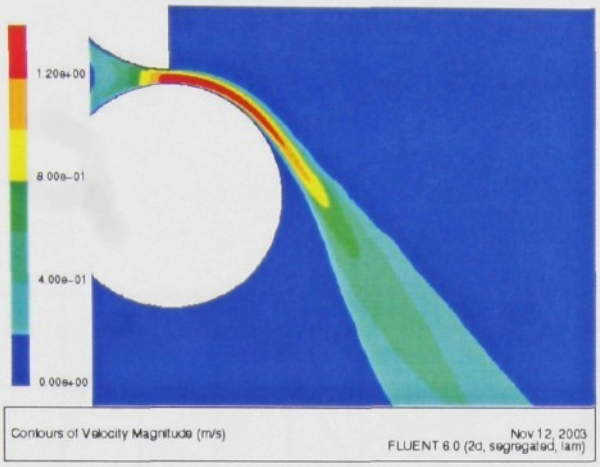

T*=1.02-Velocity

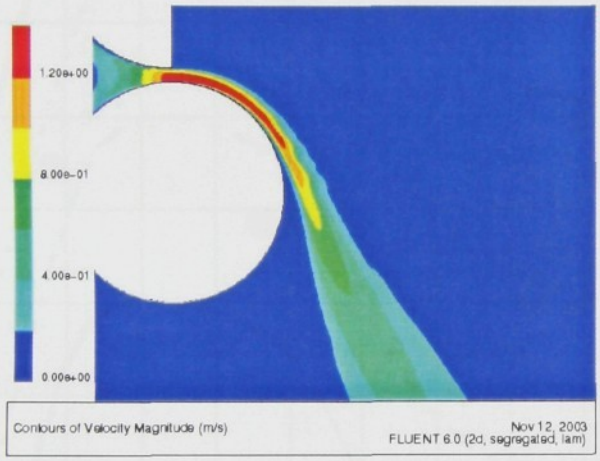

T*=1.02-Temperature

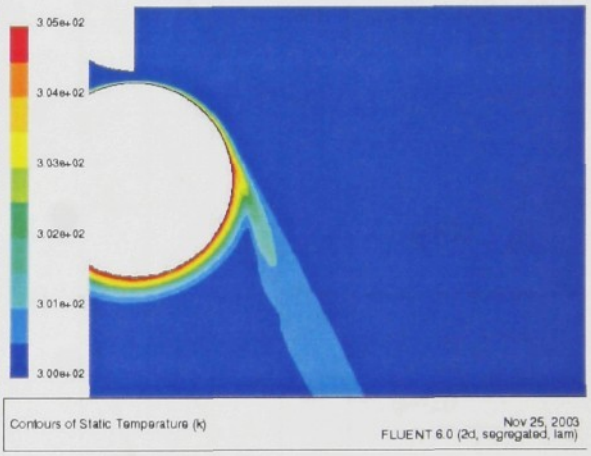

T*=1.04-Velocity

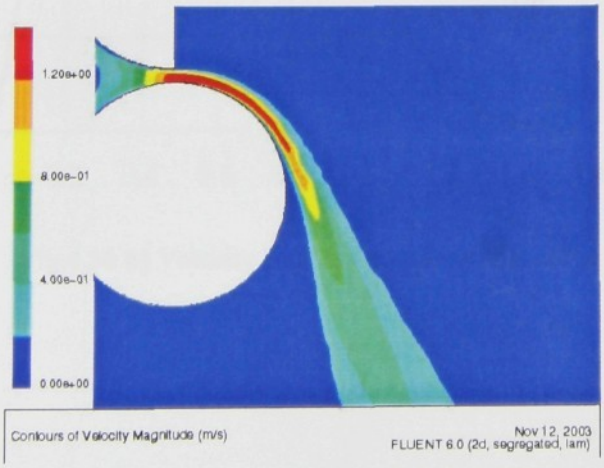

T*=1.04-Temperature

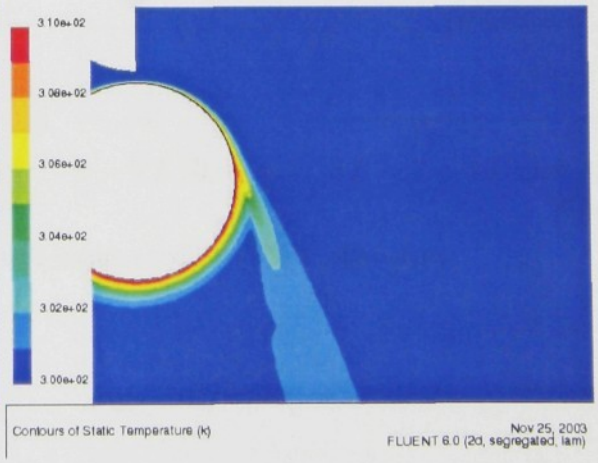

Fig.4.30 a) Results of FVM calculation of heated laminar wall jet.

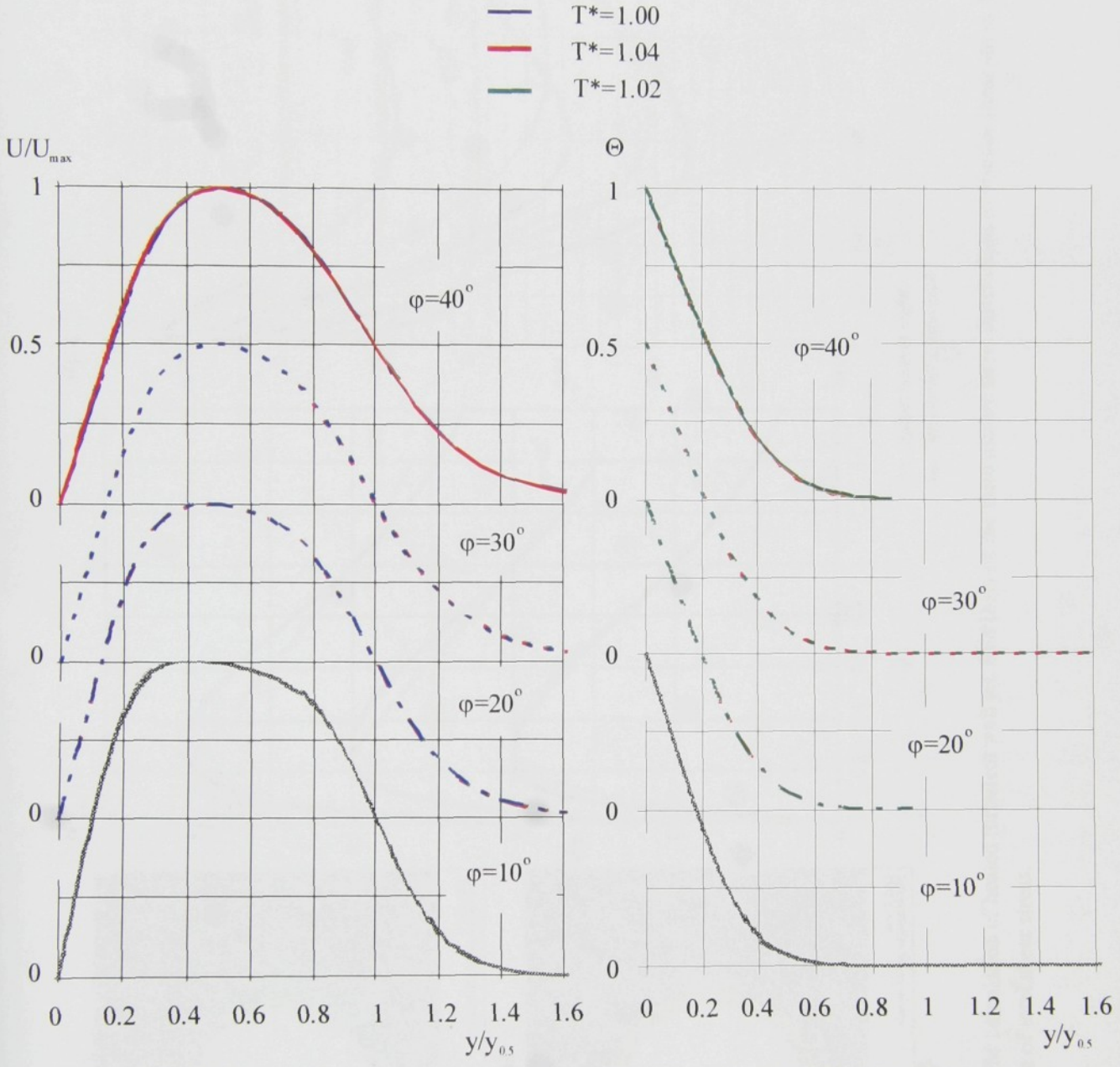

Fig.4.30 b) Velocity and temperature profiles of heated laminar wall jet (FVM calculation).

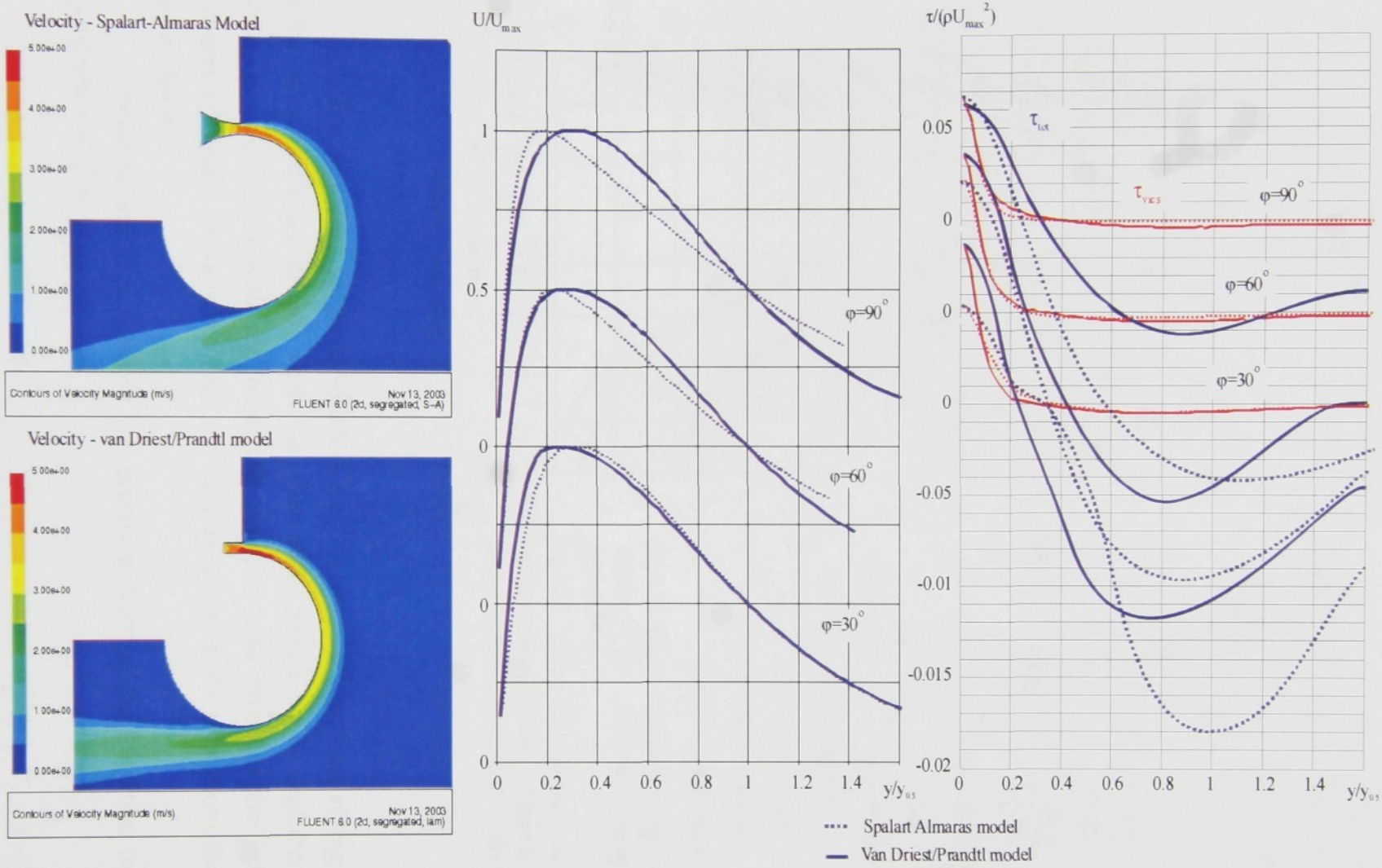

Fig.4.31 Results of FVM calculation of heated turbulent wall jet. Red lines on the third picture show distribution of viscose shear stress, blue lines show distribution of total shear stress.

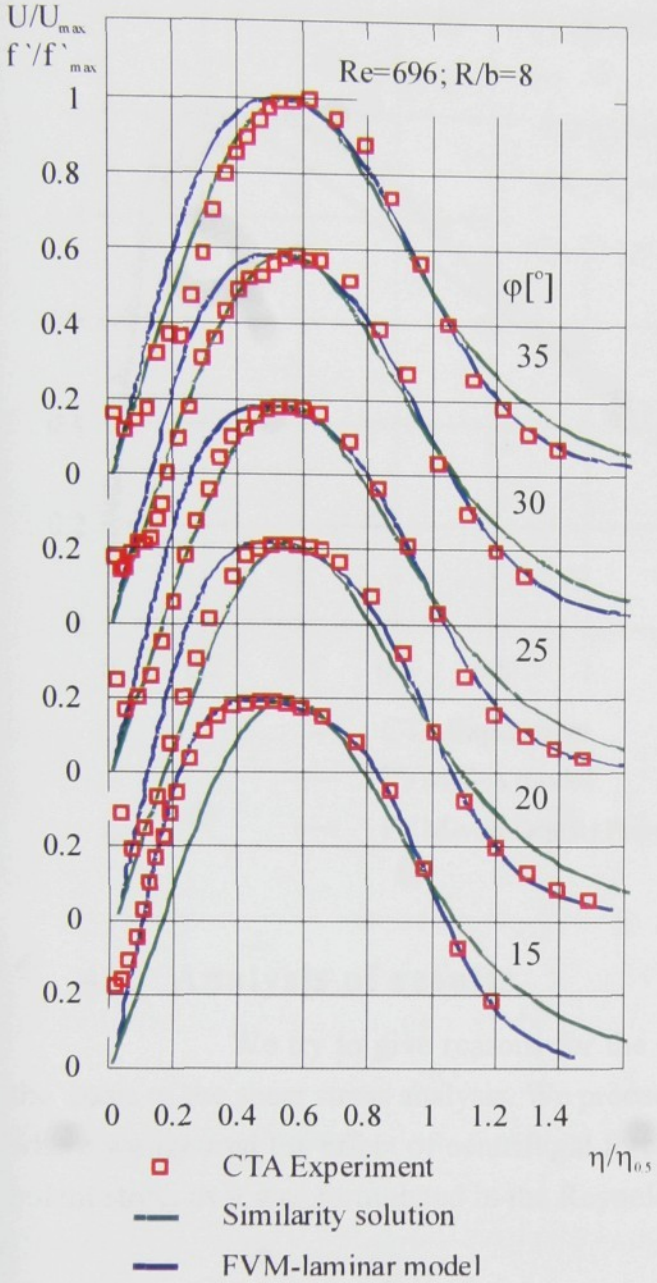

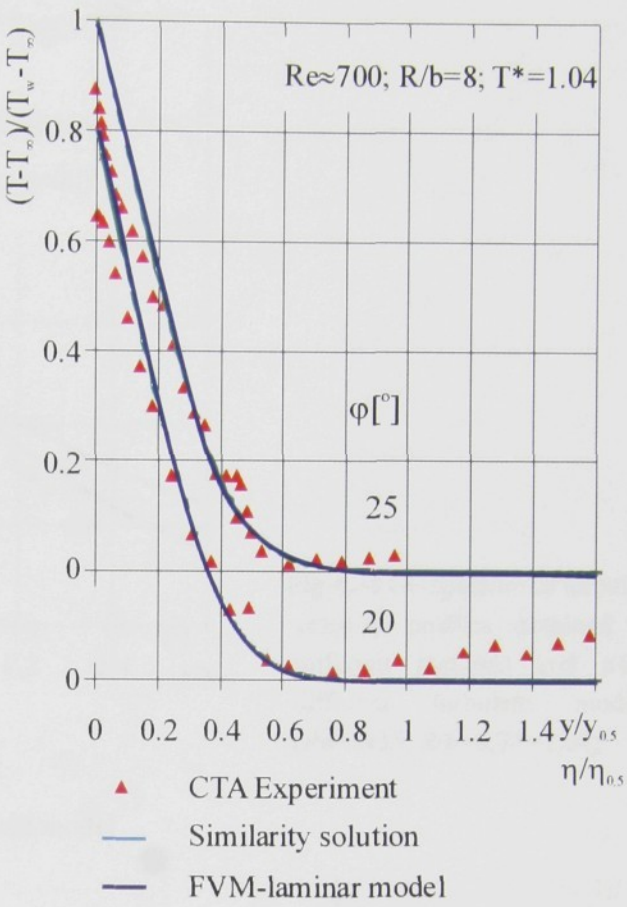

Fig.4.32 (Left) Comparison of velocity profiles obtained by different methods. (*Re*=700; *R/b*=8;*T**=1)

Fig.4.33 (Top) Comparison of dimensionless temperature profiles obtained by different methods.(*Re*=700; *R/b*=8;*T**=1.04)

The similarity solution, which is easy to solve, brings a satisfying correspondence with the experiments in positions where the effect of the nozzle can be neglected. The similarity solution, in comparison with the numerical solution, also provides the information about the course of higher derivations which can help us to obtain the idea about the stability of the boundary layer.

None of the used methods can precisely describe the transition to turbulence and the separation of flow from the wall

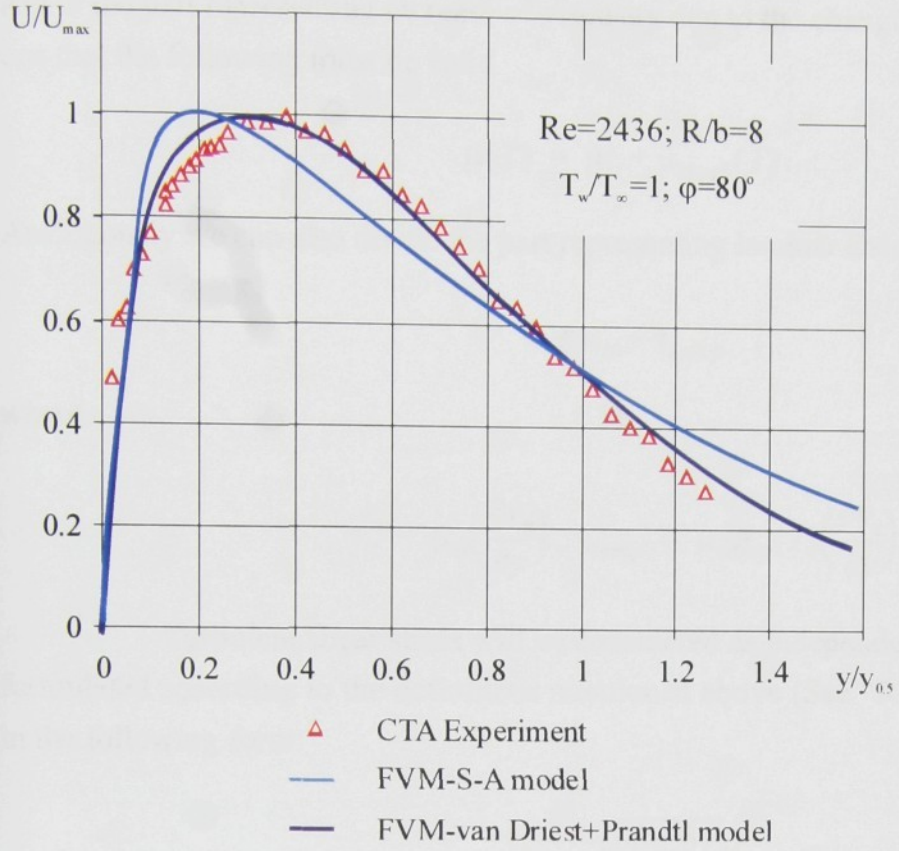

Fig.4.34 Comparison of turbulent velocity profiles obtained by different methods and using different turbulent models. (*Re*=2435; *R/b*=8;T*=1.04)

4.6 Analysis of results

We try to give reasons for the temperature gradient effect on curved wall jet on the basis of the shear stress analysis. We proceed from the momentum equation in the form (4.9), where we ignored the effect of centrifugal forces and where we added the term representing turbulent stress as it was formulated in the Reynolds equation.

$$\frac{\partial v^i}{\partial t} + \frac{\partial v^i v^k}{\partial x^k} + \rho \frac{\partial p}{\partial x^k} - \frac{\partial \tau^{ki}}{\partial x^k} - \frac{\partial \tau_t^{ki}}{\partial x^k} = 0 \qquad (4.46)$$

First we will focus especially on the magnitude of components of shear stress for individual cases of the flow.

Laminar shear stress can be formulated for two-dimensional flow as follows

$$\tau = \mu(T)\left(\frac{\partial u}{\partial y}\right) \quad , \qquad (4.47)$$

where it is necessary to take into consideration temperature dependence of viscosity for a non-isothermal case. Therefore viscosity is divided in the part corresponding to isothermal viscosity μ_{it}

and in the part representing increase of viscosity due to the changing temperature $\mu_{temp.}$ It is obvious that the following must be valid

$$\mu(T) = \mu_{it} + \mu_{temp}(T). \tag{4.48}$$

Analogously we can also divide the part representing laminar shear stresses,

$$\tau = \tau_{it} + \tau_{temp} \quad , \tag{4.49}$$

where:

$$\tau_{it} = \mu_{it}\left(\frac{\partial v_x}{\partial y}\right), \tau_{temp} = \mu_{temp}(T)\left(\frac{\partial v_x}{\partial y}\right) \tag{4.50}$$

Turbulent shear stress will be considered as independent on temperature and it can be formulated according to the definitions mentioned above (See "Reynolds equation" on page 37.) in the following form:

$$\tau_t = -(\overline{\rho \delta v_x \delta v_y}) \tag{4.51}$$

Total shear stress τ_{tot} can be written as the sum of above described three components (4.49) (4.51). Now we will gradually deal with the form of cross profile of each from above mentioned components. First we will analyze turbulent shear stress for the flow along the heated wall.

Turbulent shear stress. Individual fluctuation components of velocity were not measured in our experiments, but we measured the value that is the function of the both components δv_x and δv_y by means of a single wire probe. It was not possible, with regard to limitations of a single wire probe, to determine neither the magnitude of individual components, nor the magnitude of the product $\delta v_x \delta v_y$.

But we allow to suppose, provided that the magnitude of intensity of fluctuations for turbulent flow that we have measured does not change with temperature variation, that the magnitude of individual fluctuation components of velocity does not change either. Our measuring of intensity of fluctuations (Fig.4.20) shows insignificant temperature effect on the magnitude of velocity fluctuations in turbulent flow. Small temperature effect on the magnitude of intensity of fluctuations and on the magnitude of turbulent shear stress results also from the theses of other authors - for example Katz[21]. Therefore we will consider turbulent shear stresses as independent of temperature in our further contemplations. The typical profile of turbulent shear stress is illustrated in the Fig.4.35. Questionable is the magnitude of the turbulent shear stress in the area near the wall. From the results of the experiments and from the results of the numerical simulation

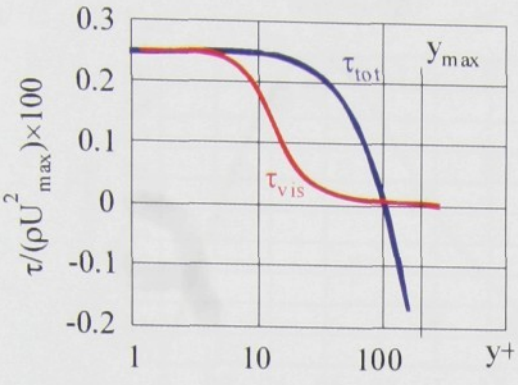

Fig.4.35 Variation of viscous and total shear stress close to the wall. Typical example of viscous sublayer (After Katz[21])

follows that turbulent viscosity near the wall is vanishing. Zero turbulent viscosity on the wall is confirmed also by supposed existence of laminar sublayer where significant molecular viscosity effect occurs.

Laminar isothermal shear stress. If the value of an isothermal component of kinematic viscosity in the boundary layer is constant, the course of shear stress depends only on the magnitude of the first-order derivative of velocity as it is obvious from the expression (4.50). Variation of the first derivation of velocity in the boundary layer was calculated on the basis of the similarity solution. Development of the first derivatives of velocity in dependence on the magnitude of parameter $4/\alpha$[1] is illustrated in Fig.4.36.

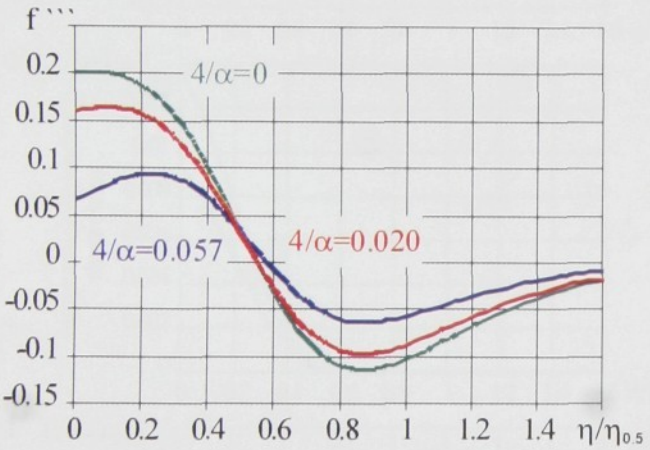

Fig.4.36 First derivation of velocity profile

From the results of the similarity solution in Fig.4.26 and from the measured velocity profiles in Fig.4.14 results that temperature effect on the form of velocity profile is not obvious for low values of T*. However there is a significant effect of temperature on the first derivation of the velocity profile. The courses of the first derivation of velocity illustrated in the Fig.4.36 can be considered in our case as similar to the courses of isothermal shear stress. It is clearly visible that the shape of isothermal shear stress profile changes with increasing the temperature ratio. For higher temperature ratios there is visible a lower isothermal shear stress near the wall.

Non-isothermal shear stress. The course of non-isothermal shear stress is affected by the temperature profile in the boundary layer and by temperature dependence of viscosity. Within a narrow temperature range it is possible to formulate temperature dependence of viscosity by

1. As mentioned above, parameter $4/\alpha$, which is defined as: $\alpha = \tilde{R}/\tilde{x}^n$, corresponds to the position of the calculated velocity profile (profile of the first derivation of f) on the circumfluenced curved surface. The value $4/\alpha \rightarrow 0$ corresponds to the Gilbert solution of a wall jet. It was established on the basis of the measured velocity profiles that the measured velocity profiles (Chapter 4.2) correspond to the magnitude of parameter α within the range of values $4/\alpha = 0.005 \div 0.013$.

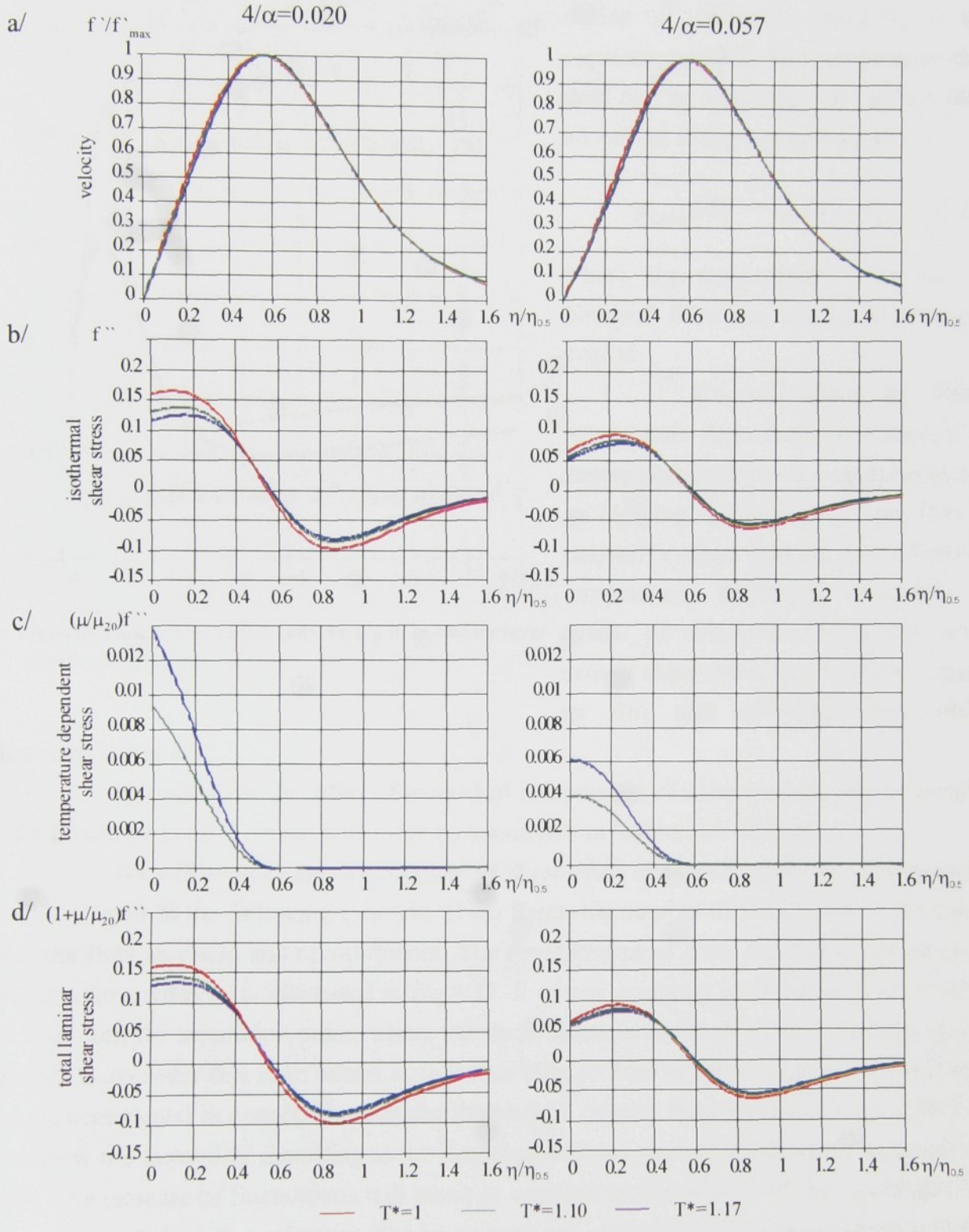

Fig.4.37 Components of shear stress for various values of temperature ratio T^* and curvature parameter $4/\alpha$ (results from similarity solution): $f' = \frac{\partial f}{\partial \eta} \approx \tilde{v}_x$ (4.22), $f'' = \frac{\partial^2 f}{\partial \eta^2} \approx \frac{\partial \tilde{v}_x}{\partial \tilde{y}}$ (4.23)

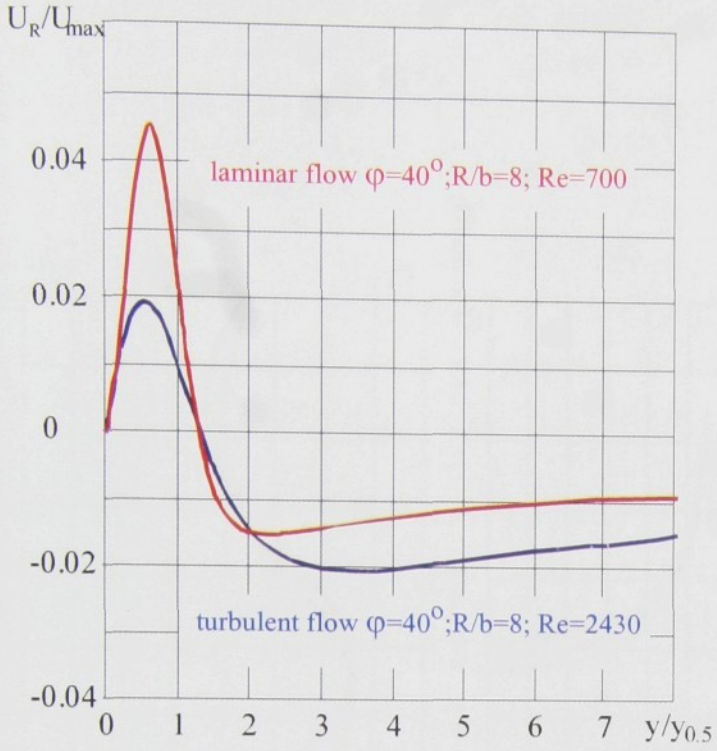

Fig.4.38 Variation of radial velocity U_R in boundary layer (CFD calculation).

means of a function, similarly as in the expression (4.35). The temperature-dependent part of viscosity can be then defined according to the equation (4.48)

$$\mu_{temp}(T) = \mu(T) - \mu_{it}, \qquad (4.52)$$

where the temperature T is the value obtained from the calculated temperature profile.

We will obtain the value of temperature-dependent component of shear stresses according to the equation (4.50) by multiplying the function of the first-order derivative of the velocity by the function of temperature dependent viscosity. The course of temperature-dependent component of shear stress as a function of parameter $4/\alpha$ and of temperature ratio is illustrated in Fig.4.37.

We will show the effect of individual components of shear stress tensor on conditions in the boundary layer. First we will focus on conditions in isothermal wall jet.

We will analyze the development of shear stress and its effect on the separation of the boundary layer in the following example. If the Reynolds number of flow is small, we can consider the flow as viscid and non-turbulent. The development of shear stresses in the streamwise direction for such flow is illustrated in Fig.4.37. It comes gradually to decrease of shear stress at the wall until the separation point, where the shear stress on the wall is zero. Unfortunately it is possible to consider this state unreal as the separation of flow is (according to the presumptions and measurements) in connection with the increase of velocity fluctuations. All the velocity profiles show the instability according to the Rayleigh criterion and thermodynamic criterion of stability. The increase of fluctuations will occur in unstable profile which will be manifested by the increase of turbulent shear stresses. The increase of turbulent shear stress occurs both in the inner and the outer regions. New equilibrium state will be reached when the maximum in total stress profile in the inner region disappears. The analysis of other cases of flow, for example free jet, shows the tendency of flow to reach the states with low total shear stress gradients. Together with the increase of total shear stress at the wall according to the similar principle (instability of the

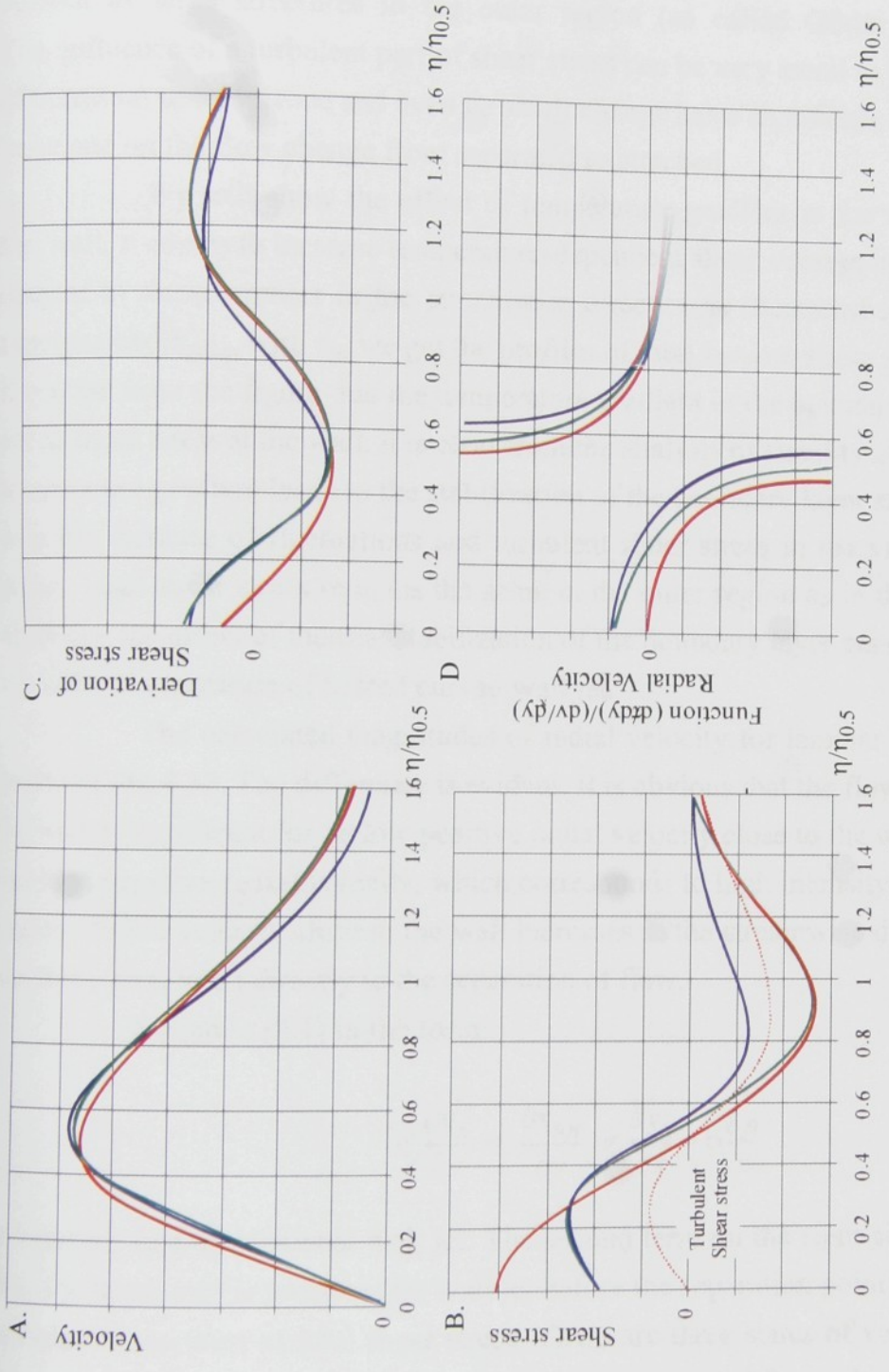

Fig.4.39 Sketches of development of total shear stress and its derivation.

shear layer), the increase of total shear stress in the outer region occurs. The flow in the outer region has the character of free jet and the tendency to decrease the gradient of total shear stress leads to the increase of the thickness of the boundary layer.

Separation of flow is also affected by the centrifugal effect and probably by the development of large structures in the outer region (so called Görter vortices - see Tesař[43]). The influence of a turbulent part of shear stress can be very small in the beginning of the process of transition to turbulence and even its small change has a significant effect on transition to turbulence and on the flow change from separated to attached.

We will show the effect of temperature gradient at the wall in this part. If we heat the wall, it comes to increase temperature-dependent shear stresses in the boundary layer. Development of these stresses in the streamwise direction is illustrated in Fig.4.37c. If we perform superposition τ_{temp} with τ_{it}, we get the profiles of total laminar shear stress as shown in Fig.4.37d. It is clear from the figure that the temperature gradient in the boundary layer decreases the gradient of shear stress at the wall. It is clear from the analysis of stability of the boundary layer that the temperature gradient leads to the stabilization of the boundary layer at the wall (Fig.4.27). That is why the increase of fluctuations and turbulent shear stress in the vicinity of the wall does not occur. Total shear stress remains the same in the outer region as in the isothermal case. We will show that the effect of thermal stabilization of the boundary layer near the wall plays a key role at the issue of separation of heated curved wall jet.

The calculated magnitudes of radial velocity for laminar and turbulent flow are presented in Fig.4.38. The difference is evident. It is obvious that the flow which remains attached to the wall is significant for its low positive radial velocity close to the wall and on the other hand it has high negative radial velocity, which corresponds to high intensity of entrainment in the outer region. Radial velocity close to the wall increases in the streamwise direction in case of the laminar flow. That leads directly to the separation of flow.

Equation (9.1) in the form:

$$v_y \frac{\partial v_x}{\partial y} = \frac{\partial \tau_{tot}}{\partial y} - v_x \frac{\partial v_x}{\partial x} - \rho \frac{\partial p}{\partial x} \tag{4.53}$$

is valid for two-dimensional wall jet. The second term on the right side of the equation is negative, the third term is positive (for wall jet before the separation point). The effect of curvature is included in the term of total shear stress. There are three states of velocity profiles presented in Fig.4.39. The state a/ corresponds to the laminar isothermal flow where $Re=Re_{lam}$. State b/ corresponds to the flow at $Re_{turb}>Re_{lam}$ where the effect of turbulent shear stresses starts to occur but it is not a developed turbulent flow. State c/ corresponds to the flow at Re_{turb}, where the velocity fluctuations and turbulent shear stress close to the wall are inhibited due to the effect of tempera-

ture. The sketches of velocity profiles (Fig.4.39-A), profiles of total shear stress (Fig.4.39-B), profiles of derivation of total shear stress(Fig.4.39-C) and finally the course of the function

$$v_y = \frac{\partial \tau_{tot}}{\partial y} / \frac{\partial v_x}{\partial y} \tag{4.54}$$

which is proportional to the course of radial velocity (Fig.4.39-D) are presented there. Owing to the simplification of the original equation (4.46) only the development of tendencies is presented here. But even the simplified analysis clearly shows that the boundary layer of curved wall jet, which is affected by the temperature gradient has higher tendency to separate from the wall than the isothermal turbulent flow at same values of the Reynolds number.

If the flow velocity increases in that way that the effect of turbulent shear stresses significantly predominates, it comes to flow reattachment and temperature effect is insignificant. It is obvious from our experiments that even a small temperature change can postpone the flow reattachment until the state where turbulence effect already plays an important role.

Conclusions formulated in this way correspond well to the results of the analysis performed on the basis of thermodynamic stability criterion as it is presented in the 4.4 "Stability of curved laminar flow" on page 93.

Chapter 5

CONCLUSIONS

5.1 Attainment of objectives

The main results of the theoretical and experimental investigation of the temperature effect on a curved wall jet can be summarized as follows:

i) From the "Smoke Wire" experiments the following conclusions can be formulated:

* At a certain value of the Reynolds number (Re_c) the reattachment of the separated flow occurs. For the isothermal case, the magnitude of Re_c depends on the slot width b and on the radius of curvature of the cylindrical surface R
* The heating of the circumfluenced surface causes the increase of Re_c with increasing ratio $T^* = T_w/T_\infty$. This phenomenon is significant even for small values of T^*.
* The increase of Re_c with T^* is not linear - the rate of the increase is reduced with increasing T_w/T_∞

ii) On the basis of velocity and temperature profiles and profiles of turbulence intensity obtained on the basis of the HWA experiments it is possible to show that:

* The separated flow has a laminar character until the separation point. The measured values of turbulence intensity in the boundary layer do not exceed 5%. A significant increase of turbulence intensity occurs near the separation point.
* For values of Re_c that we investigated the attached flow has the character of transitional turbulent flow. It is not possible to consider the turbulent flow as completely developed with regard to the velocity range that we observe.
* The measured course of the intensity of velocity fluctuations in the streamwise direction shows a gradual increase of the turbulence intensity.

* Neither significant changes of the velocity profile, nor any significant profile changes of the turbulence intensity with the temperature gradient for the investigated ranges of the temperature gradient and the Reynolds numbers were observed

iii) Our theoretical analysis based on the similarity solution and the numerical simulation of the heated curved wall jet yields the following stability conditions

* According to thermodynamic and the Rayleigh stability criterion, the laminar velocity profile in a non-heated case of curved wall jet is unstable.
* According to the Rayleigh stability criterion, the laminar velocity profile is unstable even for the velocity profile in case of heated curved wall jet.
* According to the thermodynamic stability criterion, significant stabilization of the velocity profile occurs in case of heated curved wall jet. The stabilization effect increases with the rise of the ratio T_w/T_∞ and decreases with the rise of the velocity. According to all the assumptions, the rise of the flow velocity has a destabilization effect.
* Both the experiments and the numerical simulation show that laminar flow tends to separation, on the contrary turbulent flow, even though calculated on the basis of simple turbulence model, leads to flow reattachment. The rise of velocity of turbulent flow leads to magnification of the angle of turbulent separation.
* Also the courses of pressure gradient $\partial p / \partial x$ along the cylindrical surface show different behavior. Magnitude of pressure gradient in streamwise direction is in case of laminar flow bigger than in the case of turbulent flow (except of areas near the separation point).

5.2 Application of results and further research

As it was presented in the introductory chapter, the main aim of this thesis was to investigate in detail the effect of the temperature gradient on a boundary layer in curved wall jet. In the course of solution it turned out that it concerns a very complex problem and that it is necessary to take into consideration also knowledge from the theory of turbulence and the theory of stability of a boundary layer. We have met the problem which is distinguished by separation of the boundary layer and by flow transition into turbulence. Both flow separation and flow transition into turbulence are phenomena that have not been so far satisfactory described by any of complex theories. Therefore it was necessary to make some simplifications in our contemplations and to use assumptions that are valid in the laminar case of turbulent flow regime, but the validity of which in transitional flow or in flow with separation of the boundary layer is questionable. One

of such simplifications is the presumption that transitional flow can be considered as a superposition of laminar and turbulent flow. These assumptions do not generally influence conclusions of this thesis.

A new experimental setup that enabled to perform precise experiments for a large range of boundary conditions was designed and constructed to solve the given problem. In the first phase, visualization of flow was performed by means of the "Smoke Wire" method. During the visualization flow within a large range of the Reynolds numbers and within a large range of temperature ratios was investigated. With regard to the extent of this thesis it is not possible to publish all the results obtained in this way and therefore only the most important information is presented here. But the other results serve and it is certain that they will serve in the future for a comparison with other, nowadays already planned and realized experiments that concern curved wall jet.

The "Smoke Wire" visualization gives us a good idea about flow development, but it does not enable a better understanding of the phenomenon. Hence we got down to measure velocity and temperature profiles in the boundary layer by the HWA method. These measuring proved the effect of flow velocity and temperature ratio on the character of flow (See Fig.4.19). Besides that we succeeded in measuring the development of the velocity profile and in measuring the profiles of intensity of turbulence in the streamwise direction. Detailed measuring of development of the intensity of turbulence for various values of the Reynolds number and for various values of temperature ratio shows a gradual flow transition from laminar into turbulent state.

Subsequent analytically performed calculations of temperature and velocity profiles by using the similarity solution, and these calculations performed numerically by using the Final volume method, enabled to have a look in the flow structure in detail and to get an idea about magnitudes of quantities that cannot be obtained by experiments. That concerns especially the distribution of static pressure on the circumferenced wall and courses of the first-order derivations and second-order derivations of the velocity profile. On the basis of these calculations the value of thermodynamic stability criterion could be calculated. The course of the thermodynamic stability criterion clearly showed the stabilization effect of temperature and the temperature gradient. It is necessary to mention, referring to the performed calculations, the derivation of the similarity solution of curved wall jet for non-isothermal flow and formulation of the thermodynamic stability criterion in curvilinear orthogonal co-ordinates. Although the formulation in curvilinear orthogonal co-ordinates is not so difficult, it does not occur in available literature.

Except for the often mentioned thesis by Tesař [41], which was the way out to design our experimental setup and for the determination of the range of experiments, we are not aware of any other similar problems being treated in a similar way in available literature. Therefore it is possible to consider most of here published conclusions as original. The most investigated is the

character of turbulent curved jet that is certainly widely applied in technical practice. But wrongfully are neglected here the described laminar curved wall jet and transition from the state of separated flow into attached flow. There are only few theses (most of them are mentioned in the Chapter 1) that deal with the temperature effect on turbulent wall jet and turbulent curved wall jet.

As mentioned several times before in the thesis, the problems of the curved wall jet and the curved wall jet with the temperature gradient are very complex problems, detailed analysis of which requires performance of a great number of experiments and numerical simulations. We succeeded in constructing an experimental setup and in creating a workplace where it is possible to perform a lot of other experiments. One of the most important steps will be a detailed investigation of a buoyancy effect on the observed phenomenon. Even though the effect we describe is significant also at low values of the temperature ratio, and therefore we suppose the buoyancy effect being insignificant, other experiments will have to be performed with the experimental setup turned upside-down with regard to the applied gravity, so that the buoyancy effect can be well described. For the near future, experiments with the reversed temperature gradient, that means experiments dealing with the cooling curved wall, are planned. Also construction of a new setup is planned for the future. We will profit by the mistakes of the contemporary setup by its construction and this new setup will enable measuring of all fluctuation components of velocity and temperature. Next construction of the setup is planned to perform similar experiments in water. On the basis of the thermodynamic criterion we can suppose the flow development in these cases. An experiment, and especially the experiment in so little described area as the curved wall jet with the temperature gradient is, can show surprising results.

REFERENCES

[1] BIRD, R. B., STEWARD, W. E., LIGHFOOD, E.N.: *Transport phenomena*, J.Wiley, New York, 1960, (Translated.: *Přenosové jevy*, Academia, Praha, 1968)

[2] BRADBURY, L. J. S.: The structure of a self-preserving turbulent plane jet, *Jour. Fluid Mech.*, **23** part 1, 1965, p. 31-64

[3] BETCHOV R.,CRIMINALE W. O.:*Stability of Parallel Flows*, Academic Press, New York, 1967

[4] BRUUN, H. H.:*Hot wire anemometry*, Oxford Univ. Press, 1995

[5] CHENG K.C.:A history of flow visualization: chronology, *The 1st Pacific Sympos. on Flow Visualization*, Honolulu, 1997

[6] CORNELL, D.: Smoke generation for Flow Visualisation, Mississippi State Univ, *Aerophysics Res. Rep*, **54**, 1964

[7] DAKOS, T.,VERRIOULOS C.A.,GIBSON M.M.:Turbulent flow with heat transfer in plane and curved wall jets, *Jour. Fluid Mech.*, **145**, 1984, p. 339-360

[8] DANTEC *StreamLine/StreamWare Installation & User's guide*, Dantec M. T. A/S, 1996

[9] FLUENT INC.:*User's Guide Vol. 1-5*, Fluent Inc., 1998

[10] GIBSON, M. M., VERRIOPOULOS, C. A.:Turbulent boundary Layer on a mildly curved convex surface: II. Temperature field measurements. *Expts Fluids*, **2**, 73, 1984

[11] GIBSON, M. M., VERRIOPOULOS, C. A.:Turbulent boundary Layer on a mildly curved convex surface: I. Mean flow and turbulence measurements, *Expts Fluids*, **2**, 17, 1984

[12] GLAUERT, M. B.: The Wall Jet, *Jour. Fluid Mech.*, **1**, 1956, pp. 625-644

[13] GOLDSTEIN, R. J.: *Modern Developments in Fluid Dynamics, Vol. 1*, Oxford University Press, 1938,

[14] GUITTON, D.E., NEWMAN, B.G.: Self-preserving turbulent wall jets over convex surface, *Jour. Fluid Mech.*, **81**, 1977, pp. 155-185

[15] HILSENRATH, J, TOULOUKIAN Y.S.: The viscosity, thermal conductivity, and Prandtl number for air, O_2,N_2, NO, H_2, CO, CO_2, H_2O, He, and A, *Trans. ASME*, **76**, pp. 967-985, 1954

[16] HINZE, J. O.: *Turbulence. An introduction to its mechanism and theory*. McGraw-Hill, New York, 1959

[17] IRVIN, H. P. A. H.:Measurements in a Self-Preserving Plane Wall Jet in a Positive pressure Gradient, *Jour. Fluid Mech*, **61**, Part1, pp.33, 1973

[18] JANKE, G.: Hot wire in wall proximity, in *Advances in Turbulence*, Comte-Bellot, Mathieu J. (ed), p. 488-498, Springer, Berlin, 1987

[19] JONÁŠ, P.: Měření turbulentních fluktuací rychlosti a teploty jednodrátkovým anemometrem se žhaveným drátkem, *Strojnický časopis*, **24**, 1973

[20] KACKER,S.C., WHITELAW, J.H.: The turbulence characteristics of two-dimensional wall-jet and wall-wake flows, *Trans. ASME E: J. Appl. Mech.*, **39**, pp.7., 1971

[21] KATZ, Y., HOREV, E., WYGNANSKI, I.: The forced turbulent wall jet, *Jour. Fluid Mech.*, **242**, p. 577, 1992

[22] KREITH, F.:The influence of curvature on heat transfer laws for fully turbulent wall flows, *Mech. Engng 77*, pp.265, 1955

[23] KRUKA, V., ESKINAZI, S.: The Wall Jet in a Moving Stream, *Jour. Fluid Mech.*, **20**, Part 4, 1964, pp.555

[24] LIGRANI,P.M., BRADSHAW, P.:Spatial resolution and measurement of turbulence in the viscous sublayer using miniature hot-wire probes, *Exp. in Fluids*, **5**, pp. 407-417

[25] MARŠÍK, F.:*Příklady ke cvičení z Termodynamiky kontinua*

[26] MARŠÍK, F.: *Termodynamika kontinua, Academia*, Praha, 1999

[27] MAYLE, R. E., BLAIR, M. F., KOPPER, F. C.:Turbulent boundary layer heat transfer on curved surface. *Trans. ASME C: J. Heat Transfer,* **101**, pp.521, 1979

[28] NEWMAN, B. G.: The deflection of Plane Jets by Adjacent Boundaries, Coanda Effect, p.232-264 in *Boundary Layer and Flow Control*, G. V. Lachman (ed), Pergamon Press, 1961

[29] NIZOU, P. Y.: Heat and momentum transfer in a plane turbulent wall jet, *Trans. ASME C: J.Heat Transfer,* **103**, pp.138, 1981

[30] PERRY, A. E.: *Hot Wire Anemometry*, Clarendon Press, Oxford, 1982

[31] POLYAKOV, A. F.,SHINDIN, S. A.:Peculiarities of hot-wire measurements of mean velocity and temperature in the wall vicinity, *Lett. Heat Mass Transfer*, **5**, pp. 55.

[32] PŘÍHODA, J.: *Algebraické modely turbulence a jejich použití při řešení středovaných Navier-Stokesových rovnic*, Rep. ČSAV Z-1153/90, 1990

[33] PULLIAM, T. H., LOMAX, H.:*Fundamentals of Computational Fluid Dynamics*, Springer Verlag, 2001

[34] SCHLICHTING, R.: *Boundary-layer theory*, Pergamon Press, 1955

[35] SHERMAN, S. F.: *Viscous Flow*, McGraw-Hill, London, 1990

[36] SWAMINATHAL, M. K., RANKIN, G. W., SRIDHAL, K.: A note on the response equations for hot-wire anemometry, *Jour. Fluids Eng*, **108**, 1986, p. 115-118

[37] ŠESTÁK, J., RIEGER, F.: *Přenos hybnosti, tepla a hmoty*, ČVUT, Praha, 1993

[38] SQUIRE, H. B.: jet flow and its effect on aircraft, *Aircraft Enginering*, **22**, pp.62, 1950

[39] TENNEKES, H.,LUMLEY, J. L.: *The First Course in Turbulence*, MIT Press, 1972

[40] TESAŘ, V.: *Vyšetřování bistability u proudění s charakterem zatopeného tekutinového proudu*, Final report from the Grant project num. 101/99/00959, 2001

[41] TESAŘ, V.:Objev lokálního minima na stěně obtékané přilnutým proudem, *Acta Polytechnica,* **1**, Praha, 1974

[42] TESAŘ, V.:Přechod do turbulence u Coandova jevu, *Acta Polytechnica,* **17**, Praha, 1985

[43] TESAŘ, V.: *Mezní vrstvy a turbulence*, ČVUT, Praha 1996

[44] TESAŘ, V.: Control of flow separation by temperature gradient, in *Euromech Colloquium 377, IT-CAS, Praha*, pp. 54-55, 1998

[45] TRÁVNÍČEK, Z.: *Coandův efekt užívaný při impaktním proudění*, PhD Thesis, Praha 1993

[46] TRAVNÍČEK, Z., WANG, A-B., MARŠÍK, F.: Flow visualization of the laminar vortex shedding behind a cooled cylinder, In: *Int. Symposium on Experimental Mechanics ISEM (CD- proceedings),* 2002 - Taipei, **C209**

[47] TOWNSEND, A.A.: *The structure of turbulent shear flow*, Cambridge Univ. Press, 1956

[48] VAN DER HEGGE ZIJNEN, B. G: Modified correlation for the heat transfer by natural and by forced convection from horizontal cylinders, *Appl. Sci. Res*, **A6**, 1956, pp. 129-140

[49] WANG, A-B, TRÁVNÍČEK, Z.: On the linear heat transfer correlation of a heated circular cylinder in laminar cross flow by using a new representative temperature concept, *Int. J. Heat Mass Transfer*, **44**, No. 24, pp. 4635-4647.

[50] WANG, A-B., TRÁVNÍČEK Z, CHIA, K-C.: On the relationship of Effective Reynolds number and Strouhal number for the laminar vortex shedding of a heated circular cylinder. *Physics of Fluids*, **12**, No. 6, pp.1401-1410.

[51] WHITE, F.M.: *Viscous fluid flow*, McGraw-Hill, 1974

[52] WYGNANSKI, I. J.,CHAMPAGNE F. H.: The laminar wall-jet over a curved surface, *Jour. Fluid Mech.*, **31**, Part 3, pp.459, 1968

[53] WILCOX, D. C.: *Turbulence modeling for CFD*, DCV Industries, 1993

[54] WILLS, J. A. B.:The correction of hot-wire readings for proximity to a solid boundary, *Jour. Fluid Mech.*, **12**,pp. 388

[55] WILSON, D. J., GOLDSTEIN R.J.: Turbulent Wall Jets With Cylindrical Streamwise Surface Curvature, *Jour. Fluid Mech.* **98**, 1976, pp. 550-557

[56] WYNGAARD, J. C., LUMLEY, J. L.: A constant temperature hot-wire anemometry, *Jour. Sci. Instr.*, **49**, 1978, pp. 363-365

[57] YANG, W-J.: *Handbook of flow visualization*, Hemisphere Publish. Corp., 1989

[58] YOUNG,A.D.: *Boundary Layers*, London PSP Prof. Books, 1989

[59] ZEBIB, A.:Stability of viscous flow past a circular cylinder, *Jour. Engng. Math.* **21**, pp.155-165, 1987